A FRAMEWORK FOR LIQUEFACTION SUSCEPTIBILITY MAPPING OF DHAKA CITY USING LATEST SPT BASED CO-RELATIONSHIP AND REGIONAL FACTORS

A Thesis

by

SAMIUL ISLAM

MASTER OF SCIENCE IN CIVIL ENGINEERING

DEPARTMENT OF CIVIL AND ENVIRONMENTAL ENGINEERING
ISLAMIC UNIVERSITY OF TECHNOLOGY
GAZIPUR, BANGLADESH

SEPTEMBER, 2023

A FRAMEWORK FOR LIQUEFACTION SUSCEPTIBILITY MAPPING OF DHAKA CITY USING LATEST SPT BASED CO-RELATIONSHIP AND REGIONAL FACTORS

A Thesis

by

Samiul Islam

Submitted to the Department of Civil and Environmental Engineering, Islamic University of Technology (IUT), Gazipur in partial fulfilment of the requirements for the degree

of

MASTER OF SCIENCE IN CIVIL ENGINEERING

September, 2023

ISLAMIC UNIVERSITY OF TECHNOLOGY

GAZIPUR, BANGLADESH

Recommendation of the Board of Examiners

The thesis titled *"*A Framework for Liquefaction Susceptibility Mapping of Dhaka City Using Latest SPT Based Co-relationship and Regional Factors*",* submitted by Samiul Islam, Student ID. 171051008 of Academic Year 2017-2018 has been found as satisfactory and accepted as partial fulfillment of the requirement for the degree of Master of Science in Civil Engineering.

1.

_____

Dr. Hossain Md. Shahin (Supervisor)   Chairman
Professor and Head   and Ex-officio
Department of Civil and Environmental Engineering (CEE)
Islamic University of Technology (IUT)
Gazipur, Bangladesh

2.

_____

Dr. Md. Tarek Uddin, PEng.   Member
Professor
Department of Civil and Environmental Engineering (CEE)
Islamic University of Technology (IUT)
Gazipur, Bangladesh

3.

_____

Dr. Shakil Mohammad Rifaat   Member
Professor
Department of Civil and Environmental Engineering (CEE)
Islamic University of Technology (IUT)
Gazipur, Bangladesh

4.

_____

Dr. Md. Abu Taiyab   Member
Professor   (External)
Department of Civil Engineering,
Dhaka University of Engineering and Technology (DUET),
Gazipur, Bangladesh

DECLARATION

It is hereby declared that this thesis and the studies embodied in it are the result of the research carried out by the author under the supervision of Dr. Hossain Md. Shahin, Professor, Department of Civil and Environmental Engineering, Islamic University of Technology, Gazipur, Bangladesh. Wherever contributions of others were involved, every effort has been made to indicate this clearly with due reference to the literature and acknowledgement of collaborative research and discussions. Neither thesis nor any part of it has been submitted to or is being submitted to for any other purposes (except for publication).

Name of Supervisor:
Dr. Hossain Md. Shahin
Professor
Department of Civil and Environmental Engineering
Islamic University of Technology,
Board Bazar, Gazipur, Bangladesh

Name of Candidate:
Samiul Islam
Student No: 171051008
Academic Year: 2017-2018

ACKNOWLEDGEMENT

ABSTRACT

Integration of regional code-based provisions considering local site effects and updated analytical techniques is a must in the field of seismic site characterization and liquefaction susceptibility assessment. This study introduces provisions from latest regional guidelines to define seismic site class and assess liquefaction susceptibility, utilizing the most comprehensive database developed for Dhaka City and produces vulnerability maps, categorizing regions into various zones based on potential risk factors. Utilizing the latest SPT based co-relationship, coupled with code-based stress reduction factors, liquefaction susceptibility assessment was conducted. Additionally, classification-based supervised machine learning algorithms were utilized to evaluate the performance of the liquefaction susceptibility calculations, which were subsequently used as an input parameter for conducting geo-statistical interpolation, resulting in risk-based zonation maps in terms of liquefaction hazard for the city. The results show that the deposition type of soil plays a significant role in triggering liquefaction in different areas of Dhaka City and the majority portion of the recent artificial fill areas are subjected to high liquefaction potential for 7.0, 7.5 and 8.0 magnitude earthquake. This study also supplements the newly published mandates and provides guidelines according to the code to conduct engineering studies as per recommended seismic site class and liquefaction susceptibility for design applications. A significant increase in the coverage area of seismic site class with low shear wave velocities have been observed, necessitating special infrastructural considerations as per the new codal guidelines compared to past researches. Areas of improvement to evaluate liquefaction susceptibility in the newly published mandate also have been identified.

Furthermore, this study also outlines a generalized framework with supplementary policies integrating regional factors into consideration for development of liquefaction susceptibility-based risk maps for any location. The developed liquefaction susceptibility-based zonation map provides a clear visual representation of areas prone to liquefaction, enabling better-informed decision-making for disaster preparedness, risk reduction, and sustainable urban development.

TABLE OF CONTENTS

LIST OF FIGURES

LIST OF TABLES

NOTATIONS

τ_{av} Average earthquake induced cyclic shear stress

σ_v Total stress

σ'_v Effective vertical stress

Φ^{-1} Inverse of the standard normal cumulative distribution

a_{max} Maximum peak ground acceleration factor

AHP   Analytical Hierarchy Process

ANN   Artificial Neural Network

AUC   Area Under the Curve

CSR   Cyclic Stress Ratio

CRR   Cyclic Resistance Ratio

CPT   Cone Penetration Test

CV   Cross-Validation

DNN   Deep Neural Network

FS   Factor of Safety

GBM   Ganges Brahmaputra Meghna

I   Structural importance factor

Ic   Soil behaviour type index

IDW   Inverse Direct Weight

LPI   Liquefaction Potential Index

MSF   Magnitude Scaling Factor

M_W Moment magnitude of an earthquake

NCEER   National Center for Earthquake Engineering Research

NEHRP   National Earthquake Hazard Reduction Program

N_{60} SPT blow count normalized to hammer energy efficiency of 60%

$N_{1(60)}$ SPT blow count normalized to an overburden stress and energy efficiency of 60%

P_L Probability of Liquefaction

PGA   Peak Ground Acceleration

PSHA   Probabilistic Seismic Hazard Assessment

R   Response modification factor

R_f Friction Ration

ROC   Receiver Operation Characteristics

q_c Cone resistance of piezocone penetration test

r_d Stress reduction factor

r_u Pore pressure ratio

S   Soil factor depending on site class

SPT   Standard Penetration Test

SVM   Support Vector Machine

SCPT   Seismic Cone Penetration Test

USCS   Unified Soil Classification System

Vs   Shear wave velocity

Vs_{30} Average shear wave velocity of upper 30m soil layer

Z   Seismic zone co-efficient

CHAPTER 1: INTRODUCTION

1.1   General

Dhaka, the capital city of Bangladesh, is the world's most densely populated mega-city. Around 20 million people are living in this city with a growing rate of 4.2 percent per year (Islam, et al., 2019), and following similar growth trends the population may reach 22 million by the year 2025 (Rahman, et al., 2013). On the other hand, based on UN projections, the population of Dhaka metropolitan will be reach to 27 million in the year 2035 (Khaleda et al., 2019). Dhaka City is located at the centre of Bangladesh which is a part of Ganges-Meghna-Brahmaputra basin as its lowermost riparian. Being one of the fastest growing cities in the world the expansion of the city has taken place both horizontally and vertically to accommodate the continuous influx of people from all around the country.

The transformation of Dhaka into a megacity has engendered a multitude of pressing issues for both the city itself and its encompassing environs. Among the swiftest expanding urban areas on the global scale, Dhaka confronts an array of challenges, encompassing traffic congestion, effective waste management, inundation due to excessive rainfall, habitation deficiencies, as well as concerns relating to water, atmospheric, and auditory pollution. Furthermore, the city contends with the depletion of its groundwater resources, insufficiencies in basic services, and the depletion of wetland ecosystems. These complexities arise predominantly from an unprecedented surge in population.

In parallel, the unregulated and haphazard progression of urbanization has rendered Dhaka acutely susceptible to assorted natural disasters, such as earthquakes, floods, and fire incidents. These incidents are observing an escalating frequency due to this unchecked urban expansion.

To add to the problem state, in the recent past geologists anticipated severe seismic threats from yet undefined tectonic structures and seek to determine their consequential geo-structural responses and conformance to the national building codes.

Dhaka is largely an alluvial plain consisting of fine sand and silt deposits with shallow ground water table in most places which triggers factors of soil liquefaction due to earthquakes. The past

historical records, coupled with recent low to moderate-magnitude earthquakes near Dhaka, are indications of its earthquake source and vulnerability.

Seismic soil liquefaction is a phenomenon of special concern for cities going through a rapid urbanization process where low-lying lands are being filled up with sand as a part of the expansion process. Such phenomena have been recorded and developed in many parts of the world (Seed and Idriss 1971, 1982; Youd and Idriss, 2001).

Liquefaction in saturated deposits is one of the most significant causes of damage to structures during earthquakes. If the soil is wet and generally unable to drain during ground shaking, normal stress from the soil matrix can be transferred onto the pore water. The result is a reduction in the effective confining stress within the soil and an associated loss of strength and stiffness that contributes to deformations of the soil deposit.

According to Samui et al. (2011), the process by which a granular material undergoes a transition from a solid state to a liquefied state as a result of an increase in the pore water pressure is referred to as liquefaction. Ground deformation takes place as an aftermath of cyclic mobility due to static and dynamic pressure.

Damages that can be ascribed to the phenomena of earthquake-induced liquefaction have resulted in hundreds of millions of dollars' worth of costs for society (Seed and Idriss, 1982). Furthermore, most soil improvement techniques are not always feasible for large areas associated with the probability of liquefaction. Hence, accurate soil liquefaction prediction is necessary for safe foundation engineering practices and post-earthquake emergency evacuation design in liquefaction-prone areas. However, identifying and integrating regional factors according to latest building codes that have a greater influence on seismic liquefaction triggering is a demand of time and is expected to yield as sustainable outcome in the form of vulnerability maps which can be valuable information for policymakers, engineers and planners to implement and execute measures that promote safety restraints during substructure construction. The current study attempts to utilize provisions of BNBC (2020) coupled with latest SPT based deterministic liquefaction evaluation method to develop seismic site characteristic and liquefaction vulnerability map of Dhaka City using an up-to-date geotechnical database of the last decade. Furthermore, the study also aims to validate and evaluate the performance of the liquefaction assessment results using variety of machine learning algorithms.

Liquefaction has been investigated with different methods, including experimental and numerical methods. However, this research adopted the latest SPT (Cetin et al., 2004, 2018) based evaluation techniques to determine liquefaction susceptibility for different investigation points distributed in different locations of Dhaka City.

1.2   Objectives of the Study

The focal objectives of this study are:

i.   Evaluation of liquefaction susceptibility along different locations of Dhaka city using latest SPT based deterministic liquefaction evaluation method and identify vulnerable hotspots within the city boundary.

ii. Integration of BNBC 2020 provisions for regional stress reduction factor (r_d) as well as surface PGA value in liquefaction triggering relationships.

iii. Use BNBC 2020 provisions to characterize seismic site class based on shear wave velocity data.

iv. Produce vulnerability maps in terms of seismic site class and liquefaction susceptibility in the context of Dhaka city for different seismic scenarios.

v.   Evaluate the performance of liquefaction susceptibility assessment outcome using different machine learning algorithms (e.g Logistic Regression, Support Vector Machine etc.)

vi. Develop a generalized framework for liquefaction hazard mapping.

1.3   Scope of the Study

The scope of the study is to outline an appropriate hazard mapping scheme using up to date database and research integrating with regional factors based on local mandates and validation of the results with machine learning techniques as a guideline for usage by policy makers, engineers, researchers for liquefaction hazard assessment. Even though the current study focuses on a case study based on Dhaka City however, the results are expected to yield in a global benefit for all paving the way for future studies.

1.4 Outline of Thesis

There are total six chapters which are chronologically developed on the basis of the research work towards its main objective. Brief descriptions of the six chapters are given below:

Chapter One deals with the background, objectives and scope of the research. It also gives a brief overview of the other chapters.

Chapter Two is devoted to reviewing past research related to the theme of this research.

Chapter Three describes the geology and seismicity of the study area along with an overview of data collection for the research.

Chapter Four describes analytical approach and methodology of the overall research.

Chapter Five illustrates results and discussions with specific findings.

Chapter Six describes key findings, conclusions and recommendations for future studies.

CHAPTER 2: LITERATURE REVIEW

2.1   General

Seismic site classification (SSC) and liquefaction susceptibility are critical components in the field of geotechnical and earthquake engineering. The chapter is organized into several sections, starting with an overview of seismic site classification, followed by insights into past studies related to liquefaction susceptibility maps, liquefaction potential assessment, and the history of application of machine learning. It concludes with a discussion on the research gaps and a proposed framework of the studies carried out in the past.

2.2   Overview of Seismic Site Classification

Seismic site classification (SSC), which defines engineering properties of the soils by means of V_S or SPT-N values, is the simplest method to consider the site effects for numerous purposes including engineering projects and micro-zonation studies (Pitilakis, 2004). Many classification systems utilize the SPT-N and V_S values measured in upper 30m to provide an SSC assessment (NEHRP 2000, IBC 2009, Eurocode 8).

Amongst the different available methods National Earthquake Hazard Reduction Program (NEHRP) is one of the widely used systems for the SSC applications and has been used to classify soils by using their V_S values in designing building codes and characterizing site response. Countries like the USA (Chung et al., 2012), Turkey (Naji et al., 2021) and India (Sreejaya et al., 2022; Maheswari et al., 2010) have already compiled seismic site classification-based maps for delineating zones of respective seismic site class according to regional code provisions.

In absence of local mandates in the past, similar seismic site classification map has been produced for Dhaka City using Eurocode 8 and NEHRP guidelines (Rahman et al., 2018). The map produced under the aforementioned research (Rahman et al.,2018) is shown in Figure 2.1.
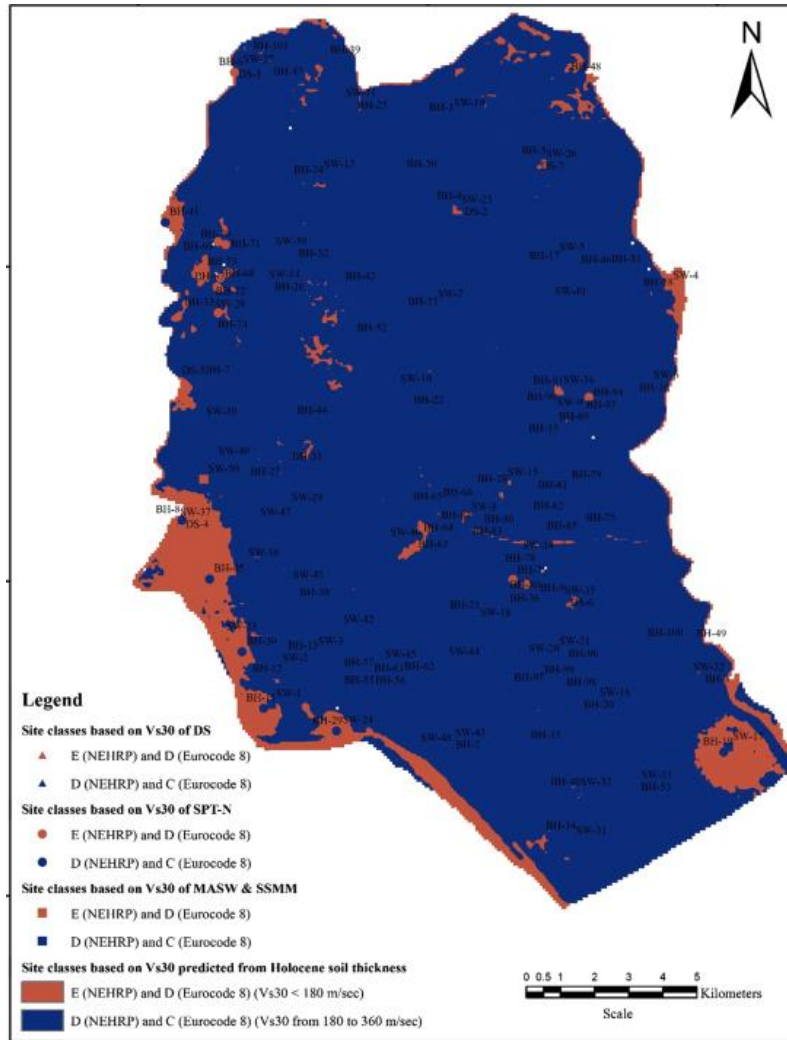
Fig. 2.1 Seismic site class map of Dhaka city (Rahman et al. 2018)

It is to be mentioned here that, even though the older version of the Bangladesh National Building Code (2006) did not include provision of seismic site characterization, the newly published mandate BNBC (2020) outlines soil type classification system based on shear wave velocity of top 30m soil layer and according to each classified category, guidelines for design considerations have been recommended.

Our current study focuses on integration of the provisions of BNBC (2020) and classify sites-based shear wave velocity information at different data point locations and produce a continuous map delineating respective zones according to the code.

2.2 Liquefaction Susceptibility Maps

Liquefaction hazard maps increasingly are being incorporated into earthquake risk mitigation practice. These maps initially resulted from research efforts by engineering geologists and geotechnical engineers and their application by communities was voluntary (Toprak and Holzer, 1996). However, the mapping methods have matured from time to time, maps have been incorporated into community earthquake safety plans and, also have been used for regulatory purposes in the field of disaster management (e.g CDMP 2009). Since the maps cover large areas of hazard it is deemed to be a strong tool for policy level decision making.

Mapping liquefaction hazard at a regional scale is important for both planning for earthquake events as well as guiding relief efforts by positioning resources once the events have taken place. Initial attempts to mapping vulnerability of soil liquefaction was developed by Youd and Perkins (1978). Starting with that subsequent mapping approaches (Youd and Hoose, 1978; Brankman and Baise, 2008) all used geologic characteristics such as age of deposition, geological units into quantitative susceptible classes, such as high, moderate or low. Additionally, site specific data in the form of geotechnical as well as geophysical field and laboratory testing are also taken into account for site specific evaluation of the vulnerability which is the basis of the simplified procedure developed by Seed and Idriss (1971). Even though the simplified procedure was based on SPT data, however, it has been adapted for Cone Penetration Test (CPT) data (Juang and Jiang, 2000; Boulanger and Idriss, 2016), shear wave velocity (Vs) data (Vs) (Andrus and Stroke II, 2000).

2.2.1 Global Perspective

Liquefaction susceptibility maps delineate zones estimated to be liquefiable under given earthquake parameters and have been compiled for several regions and countries including USA, Greece, Japan, Iran, Turkey etc. as well as southeast asian countries like India, Nepal and Myanmar.

In particular, maps were developed in USA for the San Francisco Bay region (Youd and Perkins, 1987; Knudsen et al., 2000; Holzer et al., 2002), for Los Angeles urban area (Tinsley et al., 1985),in Australia at national scale (Jena et al., 2023), in Greece for the region of Thrace, Greece

(Papathanassiou et al., 2008), in Japan for Saitama City (Pokhrel et al., 2010), in Turkey for Balikesir (Ceryan et al., 2021), Canakkale (Tunusluoglu and Karaca, 2018) cities etc. On the other hand, for southeast asia such maps have been produced in India for Mumbai (Mhaske and Choudhuey, 2010), Kolkata (Nath et al., 2014; Gurung and Chatterjee, 2023), Chennai (Anbazhagan et al., 2011), Guwahati (Sharma and Chetia, 2016), Jammu and Kashmir (Ansari et al. 2023) etc. Apart from that, in Nepal as an after math of Gorkha (2015) earthquake, maps showing vulnerable areas of Kathmandu Valley (Pokhrel et al., 2022) was generated**.**
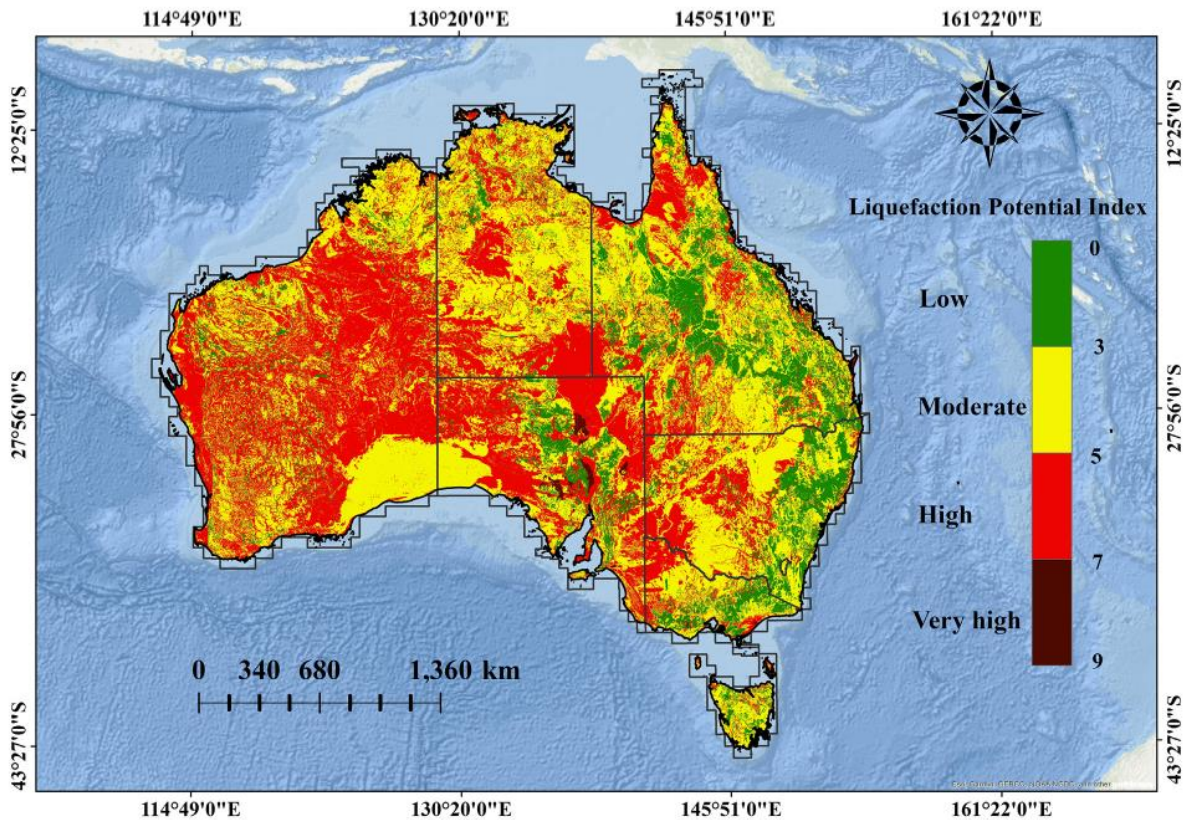
Fig. 2.2 Liquefaction susceptibility map of Australia (Jena et al., 2023)
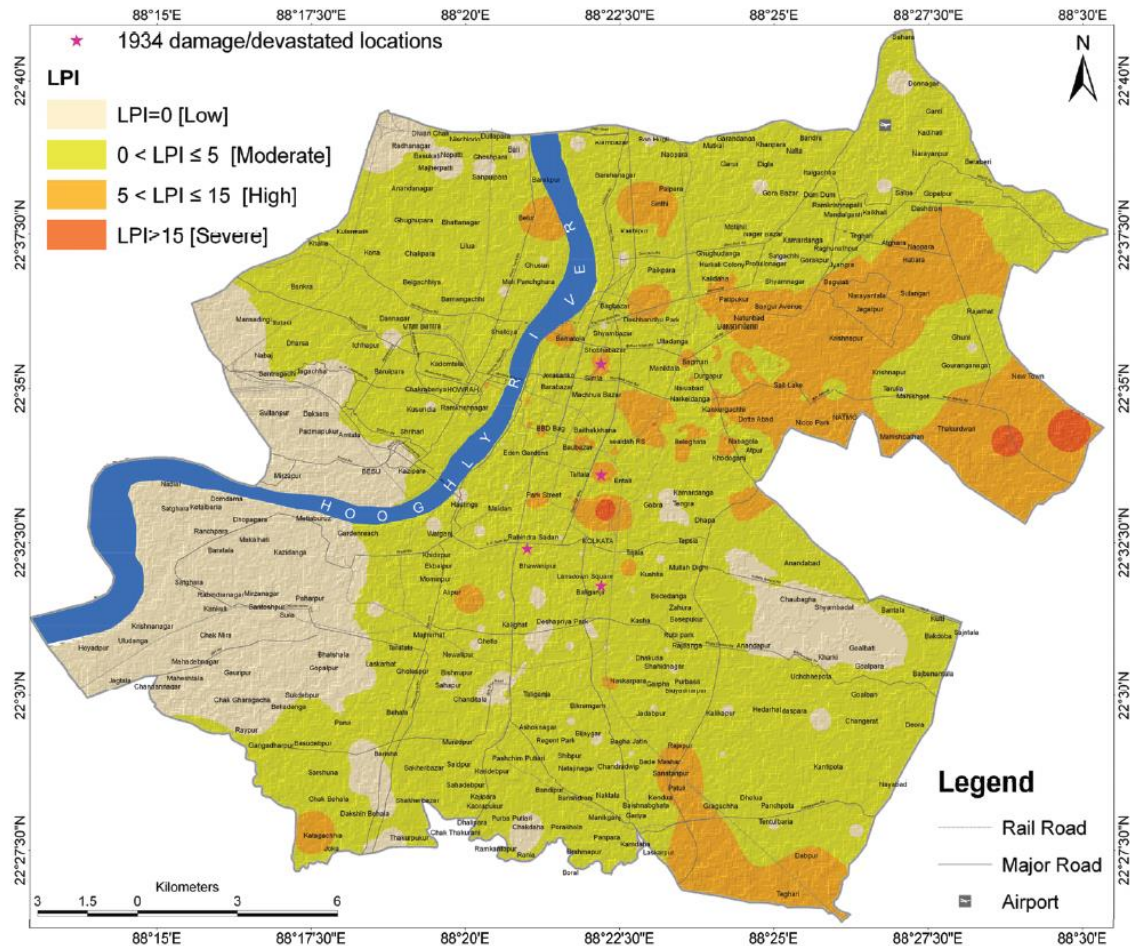
Fig. 2.3 Liquefaction susceptibility map of Kolkata (Nath et al., 2014)

Even though these maps do not predict liquefaction-related ground failures, however ground failures may accompany liquefaction and are more likely to occur in areas with higher liquefaction susceptibility (Tinsley et al., 1985). Moreover, large scale maps, regarding the liquefaction-induced ground disruption, were published for urban areas using data provided by in situ tests (mainly SPT and CPT). These "micro-zonation" maps were compiled based on the LPI methodology, suggested by Iwasaki et al. (1978).

2.2.2 Bangladesh Perspective

The concept of hazard mapping is also not new to the researchers of Bangladesh. Studies conducted in the past used SPT data for generating Liquefaction Potential Index (LPI) based maps for Dhaka (Ansary and Rashid, 2000; Rahman et. al, 2015; Rahman and Siddiqua, 2017), Chattagram

(Rahman and Siddiqua, 2017), Sylhet (Rahman and Siddiqua, 2017), Dinajpur (Hossain et al., 2022) and Rajshahi (Ashikuzzaman et al., 2023) cities.

In 2000, M. A. Ansary and M. A. Rashid studied liquefaction potential in Dhaka by Standard Penetration Test (SPT) and provided the first liquefaction potential map for Dhaka. A total of 190 boreholes of SPT data were collected for liquefaction study of Dhaka city under that research. Among these data, 16 bore holes with SPT-N data up to a depth of 100 ft were directly collected for this study. The rest of the data were collected from different private and government soil testing agencies. The typical soil data were up to a depth of 50 ft. but some of the data collected are up to a depth of 150 ft. Figure 2.4 shows the 1st map developed by Ansary (Ansary and Rashid, 2000).
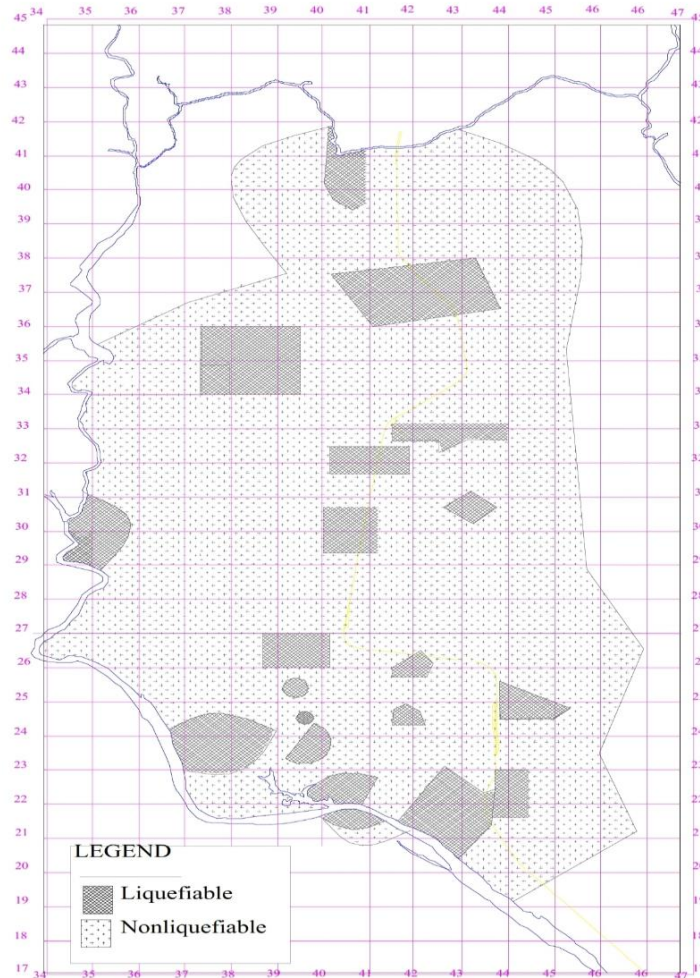
Fig. 2.4 First liquefaction susceptibility map of Dhaka city (Ansary and Rashid, 2000)

After a long gap in 2015, another study for predicting (Rahman et al., 2015) liquefaction potential of Dhaka city was conducted by establishing a database containing 53 borehole data based on the investigation carried out under Comprehensive Disaster Management Program (CDMP 2009). Boreholes data had sufficient information, such as SPT N-values, geotechnical properties, and geological information for determination of liquefaction potential index (LPI) were utilized for that study. The borehole locations were classified based on the surface geological units of the city. The contour showing LPI values along different locations of Dhaka City according to the study (Rahman et al., 2015) is shown in the following Figure 2.5.
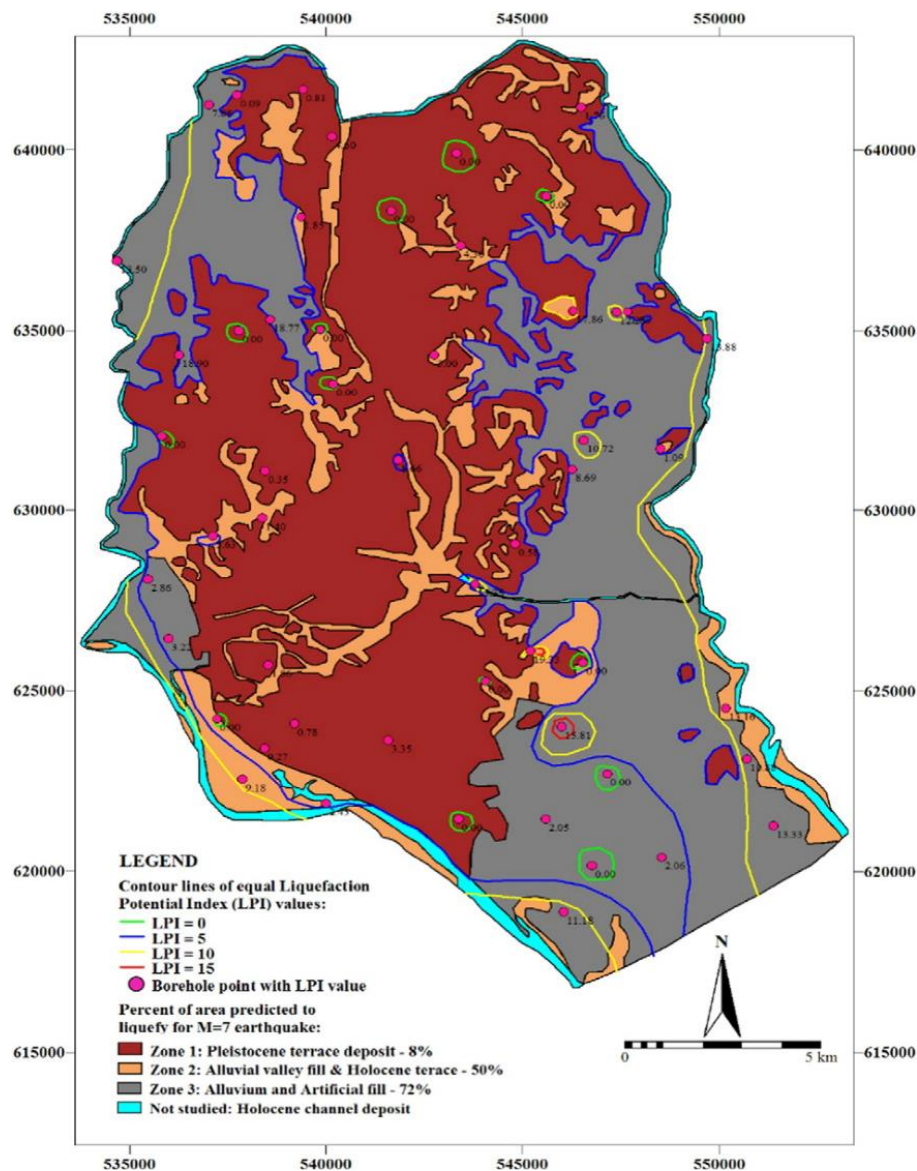
Fig. 2.5 Liquefaction susceptibility map of Dhaka city (Rahman et al., 2015)

Even though majority of such studies have been conducted for Dhaka, however, in the recent past in 2022, Hossain (Hossain et al., 2022) utilized 160 data points for furnishing LPI based maps for Dinajpur City considering an earthquake magnitude of 6.5.

On the other hand, under a separate study Rahman and Siddiqua (Rahman and Siddiqua, 2017) used only 6 nos. of SPT data for Dhaka City and 7 nos. of SPT data for Sylhet and Chattagram respectively to generate liquefaction potential based hazard maps.

2.3   Liquefaction Potential Assessment

Evaluation of soil liquefaction resistance is an important aspect of geotechnical engineering practice. The assessment of potential liquefaction hazards involves two questions: (1) will liquefaction be triggered by the earthquake ground motions under consideration and (2) what is the liquefaction potential due to the triggering of liquefaction. This section covers and extensive literature review of the procedures used to evaluate liquefaction triggering, including a discussion of compilation of historical data, geologic considerations, the analysis framework, in-situ testing, liquefaction triggering correlations, etc.

2.3.1   Liquefaction Triggering Procedures

Over the past 25 years a methodology termed the ''simplified procedure' has evolved as a standard of practice for evaluating the liquefaction resistance of soils. Following disastrous earthquakes in Alaska and in Niigata, Japan in 1964, Seed and Idriss (1971) developed and published the basic ''simplified procedure.'' That procedure has been modified and improved periodically since that time, primarily through landmark papers by Seed (1979), Seed and Idriss (1982) and Seed et al. (1985). In 1985, Professor Robert V. Whitman convened a workshop on behalf of the National Research Council (NRC) in which 36 experts and observers thoroughly reviewed the state of knowledge and state of art for assessing liquefaction hazard. The workshop produced a report that has become a widely used standard and reference for liquefaction hazard assessment (Youd and Idriss, 2001).

In January 1996, T. L. Youd and I. M. Idriss convened a workshop of 20 experts to update the simplified procedure and incorporate research findings from the previous decade that is known NCEER 1996 and two years later the workshop was rearranged by T. L. Youd and I. M. Idriss in 1998 that is known as NCEER 1998 (Youd and Idriss, 2001). However, further updates have been

made by different researchers within the last decade (Idriss and Boulanger, 2012; Cetin et al., 2004, 2018).

The references cited are among the most reputable and authoritative sources for assessing the potential for soil liquefaction. In this study, "Liquefaction Potential Assessment," methodologies were employed based on these aforementioned references. The simplified approach that was formulated is based on empirical analyses of both field observations and data from field and laboratory tests. Manifestations of liquefaction in the field typically include surface-level indicators such as sand boils, ground fissures, or lateral spreads. The data predominantly originated from sites characterized by level to gently sloping terrain, underlain by Holocene alluvial or fluvial sediments at shallow depths (less than 15 meters).

The investigation of soil liquefaction potential is a part of modern seismic engineering design. An abundance of approaches for assessing soil liquefaction potential have been developed as an aftermath of the devastating liquefaction damaged induced by the aforesaid earthquake events in Japan.

The robustness and applicability of these methods have been comprehensively compared and discussed from time to time. However, those methods that exploit in situ tests such as the blows of standard penetration tests (SPT – N), the cone resistance of piezocone penetration test (qc) and the shear wave velocity (Vs) for liquefaction potential evaluations are prevalent in engineering practice.

Even though CPT – qc-based methods (e.g., Chen and Mayne, 1996; Robertson 2009, 2016) have attracted considerable attention in geotechnical engineering, however SPT based approaches have been widely accepted in various seismic design codes for civil structures (e.g., AASHTO 2017; JRA 2017) including the newly published Bangladesh National Building Code 2020 (BNBC 2020).

SPT-N methods have been diversely developed over the past few decades (e.g., Seed et al., 1985; Youd and Idriss 1997; Juang et al., 2000; Youd et al., 2001; Cetin et al., 2004; Idriss and Boulanger 2010; Boulanger and Idriss 2014; Cetin et al., 2018) compiling field case history datasets from time to time starting from its inception with the simplified procedure attributed to Seed and Idriss (1971). Among these methods, the one featured in the 1998 NCEER/NSF workshop (Youd et al., 2001) is the earliest procedure on which geotechnical experts and scholars have reached a

consensus and also usually appears in relevant comparative research work (e.g., Hwang et al., 2005; Boulanger and Idriss 2014; Cetin et al., 2018).

2.3.2 Development of Liquefaction Triggering Co-relationship

Published collections of triggering case histories date back to at least 1971. Whitman (1971) assembled 13 different cases from 8 earthquakes in Chile, Japan, Mexico, the Philippines, and the United States. Entries for each case included the depositional environment of the soil inferred to have liquefied; the estimated peak ground acceleration (PGA) at the ground surface; the depth of the groundwater table; the depth of the soil inferred to have liquefied (i.e., the "critical layer"); a representative SPT blow count (or N-value) for the critical layer; and the estimated duration of strong earthquake shaking. Seed and Idriss (1971) compiled 35 cases from 12 earthquakes in Chile, Japan, and the United States. Entries in that database included earthquake magnitude, distance from the earthquake source, and soil type in addition to water-table depth, critical-layer depth, representative SPT N-value for the critical layer, and estimated values of PGA and strong shaking duration. The Seed and Idriss (1971) database included 23 cases where liquefaction is known to have occurred and 12 cases in which no liquefaction is inferred. Seed et al. (1985) compiled 125 case histories which was the best that had been assembled at that time. Later on, Cetin et al. (2004) employed a well-defined screening system with regards to data completeness, documentation and reliability. Idriss and Boulanger (2004) had accepted the screening process employed by Cetin et al. (2004) and had adopted it in their database. The Idriss and Boulanger (2010) field performance case history database has 230 case histories. Most of these are from the database screened and compiled by Cetin et al. (2004), but there are also 33 new cases added by Idriss and Boulanger (2010). Twenty-seven of these are cases from Iai et al. (1989), compiled after the 1983 Nihonkai-Chubu M=7.7 earthquake. There are also three case histories from the 1989 Loma Prieta earthquake, one from the 1964 Niigata earthquake, one from the 1968 Hyūga-nada earthquake, and one from the 1982 Urakawa-Oki earthquake. Later, Boulanger and Idriss (2014) compiled additional 24 cases from the Kocaeli (1999) and Chi-Chi (1999) earthquakes.

Cetin et al. (2016) re-evaluated these 57 (=33+24) new cases and accepted 13 of them. The same screening criteria for admission of these 57 new case histories to the Cetin et al. (2004) database was again employed here. Thirteen of these new cases (10 of the Nihonkai-Chubu case histories, and 3 of the Loma Prieta earthquake case histories) satisfied the screening criteria and were added to the updated Cetin et al. (2016) database. This is till to date the latest database compiled by

researchers and has been used to develop the latest SPT based triggering co-relationship referred as Cetin et al. (2018).

Apart from that, many other liquefaction triggering databases have been assembled since 1971, chiefly to support the development and updating of CRR curves. The databases vary in their levels of documentation. Significant contributions include the work of Yegian and Vitelli (Yegian and Vitelli, 1981), followed by the research conducted by Tokimatsu and Yoshimi in 1983 (Tokimatsu and Yoshimi, 1983). In 1984, Seed et al. made notable advancements in this field (Seed et al., 1984), and more recently, Boulanger and Idriss in 2014 furthered the understanding of SPT (Boulanger and Idriss, 2014). Moss's work in 2003 has been a significant reference point in the context of CPT based assessment (Moss, 2003), and Boulanger and Idriss continued to contribute to this method in 2014 (Boulanger and Idriss, 2014). For the assessment using Shear Wave Velocity (Vs), key research efforts have been led by Andrus (Andrus and Stokoe, 1999; Andrus et al., 2003), with subsequent work by Kayen in 2013 (Kayen et al., 2013). Other liquefaction triggering databases have been compiled in support of the development of CRR curves for other types of in situ tests, including the flat plate dilatometer test (Monaco et al., 2005) and the Chinese dynamic penetration test (Cao et al., 2013).

The current study focuses on utilizing the latest SPT based database used to develop the triggering co-relationship of Cetin et al. (2018) and evaluation of the analytical outcome based on machine learning approaches after integrating provisions of BNBC 2020 to the empirical equations.

2.4 Application of Machine Learning in the Field of Liquefaction Studies

Machine Learning (ML) is a field of artificial intelligence that uses statistical techniques to give computer systems the ability to learn from data. In general, machine learning algorithms are classified in two groups: supervised and unsupervised learning. The supervised algorithms that apply what has been learned with historical data to draw conclusions on new data and on the other hand are the unsupervised algorithms can extract inferences from data sets. Most of the civil engineering problems relate to supervised learning category.

ML - based applications have made great progress in geotechnical engineering. Different kinds of ML tools, including artificial neural network (ANN), random forest (RF), support vector machine (SVM), eXtreme gradient boosting (XGBoost), canonical correlation forest (CCF), k-nearest neighbors (kNN), deep neural network (DNN), etc. have been successfully employed in several

geotechnical applications (Demir and Sahin, 2022; Wang et al., 2020; Amiri et al., 2019; Zhang et al., 2022). The use of such algorithms are also not new in the field of liquefaction susceptibility evaluation for classification based problems and as well as in predicting liquefaction induced ground settlement (Chen et al., 2016) alongwith lateral spreading (Xie et al., 2020).

Some of the recent studies for liquefaction prediction are briefly mentioned here. For example, Zhang et al. (2021) employed the DNN strategy to predict soil liquefaction based on the Vs and SPT dataset. Zhou et al. (2021) proposed two support vector machine (SVM) models for predicting liquefaction potential using genetic algorithm (GA) and grey wolf optimizer (GWO) techniques in order to enhance the efficiency of the models. Zhao et al. (2021) developed the kernel extreme learning machine (KELM) with particle swarm optimization based on soil liquefaction potential evaluation system using CPT and Vs measurements. Hu et al. (2021) used Bayesian network (BN) model for soil liquefaction prediction under the conditions of nine different training sample size ratios. Demir and Sahin (2022) investigated the performance of three forest algorithms to predict the liquefaction potential of soils from two different CPT datasets using CCF, RF, and rotation forest (RotFor). These studies revealed that ML algorithms provide feasible solutions to tackle soil liquefaction prediction problems. Nevertheless, these studies have tended to focus on some factors, such as the applicability of ML algorithms, the effects of optimization approaches on ML algorithms, and ratios of training sample size.

Out of the different machine learning models used for classification related problems logistic regression is the most common type of supervised machine learning algorithm for classification related problems which has been used for liquefaction prediction by different researchers (Zhang and Goh, 2016; Jairi et al., 2021). On the other hand, another popular machine learning algorithm which has been widely adopted is Support Vector Machine which was used to predict soil liquefaction potential based on SPT (Samui et al., 2011) and CPT (Samui et al., 2013) data as well. Apart from that in the recent past, ensemble-based ML algorithms have gained popularity amongst the mass and produced fruitful outcome in the field of soil liquefaction prediction (Demir and Sahin, 2022).

This research uses an updated, robust and promising approach to measure soil liquefaction resistance for Dhaka City using Logistic Regression, Support Vector Machine and Ada-boost ML algorithms for validating the performance of liquefaction prediction using field case history data.

2.5 Liquefaction Susceptibility Assessment Frameworks

Computational susceptibility assessment frameworks in the field of liquefaction studies are not new considering global perspectives. Nath et al. (2017) proposed an SPT based framework integrating Probabilistic Seismic Hazard Assessment (PSHA), site response analysis and SPT based computations for liquefaction evaluation based on a case study of Kolkata City. In Europe, Analytical hierarchy processes (AHP) have been incorporated in development of liquefaction susceptibility-based risk maps. Australia (Jena et al., 2023) have recently integrated Deep Learning Techniques for developing liquefaction potential index (LPI) based maps coupled with paleo seismic studies at a national scale. The examples from Australia and Europe are shown in Figure 2.6 and Figure 2.7 respectively.
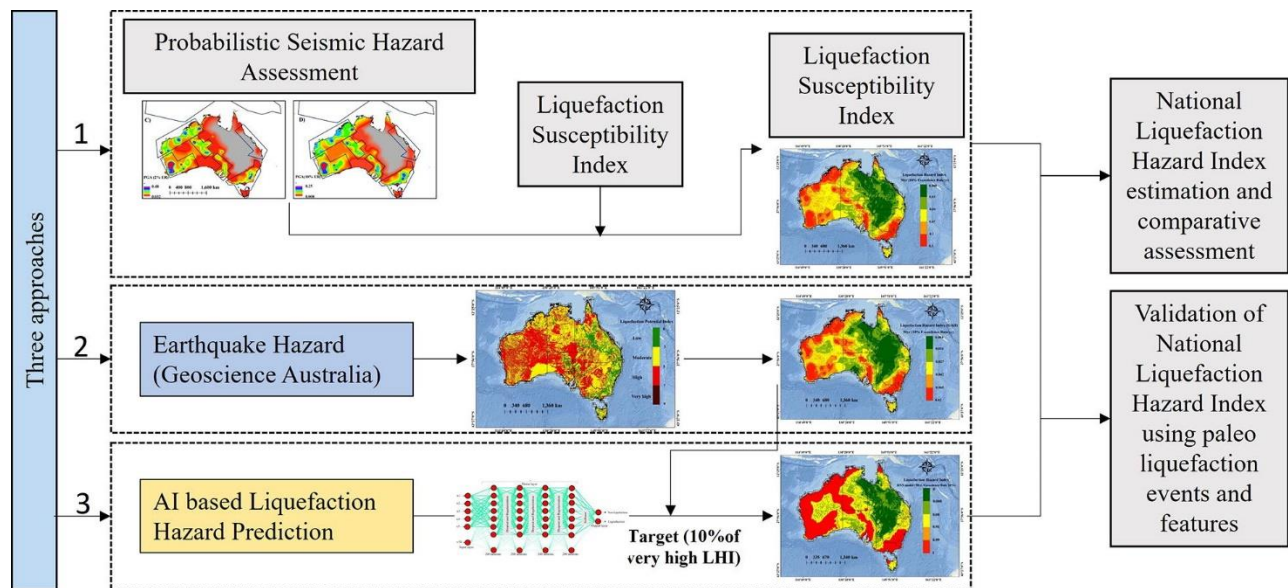
Fig. 2.6 Liquefaction susceptibility mapping framework of Australia (Jena et al., 2023)
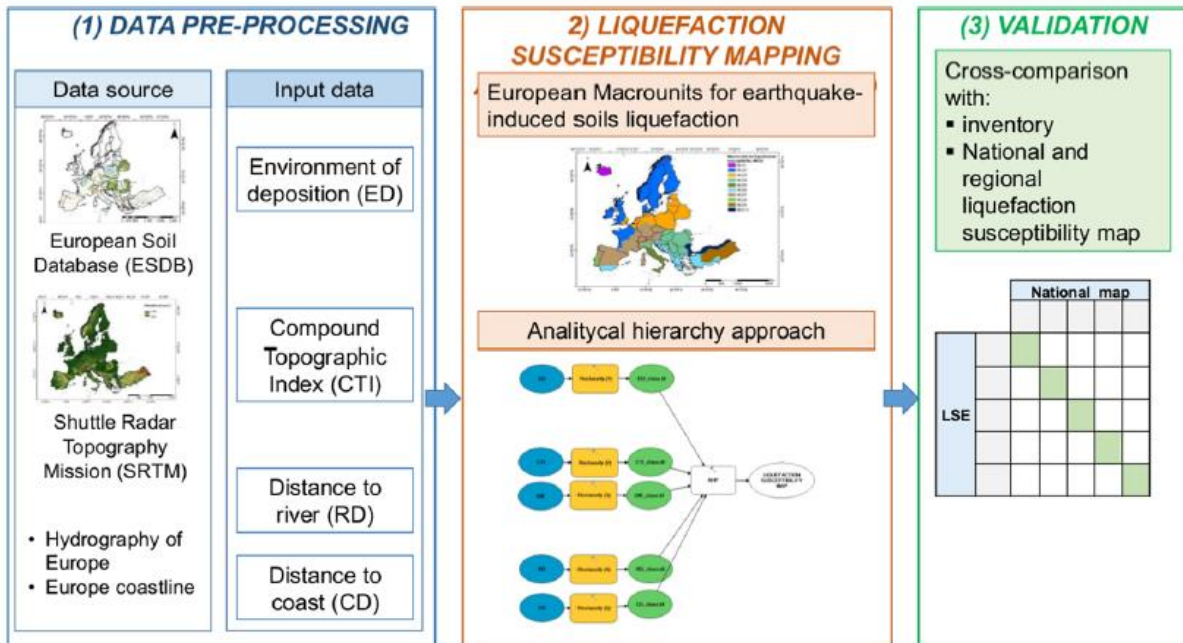
Fig. 2.7 Liquefaction susceptibility mapping framework of Europe (Meisina et al., 2022)

The point to be mentioned here is that in case of the frameworks adopted for Australia and Europe case history data related to soil liquefaction was utilized for predication and validation of results using machine learning approaches as well as geo-statistical analysis. However, in case of Bangladesh such physical evidence related to soil liquefaction related phenomenon does not exist. Hence, this research aims to produce a generalized framework using regional factors and national policies as an upgradation scheme which may be adopted not only for Dhaka City but, for a specific study area anywhere around the globe.

2.6   Research Gap

The point to be mentioned here is that past studies carried out by Ansary and Rashid (2000), Rahman et al. (2015), Rahman and Siddiqua (2017) had access to very limited high-quality datasets whereas under the current research utilizes only recently investigated boreholes where in most cases hydraulic rotary has been used was considered for the evaluation.

The study carried out by Ansary and Rahman (2000) considered the maximum ground surface acceleration estimated from the seismic map based on 200-year return period ground motion contour and earthquake data from 1900 to 1977 (Hattori, 1979). According to that study, for Dhaka

the peak ground surface acceleration is around 0.15g. and the moment magnitude considered for liquefaction susceptibility evaluation was 7.5 based on studies carried out by Ali (1997). On the other hand, Rahman et al. (2015) also used a PGA value of 0.15 and seismic moment magnitude of 7 for preparing contour maps in the context of intensity of liquefaction susceptibility along Dhaka City. In contrast to the previous researches, this study uses a variety of PGA values according to the guidelines of BNBC (2020) code and 3 different seismic moment magnitude for preparing continuous liquefaction potential index based zonation maps for Dhaka City.

Also, due to recent advancements in GIS based geostatistical interpolation techniques now it is possible to develop seismic hazard maps based on the advanced tools available which was not done by the past researchers.

In addition, considering continuous development of liquefaction triggering databases and modifications made to the empirical equations the past studies are considered to be somewhat obsolete in the current context as it used the old NCEER workshop-based methodologies for deterministic liquefaction evaluation.

The past studies also did not provide any guideline for continuous upgradation of the dataset for periodic updating of the hazard maps. On the other hand, this study provides a framework for mandatory regulations as well as future research related to similar studies.

Subsequently, machine learning approaches for the prediction of liquefaction are not available in the context of Bangladesh which has been performed under the current research.

Also, this study includes BNBC (2020) specified regulatory after it's publication in 2021.

CHAPTER 3: STUDY AREA AND DATABASE DEVELOPMENT

3.1   General

The geological and seismic characteristics of Dhaka, Bangladesh, are deeply interconnected with the city's development and its vulnerability to natural disasters. Located within the expansive Bengal Basin and encircled by the Ganges-Brahmaputra-Meghna (GBM) Delta Complex, Dhaka is shaped by the sedimentary processes of major river systems, which is a part of formation of the world's largest deltaic landmass. Apart from that, Dhaka lies within a notably seismic active zone, the Indian and Myanmar Plate Stress (IMPS) zone, which exposes it to substantial earthquake risks. This chapter provides insights into the intricate geological settings, detailed geological analyses, seismicity, and database development of the study area, providing a comprehensive overview of the geological and seismic framework that underpins the city's landscape and its associated hazard vulnerabilities.

3.2   Geological Setting

Geologically speaking, Bangladesh is positioned within the Bengal Basin, whose development is closely linked to the Himalayan mountain-building process and the resultant upward movements. The Himalayan mountain range and the Tibetan Plateau were formed due to the collision of the Indian and Eurasian tectonic plates. This collision led to the rise of the Himalayas and the creation of an extensive river system that drained the elevated terrain, carrying substantial sediment loads. This process resulted in the formation of the world's largest deltaic landmass.

As the expansive delta migrated southward and concurrently experienced rapid sinking of the basin, a substantial layer of deltaic and river-derived sediments accumulated along the broad alluvial front of the Ganges-Brahmaputra River system. The entirety of Bangladesh's surface is essentially covered by this delta system, known as the Ganges-Brahmaputra-Meghna (GBM) Delta Complex. These rivers annually transport billions of tons of sediments, ultimately discharging them into the Bay of Bengal to the south.

The GBM Delta Complex is accountable for supplying all the sediments found in Dhaka City. To summarize the local geological context of the Dhaka area, there are two primary sediment groups dating back to the Quaternary period: the first group ranges from the Pliocene to the Pleistocene, while the second group pertains to the Holocene. Dhaka City is located in the southern segment of the elevated geological formation known as the Madhupur Tract or Madhupur Terrace, a fault block tilted eastward and delineated by faults (as described in the Atlas of Urban Geology, 1999). This elongated north-south terrace possesses a gently undulating surface, slightly elevated compared to the recent floodplains. Other Pleistocene Terraces can be found to the west of the Madhupur Terrace.

This gently elevated terrace is encircled by the extensive alluvial deposits of the GBM system, bordered by the Old Brahmaputra Flood Plain to the east, the Brahmaputra-Jamuna Flood Plain to the west and southwest, and the Meghna Flood Plain to the southeast. Numerous smaller tributary rivers also contribute to this geographic arrangement.

3.3   Geological Analysis

Dhaka City is built partly on the elevated Pleistocene Terrace (Madhupur Terrace) having a maximum elevation of 14 m and partly on the Holocene floodplains having a minimum elevation of 2 m. Broadly the area is classified into two geologic formations: Holocene Deposits and Pleistocene Deposits. Each of this broad geologic formation is again divided into number of geologic units on the basis of geomorphological appearance, sediment characteristics and engineering properties gathered through auger hole and SPT bore logs distributed over different geologic and geomorphological units. (Shahtaj et al., 2019). The Pleistocene deposit is the oldest deposit within the city boundary, and it mainly covers the central part of the region. It is mainly composed of yellowish brown to reddish brown, stiff to very stiff clayey silt, silty clay and medium dense to dense silty sand. The Holocene deposit consists of dark grey to grey, very soft to soft silty clay, clayey silt, and grey to yellowish brown, very loose to medium dense silty sand. On the other hand, some low-lying marshy areas near the eastern fringes and outskirts of the city area has been filled with dredged river sand from nearby river using hydraulic deposition system. The artificial fill is composed of grey, very soft to soft clayey silt, very loose to loose silty sand and sand. Considering potential risks due to earthquakes, the artificially filled areas are lying in a danger zone in terms of liquefaction vulnerability.

The surface geology of the city has been divided into six units: 1) Pleistocene terrace deposit (Q_{pty}), 2) Holocene alluvial valley fill deposit (Q_{hav}), 3) Holocene terrace deposits (Q_{hty}), 4) Holocene alluvium (Q_{ha}), 5) Holocene channel deposit (Q_{hc}), and 6) artificial fill (Q_{af}) (Figure – 3.1).
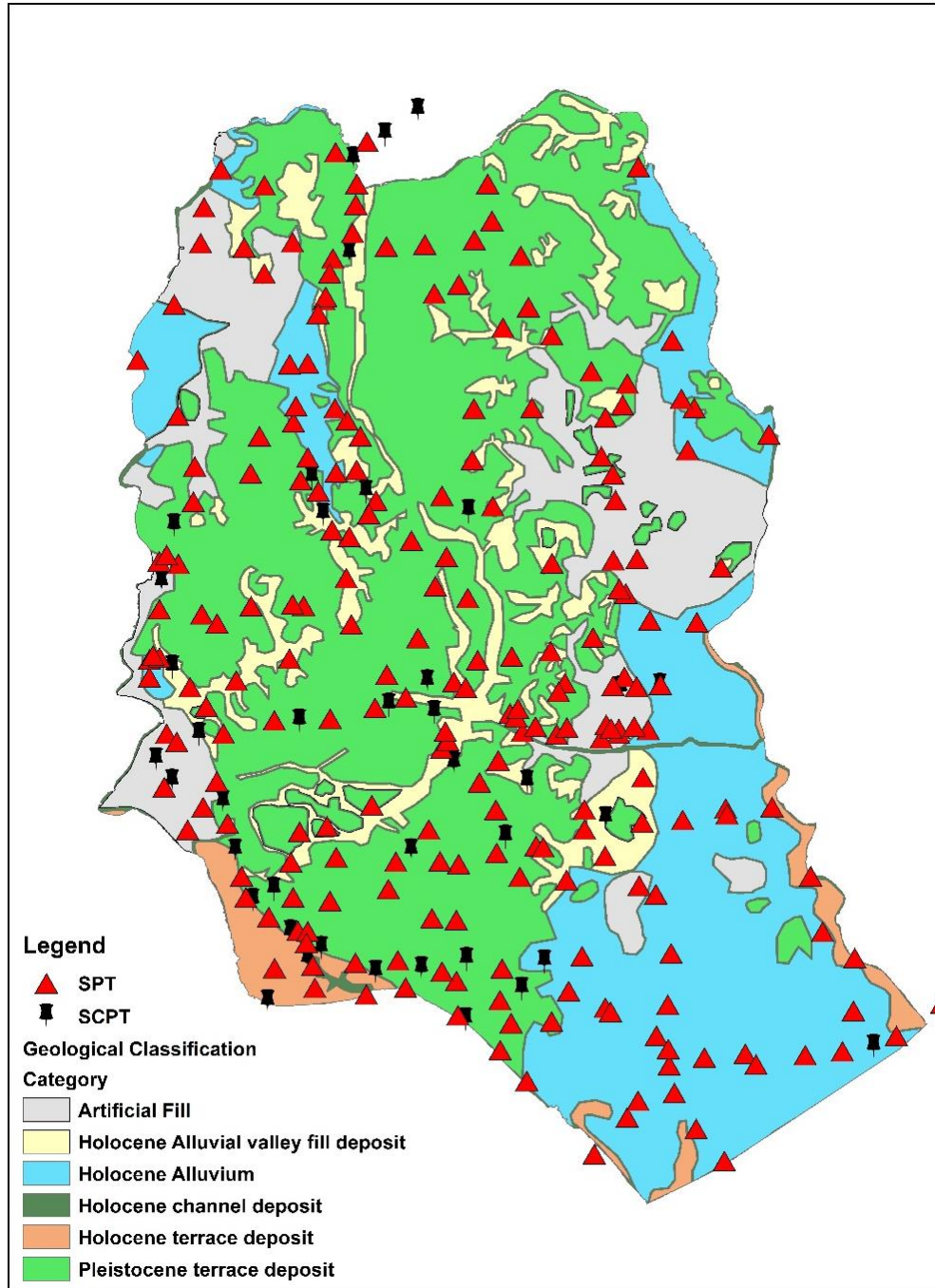
Fig. 3.1 Surface geology of Dhaka city along with distribution of geotechnical investigation points (modified after Rahman et al., 2015)

3.3   Seismicity of the Study Area

The seismic hazard present in densely populated regions constitutes a significant socio-economic concern that demands serious attention. Situated within the Bengal Basin, Bangladesh is positioned within the largest and most youthful delta globally, which is nearly twice the size of the Mississippi delta.

Bangladesh occupies a particularly active tectonic boundary area known as the Indian and Myanmar Plate Stress (IMPS) zone, extending from Sumatra through the Andaman-Nicobar region, characterized by intense seismic activity. The predominant tectonic regime in this region is compression with the northward motion of the Indian Plate relative to the Eurasian Plate. Thrusts and strike-slip faults are the consequences of this regime.

Dhaka City is situated in proximity to the actively seismic convergent plate boundary between the Indian and Eurasian plates, hosting numerous fault lines that experience seismic activity. The Himalayan System (resulting from the Eurasian plate) and the Arakan-Indo subduction collision system (resulting from the Indo-Burma plate) are the two primary tectonic systems capable of generating substantial earthquakes within the Bengal Basin, with the potential to inflict damage on Dhaka city as well. According to recent studies the Burmese plate is overriding the Indian plate and the locked faults exist near the eastern parts of Dhaka City.

3-D blockmodels of the India-Burma-Sunda system show that a significant convergence rate across the Rakhine-Bangladesh megathrust is necessary to explain the India-Burma-Sunda plate motion vectors. The dip-slip component of the convergence across the Bangladesh megathrust decreases northward from 24 to 12 mm/year from 22°N to 25°N (Figure 3.2 and Figure 3.3) due to rotation of the Indo-Burman wedge relative to India.
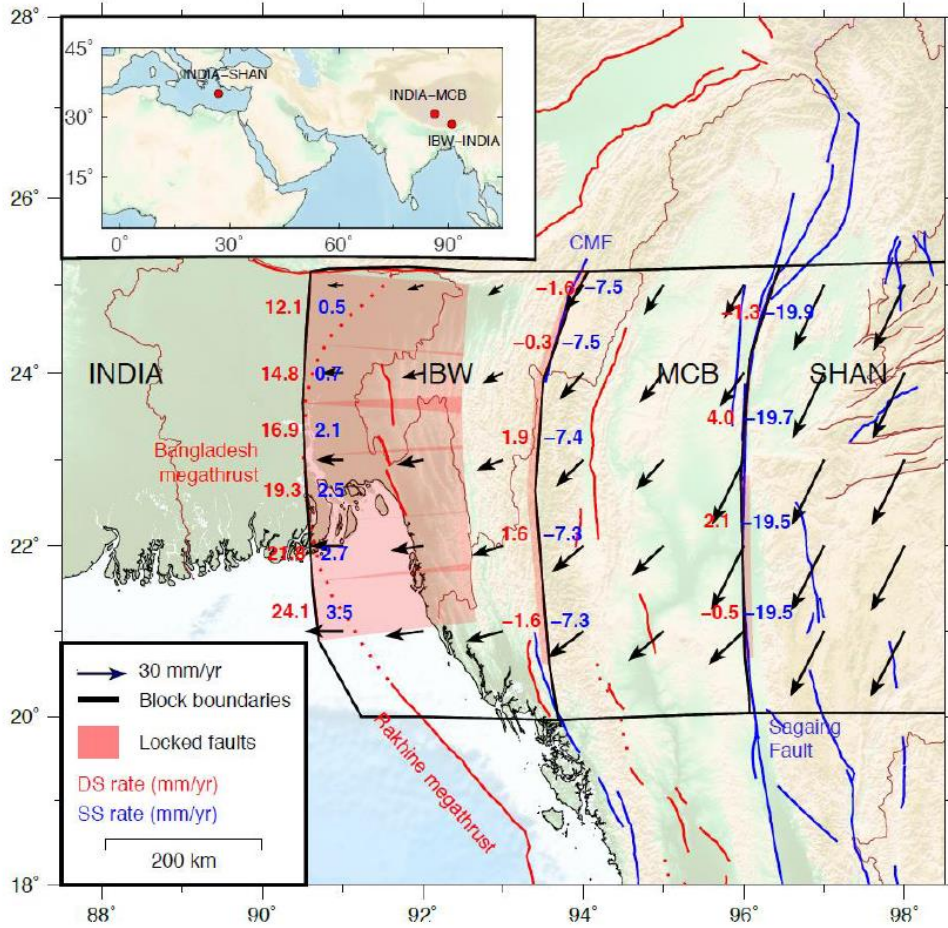
Fig. 3.2 Locked faults at convergence point of Burmese plate and Indian plate with slip rates (Mallick et al., 2019)
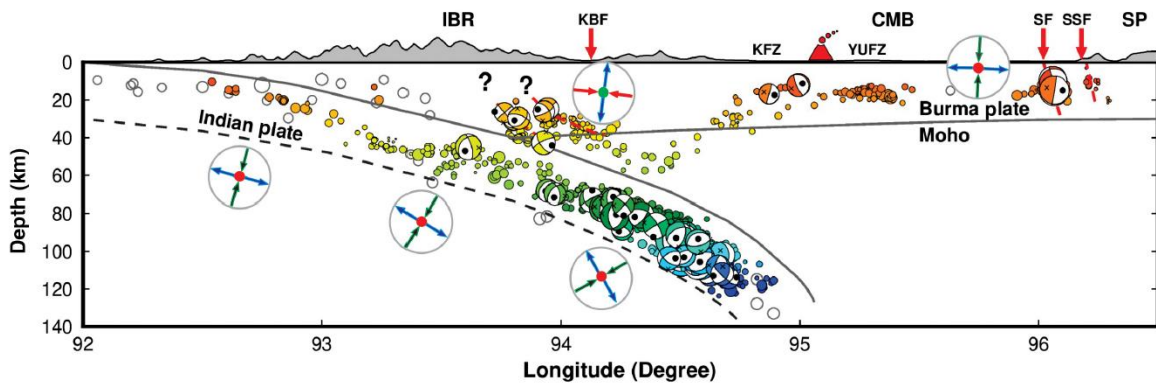
Fig. 3.3 Schematic illustration of subduction of Indian plate (Mon et al., 2020)

The major seismic events that have led to significant damage in Bangladesh are highlighted in the CDMP report and is shown in table 3.1.

24

Table 3.1 Major earthquake events near Dhaka

Earthquake	Year	Magnitude	Distance from Dhaka (km)
Cachar	1869	7.5	250km
Bengal	1885	7.0	170km
Great Indian	1897	8.1	230km
Srimangal	1918	7.6	150km
Dubri	1930	7.1	250km
Bihar-Nepal	1934	8.3	510km

Multiple earthquakes highlight the substantial seismic activity within and around the vicinity of Bangladesh. The historical record underscores the inevitable occurrence of severe infrastructural damage, loss of lives, and economic setbacks due to past earthquakes. The notable 1762 major Arakan earthquake, as documented by Cummins (2007), registered a magnitude of 8.8 (Mw). Through paleo-seismic studies, Mondal et al. (2014) confirmed occurrences of similar high-magnitude earthquakes along the Chittagong-Arakan coast, suggesting the potential for a future earthquake exceeding Mw 8. The 1869 Cachar earthquake, a profoundly destructive event near Sylhet, inflicted havoc on structures including cemeteries, jails and hospitals, leaving significant devastation in its wake (Oldham, 1882).

The 1885 Bengal Earthquake (Martin and Szeliga, 2010) measured at 7.0 magnitude (Bolt, 1987) and had its epicenter near Manikganj (Akhter, 2010). This calamitous earthquake resulted in a minimum of 75 fatalities, with the highest toll of 40 in Sherpur (Martin and Szeliga, 2010; Akhter, 2010). The Great Indian earthquake of 1897 stands as the most destructive seismic event in the India-Bangladesh region, registering an Mw of 8.1 (Bilham and England, 2001). Martin and Szeliga (2010) reported a death toll of at least 1626. The earthquake's impact led to the near-total destruction of brick and stone buildings, accompanied by violent ground shaking.

A 7.6 magnitude earthquake struck in Srimangal in 1918 (Sarkar et al., 2010), wreaking havoc in eastern Bangladesh, particularly in Srimangal (Martin and Szeliga, 2010). In Sylhet, the disaster destroyed brick structures, steel girder factories and houses. Bridges sagged and railway lines twisted.

These reports provide proof of the devastating effects of earthquakes on built structures, as well as the economic and societal costs. The country's increased seismic risk is due to the construction of many

buildings prior to the application of building rules (CDMP 2009, Sarker et al., 2010, Mazumder et al., 2018). Substandard design, inadequate detailing, construction practices and lack of proper oversight have rendered the region susceptible to earthquakes (CDMP 2009; Akhter, 2010). Sarker et al. (2010) considered the 1918 Srimangal earthquake as a hypothetical scenario and estimated potential losses in the Sylhet City Corporation area. Mazumder and Salman (2018) assessed seismic damage in Sylhet in the context of two hypothetical earthquakes. Both studies indicated that earthquakes might cause major infrastructure damage and fatalities.

Of significance is that, aside from the Bengal and Srimangal earthquakes, most events had epicenters beyond the 200 km buffer zone from the study area. To comprehend the overall seismic activity, this research focused on events with magnitudes greater than 5 within a 200 km radius of Dhaka. The most recent earthquake catalog (spanning 1762 to 2023) concerning earthquakes of more than 5 magnitude affirms the presence of seismic activities in the northeastern and southeastern regions of Bangladesh, which could substantially impact Dhaka as well (Figure – 3.4). Studies conducted under the Comprehensive Disaster Management Program (CDMP 2009) corroborate that Dhaka ranks among the cities at highest risk in terms of the severity of damage. A recent study projected that, in Dhaka City, approximately 270,604 buildings (83% of the total) would experience moderate damage, and out of these, about 238,164 buildings (73% of the total) would sustain irreparable damage from a scenario earthquake of 7.5 magnitude occurring roughly 50 km away from the city center (CDMP 2009).
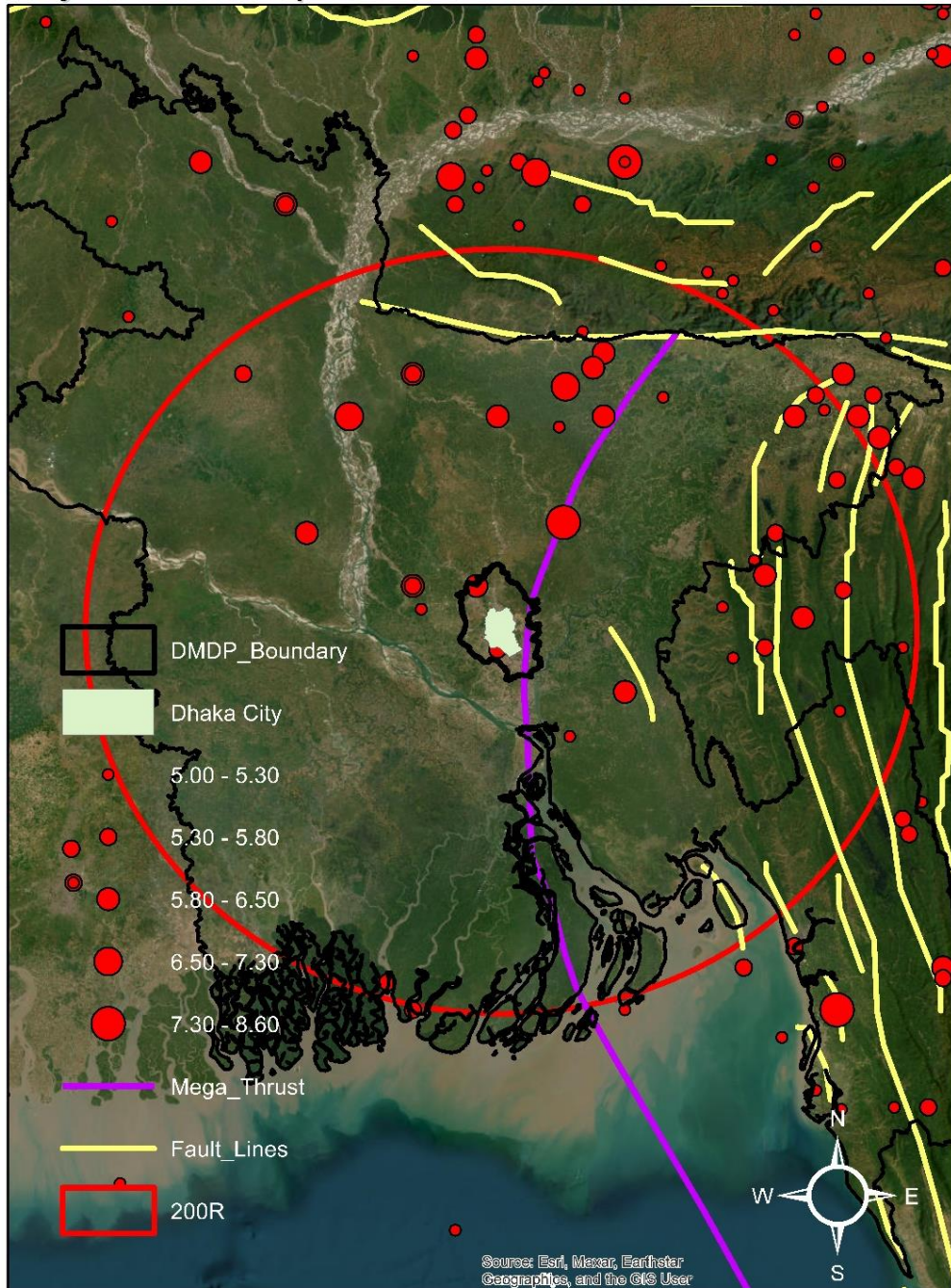
Fig. 3.4 Major seismic events and active faults near Dhaka city from 1762 to 2023

For the purpose of this study, upgradation of the earthquake event information was carried out by compiling the data used by previous (Al-Hussaini and Hasan, 2006; Chowdhury, 2016) researchers and merging it with additional event information upto 2023. The additional earthquake event

information was extracted from ISC– GEM Global Instrumental Earthquake Catalog and US Geological Survey Earthquake Catalog. The dataset used in development of the earthquake event map have been furnished in tabulated format in Appendix – A.

3.4   Database Development

A total of 224 nos. SPT drillhole data and 40 nos. of SCPT data scattered all along different areas of Dhaka City covering most of the regions were compiled as a part geotechnical database development for the research. These boreholes were later transformed in tabulated format to produce the data sets required for the evaluation of shear wave velocity, liquefaction potential index, hazard mapping and incorporation in machine learning models. The location of these boreholes were mostly confined within greater Dhaka City. Various types of geotechnical tests were performed on these boreholes to find out different soil parameters and soil classification of different locations in Dhaka.

The source of dataset illustrated in Appendix - B included 126 nos. of SPT data from Dhaka Sub-Way Project referred to as 'SW', 12 nos. of SPT data from Dhaka Metro Rail Line - 5 project referred to as MRT, 37 nos. of SPT data from Geological Survey of Bangladesh referred to as 'GSB' and 49 nos. of SPT data from Comprehensive Disaster Management Program referred to as 'CDMP'. On the other hand, all 40 nos. Seismic Cone Penetration data were compiled from Dhaka Sub-Way Project. The point to be noted here is that the SPT based dataset of 'CDMP' project was also used by Rahman et al. (2015) for his PHD research and was directly collected from him as part of overall upgradation process of the dataset and future research works.

The distribution of SPT with corresponding depth compiled for the study is shown in Figure 3.5.
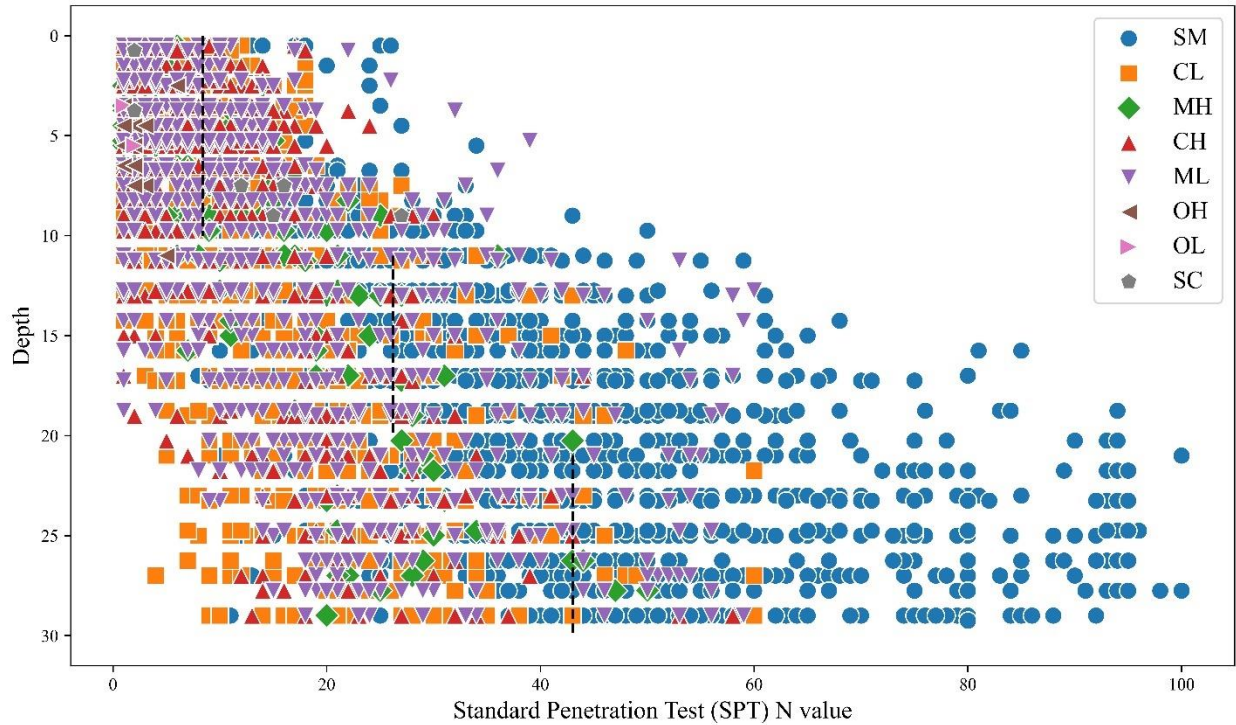
Fig. 3.5 Distribution of SPT along depth (upto 30m)

The distribution of SPT value for different soil types classified according to USCS classification system for Dhaka City illustrates that most of the cohesive layers lie within the top 15m from the surface having a combination of clay and silt deposition. On the other hand, dense sands having SPT values greater than 50 lie below 20m depth from the surface. Average SPT -N value for upto 10m depth for Dhaka City is 8.37, for 11m to 20m depth is 26.33 and from 21m to 30m depth the value is 43.06.

In addition to the SPT values the soil classification adopted from SCPT results were based on "Ic" (soil behavior type index) values proposed by Robertson (1990). The point to be mentioned here is that "Ic" is a function of cone resistance, q_c and friction ration R_f. A typical shear wave velocity profile of SCPT point "SW PZ 05" is shown in the following Figure 3.6 and subsequently distribution of shear wave velocity V_s with respect to soil type for the 40 SCPT points are illustrated on Figure 3.7
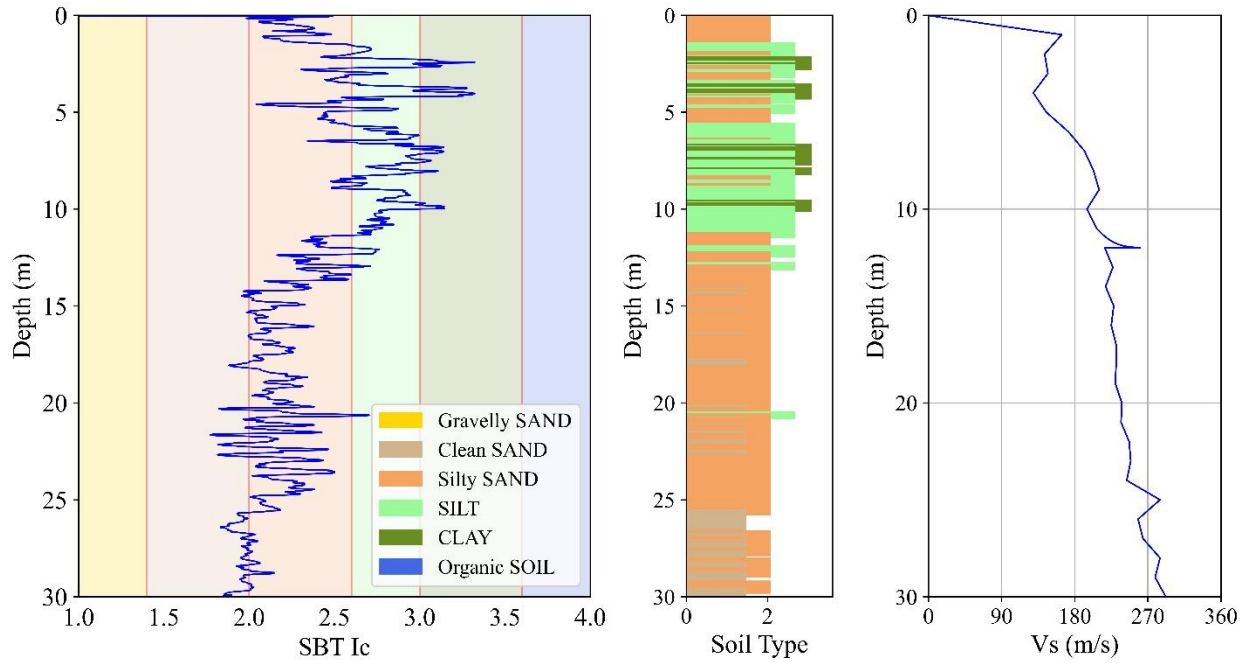
Fig. 3. 6 Typical Shear Wave Velocity Profile for BH-SW05 (upto 30m)
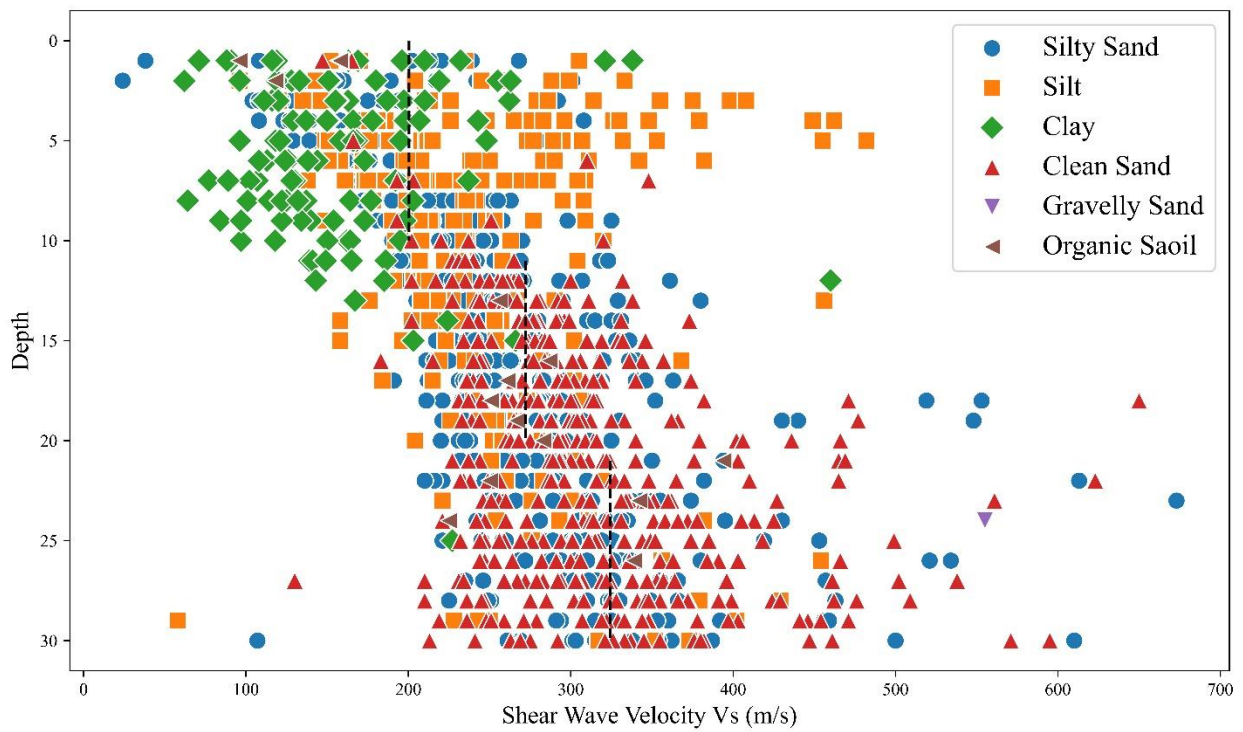
Fig. 3. 7 Distribution of shear wave velocity along depth (upto 30m)

The distribution of shear wave velocity, V_s value for different soil types for Dhaka City illustrates that silt and clay layer exists within top 10m from the surface having shear wave velocity less than 400 m/s in majority of the cases. On the other hand, clean and silty sands having V_s values greater than 200 m/s lie below 10m depth from the surface. Average V_s value for upto 10m depth for Dhaka City is 200.4 m/s, for 11m to 20m depth is 272.06 m/s and from 21m to 30m depth the value is 324.24 m/s.

CHAPTER 4: ANAYTICAL APPROACH AND METHODOLOGY

4.1   General

The research approach is structured into four phases, commencing with the seismic site characterization in alignment with the BNBC (2020) guidelines to ascertain the PGA value and seismic site class for Dhaka City. These parameters will then serve as inputs for evaluating liquefaction susceptibility through the application of relevant geotechnical data using Cetin et al. (2018) approach. The accuracy of the outcomes will be affirmed by employing machine learning algorithms in supervised classification. Ultimately, the acquired data will be employed to create liquefaction-focused zonation maps through the utilization of ArcGIS software's geostatistical interpolation method, yielding a seamless depiction.

4.2   Development of Liquefaction Susceptibility Mapping Framework

The methodology aims to provide a comprehensive framework integrating regional code provisions for evaluating the liquefaction susceptibility of a given study area. It integrates geotechnical data, seismic parameters, machine learning indicators and GIS-based geostatistical interpolation to develop vulnerability maps for liquefaction. The following steps have been followed in developing the framework in the context of Dhaka City:

- Collect up-to-date geotechnical data through geotechnical (SPT, CPT etc.) and geophysical tests (SCPT, downhole tests etc.)
- Calculate the seismic site class based on the weighted average shear wave velocity data for the upper 30m soil layer, as per BNBC (2020) guidelines.
- Characterize the seismic site class and evaluate the Peak Ground Acceleration (PGA) value according to code provisions or site-specific attenuation models as well as seismic site response analysis.
- Evaluate the Cyclic Stress Ratio (CSR) and Cyclic Resistance Ratio (CRR) using the seismic parameters and geotechnical data.

- Classify the liquefaction susceptibility outcomes into two categories: "Susceptible to liquefaction" and "Not susceptible to liquefaction," based on the estimated factor of safety value for each investigation location.

- Assess the performance of the evaluation using a variety of machine learning algorithms and evaluate their performance based on performance indicators like the Receiver Operating Characteristic (ROC) curve, confusion matrix etc.

- Utilize Geostatistical Interpolation techniques in GIS software to develop vulnerability maps for liquefaction after achieving satisfactory results.

- Recommend regulatory policies for continuous upgradation of the database, method and techniques for liquefaction susceptibility evaluation.

The methodological framework adopted for the study is shown in the following workflow diagram:
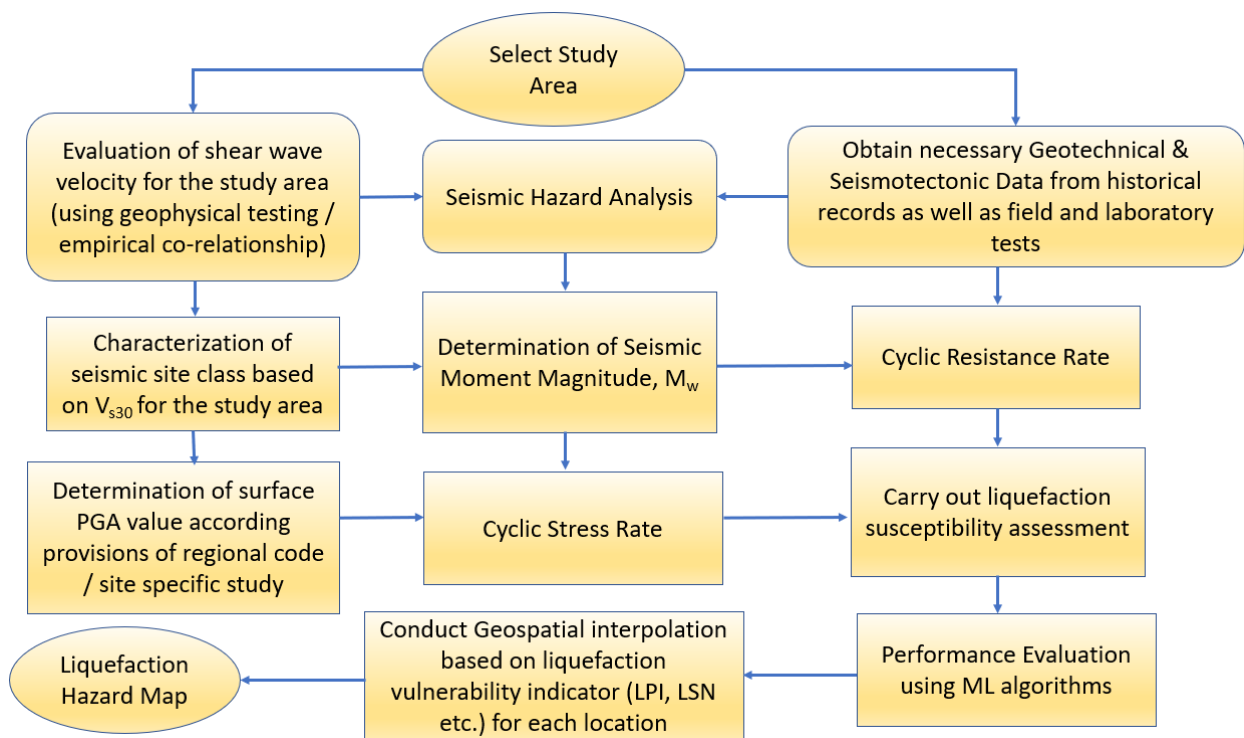
Fig. 4.1 Methodological framework for liquefaction susceptibility mapping

The point to be mentioned here is that seismic site characterization, liquefaction potential index estimation, performance evaluation using machine learning algorithms, utilization of advanced mapping techniques in the form of geostatistical interpolation such which has been discussed in

sub-sequent sections are all a part of different of types of analytical approaches undertaken under this study and is a part of the proposed framework for liquefaction susceptibility mapping.

4.3   Seismic Site Characterization

Accurate seismic site characterization stands as a pivotal prerequisite for conducting site-specific seismic hazard analysis, allowing for precise estimations of ground motion distribution at a given location. The inherent dynamic properties of geological materials find expression through shear wave velocity (Vs), wherein the time-averaged shear wave velocity within the uppermost 30 meters (Vs$_{30}$) emerges as the parameter of choice for the purpose of seismic site characterization. This approach is substantiated by multiple references within the academic domain, including works by Borcherdt (1994), BSSC (1994), Anderson et al. (1996), Xia et al. (1999) and Dobry et al. (2000).

For near-surface shear velocity (Vs) estimation both downhole survey method in the form of Seismic Cone Penetration Test and SPT based empirical co-relationship was used to evaluate Vs$_{30}$ of the investigation points.

4.2.1 Empirical Correlations between the Vs and SPT-N

The standard penetration test (SPT) constitutes a prevalent in-situ investigative technique extensively employed for the characterization of geotechnical sites. The endeavour to deduce near-surface shear wave velocity (Vs) through experimental field tests holds considerable merit. However, it's pertinent to note that geophysical methodologies necessitate adept knowledge, intricate instrumentation, and advanced software for the acquisition and analysis of data. Consequently, the estimation of Vs via geophysical approaches frequently exceeds the financial scope and logistical constraints of numerous engineering undertakings. Furthermore, a majority of these techniques demand expanses of land and an environment devoid of disturbances stemming from traffic and industrial activity, conditions that are often unavailable within densely developed urban landscapes such as Dhaka.

Consequently, predicting the shear wave velocity (Vs) using the number of blows recorded in the standard penetration test (SPT-N) has gained significant popularity in the field of geotechnical earthquake engineering. Subsequently, the standard penetration test blow count (SPT-N) enjoys

universal application on a global scale (Ohta and Goto, 1978; Andrus et al., 2006; Fabbrocino et al., 2015) to predict Vs through the empirical relationships that interlink Vs with SPT-N. The emergence of such correlation's dates back to the early 1970s, spearheaded by Japanese researchers. Notably, Ohta and Goto (1978) constituted prominent instances, grounded in Japanese databases that undergo periodic updates. Ohta and Goto's approach stands distinguished for integrating four key indices SPT value, soil type, depth, and geological age in predicting shear wave velocity, in contrast to other empirical equations that hinge solely on SPT value. Noteworthy advancement came via Andrus et al. (2007), who underscored the potential for augmented prediction precision of Vs through Age Scaling Factors which was later updated by Wair et al. (2012). Therefore, the aforementioned guideline was used for Vs evaluation. The correlation suggested by Wair et al. (2012) is shown in equation 4.1.

$$Vs = 30 \, N_{60}{}^{0.215} \sigma'_v{}^{0.275} \qquad \text{(Eq. 4.1)}$$

The age scaling factor for Pleistocene and Holocene Deposition suggested for the equation is 1.13 and 0.87, respectively.

4.2.2 Vs from Geophysical Data

The present study used data from the Seismic Cone Penetration Test (SCPT), a method ingeniously adapted from traditional cone penetration testing (CPT). By integrating a seismic add-on module with the established CPT cones, the SCPT technique was executed. Positioned directly atop the measurement cone in the CPT probe, this module encompasses an assemblage of receivers, typically accelerometers or geophones, often organized in a uniaxial or triaxial configuration. In specific scenarios, a dual array arrangement is employed, denoting the utilization of two seismic modules. Analogous to the single array, these receivers can be arrayed uniaxially or triaxially. Within each receiver, three accelerometers are aligned along orthogonal axes, two of which are horizontal (X and Y), while the third is oriented vertically (Z). During measurements, these accelerometers capture oscillations evoked by seismic waves propagating across the ground surface.
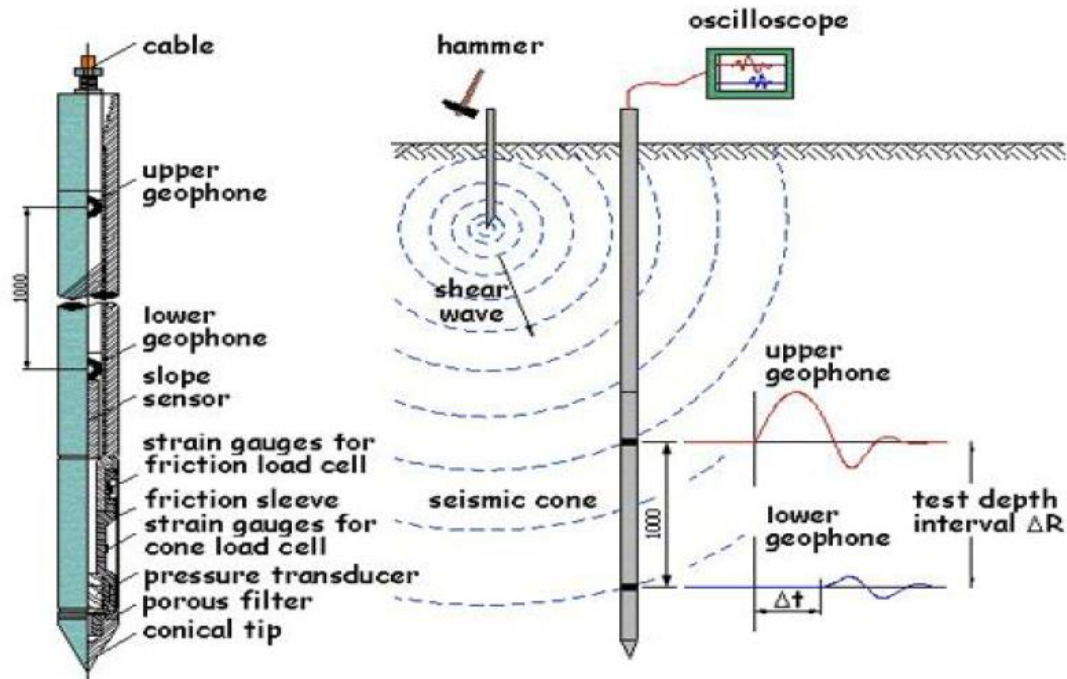
Fig. 4. 2 Typical instrumental arrangement of seismic sone penetration test

For optimal results, dual array systems are favored as they yield a genuine interval as opposed to a simulated one. To distinguish seismic data from standard CPT data, a signal conditioning box is indispensable at the surface, especially for users employing analog setups. Those utilizing analog systems will necessitate seismic cables endowed with additional pins to accommodate seismic data. A waveform generator assumes a pivotal role, serving to create seismic waves for downhole detection. In such investigations, this typically involves a striking plate coupled with a hammer, with more advanced setups being fully automated.

4.2.3 Preparation of Vs_{30} and Seismic Site Classification Map

The Vs_{30} map is an integral part of seismic micro-zonation and serves as a basis for seismic site characterization. The National Earthquake Hazard Reduction Program, Uniform Building Code, International Building Code, Eurocode 8 all have adopted Vs_{30} for site classification. In the recent past, such provisions for characterizing seismic site class have been incorporated in the newly published Bangladesh National Building Code (BNBC 2020). For the purpose of this study, BNBC (2020) based classification system was used to characterize sites according to Vs_{30} value.

Site classification provisions of BNBC 2020 is shown below:

36

Table 4. 1 Seismic site class provisions according to BNBC (2020)

Site Class	Description of soil profile upto 30 m depth	Average Properties in top 30m		
		Shear wave velocity, $\overline{Vs}$ (m/s)	SPT value, $\overline{N}$ (blows/30cm)	Undrained Shear Strength, $\overline{Su}$ (Kpa)
SA	Rock or other rock like geological formation including at most 5 m of weaker material the surface	>800	--	--
SB	Deposits of very dense sand/gravel, or very stiff clay, at least several tens of metres in thickness, characterized by a gradual increase of mechanical properties with depth	360 - 800	>50	>250
SC	Deep deposits of dense or medium dense sand, gravel or stiff clay with thickness from several tens to many hundreds of metres	180 - 360	15 -50	70-250
SD	Deposits of loose-to-medium cohesionless soil (with or without some soft cohesive layers), or of predominantly soft to firm cohesive soil	<180	<15	<70
SE	A soil profile consisting of a surface alluvium layer with Vs values of type SC or SD and thickness varying between about 5 m and 20 m, underlain by stiffer material with Vs > 800 m/s	--	--	--
S_1	Deposits consisting or containing a layer at least 10 m thick, of soft clays/silts with a high plasticity index (PI>40) and high-water content	<100 (indicative)	--	10-20
S_2	Deposits of liquefiable soils, of sensitive clays, or any other soil profile not included in types of SA to SE or S_1	--	--	--

The average soil property has been determined using the following equation:

$$\overline{Vs} = \frac{\sum_{i=1}^{n} d_i}{\sum_{i=1}^{n} d_i/Vs_i} \qquad\qquad \text{(Eq. 4.2)}$$

Where, d_i = soil layer thickness of layer i, n= number of soil layer in upper 30m and Vs_i = Shear wave velocity of i layer

In the present study, the shear wave velocity of the near-surface materials (Vs) was estimated using the SCPT records and correlation with standard penetration test blow count (SPT-N) data. Then, the Vs_{30} map was prepared from the Vs_{30} results that were estimated using the SPT based correlation and direct measurement from SCPT. According to the range of Vs_{30} values outlined in BNBC 2020, zones have been characterized according to their seismic site class and a seismic site characterization map was generated as an aftermath.

4.3   Liquefaction Susceptibility Assessment

Various methodologies and conceptual frameworks have emerged in the past 45 years to appraise the potential for triggering liquefaction. Among these, the stress-based approach has emerged as the predominant methodology, involving a comparison between earthquake-induced cyclic stresses and the cyclic resistance inherent to the soil. In contrast, the strain-based and energy-based approaches, although valuable, have gained less prominence due to their greater demand for extensive field and laboratory data. Consequently, these latter approaches have not been selected for inclusion in the present study.

The emergence of earthquake-induced cyclic stresses beneath sites situated on level ground is chiefly ascribed to the repercussions of lateral seismic shaking. Illustrated in Figure 4.3, these stresses, along with pore pressures, impact a soil element beneath a level ground surface both prior to and amid the horizontal oscillations generated by an earthquake.
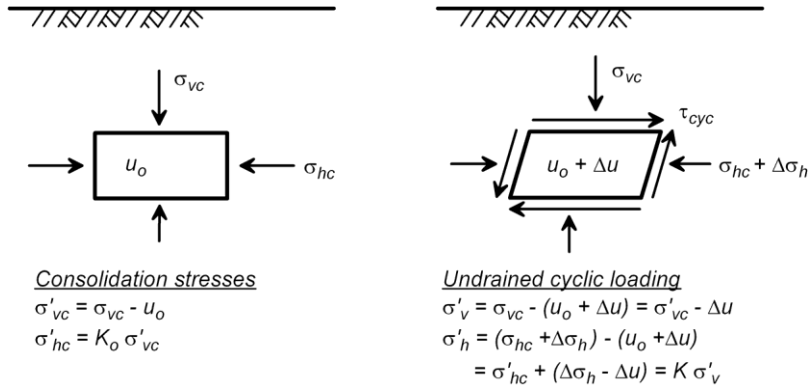
Fig. 4. 3 Cyclic stresses on a soil element beneath level ground during horizontal shaking

Vertical shaking of this profile would produce additional transient changes in the total vertical stress, total horizontal stress, and pore pressure, but the vertical and horizontal effective stresses would be unaffected. This is why the effects of vertical shaking are not considered in the analysis of level-ground profiles.

In the process of designing protocols, it becomes imperative to establish methodologies for the assessment of earthquake-triggered cyclic stresses (referred to as CSR) and the in-situ cyclic resistance ratio (CRR) as these two indicators are the fundamental parameter in assessing the susceptibility to earthquake-induced liquefaction.

The factor of safety against the occurrence of earthquake-induced liquefaction is commonly defined as the available soil resistance to liquefaction (expressed in terms of the cyclic stresses required to cause liquefaction) divided by the cyclic stresses generated by the design event (Youd, 2001). The functional form of factor of safety against liquefaction is presented in equation 4.3.

$$FS = \frac{CRR_{7.5}}{CSR} \cdot MSF \qquad \text{(Eq. 4.3)}$$

4.3.1 Cyclic Stress Ratio (CSR)

The resistance of sand to the triggering of liquefaction (i.e., its cyclic strength) depends on several factors, including the number of loading cycles, relative density, confining stress, depositional method, fabric, prior stress-strain history, age, cementation, and other environmental factors.

The induction of liquefaction in saturated sands can be evoked by diverse amalgamations of a uniform cyclic shear stress ratio (CSR) and the loading cycle count (N). Herein, an augmented

CSR, exemplified by an increased uniform cyclic shear stress relative to the initial effective confining stress, will lead to liquefaction onset (e.g., $r_u = 100\%$ or a cyclic shear strain, $\gamma = 3\%$) in a reduced number of loading cycles. Conversely, a reduced CSR necessitates a greater number of loading cycles to precipitate liquefaction.

Cyclic stress ratio calculation (CSR) commonly is named simplified procedure for estimating earthquake induced stresses. Conceptually, this ratio is defined (Seed and Idriss, 1971; BNBC 2020) in the following functional form:

$$CSR = \left(\frac{\tau_{av}}{\sigma_v'}\right) = 0 \cdot 65 \left(\frac{a_{max}}{g}\right)\left(\frac{\sigma_v}{\sigma_v'}\right) \cdot r_d \qquad\qquad \text{(Eq. 4.4)}$$

where τ_{av} is average earthquake-induced cyclic shear stress and σ_v' is pre-earthquake effective overburden stress at the depth under consideration

The shear stresses experienced at various depths within a soil deposit characterized by a level ground surface during seismic activity primarily result from the vertical transmission of horizontal shear waves. Analytical procedures are available to calculate these stresses if the characteristics of the soils comprising this deposit and the input motions are known.

However, such crucial information remains elusive for the majority of the "liquefaction/no liquefaction" instances harnessed to formulate correlations grounded in field observations. Furthermore, boreholes drilled for most projects rarely delve into the depths required to meticulously define the soil profile, thus insufficiently catering to the demands of site response investigations. Consequently, the streamlined liquefaction assessment procedure, as outlined by Seed and Idriss (1971), endures as a prevalent choice for determining the induced shear stresses, and by extension, the cyclic shear stress ratio (CSR). This approach's extensive application persists, endorsed by its inclusion in the latest design codes, including BNBC (2020).

BNBC provisions for stress reduction and PGA considerations

Since the inception stages of the stress reduction factor, r_d used for evaluating cyclic stress ratio went through lot of upgradations as different researchers used updated database from time to time and introduced new equations. Stress reduction factor is a site-specific parameter which depends on different factors such as depth, dynamic characteristics of soil as well as ground motion characteristics (Grasso and Sammito, 2021). For this study, BNBC 2020 recommended stress

reduction factor was used considering local perspectives which is shown in the following equation 4.5.

$$r_d = 1 - 0.015 \, z \hspace{3cm} \text{(Eq. 4.5)}$$

Where, z is the depth of soil column in meters.

Peak ground acceleration value, PGA for respective boreholes have been calculated according to the provisions of BNBC (2020). BNBC (2020) characterizes seismic site class based on estimation of average shear wave velocity, Vs_{30} for top 30m of the soil layer. The seismic zone co-efficient (Z) for Dhaka city according to BNBC (2020) is 0.2 which is the value for maximum credible earthquake having a return period of 2475 and 2% probability of exceedance in 50 years. The surface PGA value considering site amplification scenarios and design basis earthquake considerations have been calculated using the following equation 4.6.

$$PGA = \frac{2}{3} \cdot S. Z. \frac{I}{R} \hspace{3cm} \text{(Eq. 4.6)}$$

where $\frac{I}{R} = 1$ has been considered for free field liquefaction assessment (Al-Hussaini et al., 2012).

S has been considered 1.15 for seismic site class SC and 1.35 for seismic site class SD according to BNBC (2020). Hence, PGA value used in liquefaction evaluation is 0.15 for locations falling under site class SC and 0.18 for locations falling under site class SD.

4.3.2 Cyclic Resistance Ratio (CRR)

The cyclic resistance ratio (CRR) in the context of liquefaction pertains to a critical engineering parameter that characterizes the ability of a soil deposit to endure cyclic loading induced by seismic events without undergoing liquefaction. This parameter plays a pivotal role in assessing the susceptibility of soils to liquefaction-induced phenomena and in formulating effective strategies for seismic hazard mitigation.

The method most feasible for assessing the cyclic resistance ratio (CRR) involves procuring and subjecting undisturbed soil specimens to laboratory testing. Regrettably, the in-situ stress states encountered in the field are typically challenging to reproduce accurately within the controlled laboratory environment. Moreover, granular soil samples obtained through conventional drilling and sampling techniques frequently exhibit excessive disturbance, rendering the outcomes of

laboratory tests less meaningful. For evaluating the in-situ CRR of sandy soils, laboratory tests on field samples could potentially serve as a basis, albeit requiring the adoption of frozen sampling techniques to ensure reliable outcomes. However, the cost associated with such procedures generally renders them practicable only for projects of the utmost criticality.

To circumvent the complexities linked to sampling and laboratory evaluations, field tests have emerged as the prevalent methodology for standard liquefaction investigations. Consequently, semi-empirical correlations have been established between the in-situ CRR of sandy soils and the outcomes of in-situ tests. These correlations are formulated based on compilations of case histories where instances of liquefaction occurrence or non-occurrence have been documented, as depicted in Figure 4.4.
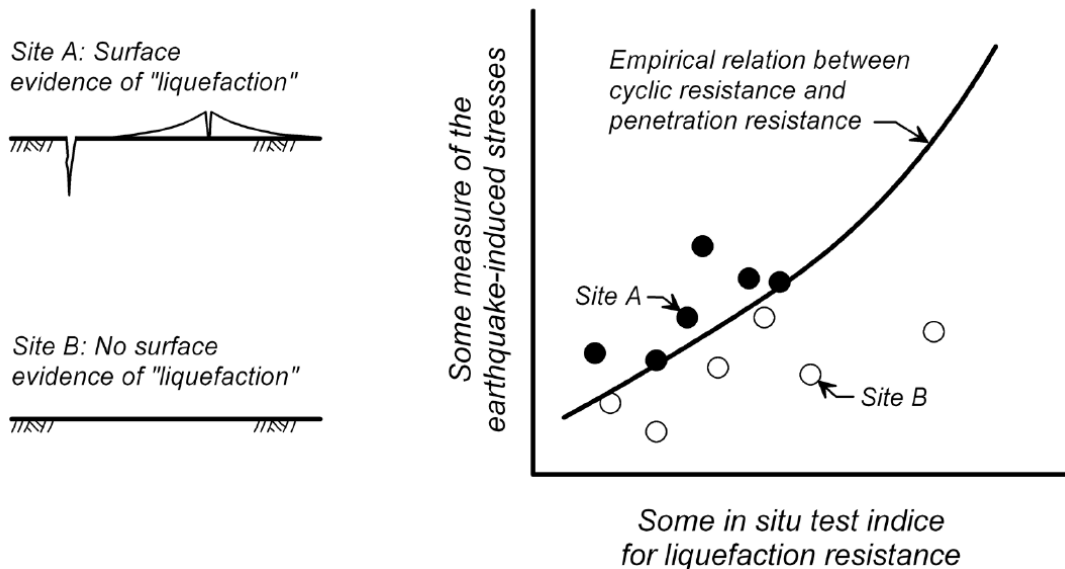
Fig. 4. 4 Schematic of the approach used to develop relationships between the in-situ CRR of sand and the results of in-situ tests

In the context of Cetin's research, the evaluation of the Standard Penetration Test (SPT) based cyclic resistance ratio (CRR) holds a significant role. This parameter quantifies the cyclic strength of a soil deposit with respect to its resistance against liquefaction-induced stresses, specifically when utilizing SPT results as a foundational metric. The SPT-based CRR is dependent on various key factors, including the $N_{1(60)}$ value, the moment magnitude of an earthquake event, the effective stress conditions, as well as fines content.

The functional form of CRR as depicted by Cetin et al. (2018) is shown in equation 4.7.

$$\text{CRR}\left(N_{1,60}, M_W, \sigma_v', FC, P_L\right) = \exp\left[\cfrac{\left(\begin{array}{c} N_{1(60)} \cdot (1 + 0.00167 \cdot FC) - 27.352 \cdot \ln(M_W) \\ -3.968 \cdot \ln\left(\frac{\sigma_v'}{P_a}\right) + 0.089 \cdot FC \\ +16.084 + 2.96 \cdot \Phi^{-1}(P_L) \end{array}\right)}{11.771}\right]$$

(Eq. 4.7)

Where, $P_L = 50\%$ has been considered for deterministic evaluation based on Cetin et al. (2018) approach for deterministic evaluation.

$N_{1(60)}$ is the SPT blow count normalized to an overburden stress and energy efficiency of 60%.

For the correction of the field SPT-N values, various factors are used, and finally calculate the normalized SPT value. The following equation 4.8 was used to find the normalized SPT value $(N_1)_{60}$:

$$N_{1(60)} = N_M C_N C_E C_R C_B C_S$$

(Eq. 4.8)

Where, N_M = field SPT value; C_N = correction for effective overburden stress; C_E = correction for hammer energy ratio (ER); C_B = correction for borehole diameter; C_R = correction for rod length; C_S = correction for samplers.

If the magnitude of the earthquake is not 7.5, then the CRR values need to be corrected for earthquake magnitude. Cetin et al. in 2004 made an approximation using different curves and the following equation 4.9 was proposed for calculating MSF:

$$\text{MSF} = \left(\frac{7.5}{M_w}\right)^{2.217}$$

(Eq. 4.9)

Where, M_W is the moment magnitude of the earthquake.

Even though past studies considered a moment magnitude of 7.5 for evaluation of liquefaction susceptibility however, recent researches have been carried out by Rahman et al. (2020) and Haque et al. (2020) where they focused on predicting PGA value based on Probabilistic Seismic Hazard Assessment (PSHA). However, outcome of the researches showed contrasting results where the PSHA study carried out by Zillur Rahman predicted a PGA value of 0.144 (Rahman et al. 2020) and on the other hand, outcome of another research conducted in the same year predicted a PGA value of 0.26 for Dhaka City (Haque et al., 2020).

It is to be mentioned here that, the parameters used based on crustal fault source model in the aforementioned researches were different. Rahman et al. (2020) predicted maximum moment magnitude to be 8.03 generated from Dauki Fault based on PSHA. On the other hand, Haque et al. (2020) considered the faults of Chittagong – Tripura fold belt which is in close proximity to Dhaka to be the biggest threat of generating 6.5 – 8.5 magnitude earthquakes at a distance of around 80 km.

For the purpose of this study, BNBC specified site class was utilized to determine PGA value for each borehole location. On the other hand, moment magnitude of 7.0, 7.5 and 8.0 was considered for liquefaction vulnerability assessment as historical records show that most of the major earthquakes had epicenters beyond 100 km from Dhaka.

4.3.3 Evaluation of Liquefaction Potential Index

To assess the damage potential of each site liquefaction potential index (LPI) originally proposed by Iwasaki et al. (1978, 1982) was utilized for risk assessment. The LPI assumes that the severity of liquefaction is proportional to the thickness of the liquefied layer, the proximity of the liquefied layer from the ground surface, and the amount by which the factor of safety (FS) is less than 1.

$$\text{LPI} = \int_0^z F(z) . W(z) . dz \qquad\qquad \text{(Eq. 4.10)}$$

Where, F (z) = 1 – FS, for FS < 1.0

      F (z) = 0, for FS $\geq$ 1.0

      W (z) = 10 – 0.5z, for z < 20 m

      W (z) = 0, for z > 20

4.4   Performance Evaluation using Machine Learning Algorithms

Supervised classification is a type of machine learning where the goal is to assign input data points to predefined categories or classes based on their features. In the context of binary classification, there are two classes: positive (or '1') and negative (or '0'). There are several algorithms commonly used for binary classification, including logistic regression, support vector machines

(SVM), tree-based algorithms (like decision trees and random forests), and boosting algorithms (like AdaBoost and Gradient Boosting).

However, in the field of liquefaction susceptibility assessment Support Vector Machine (SVM) has been used vastly by many researchers (Goh and Goh, 2007; Lee and Char, 2013) and some researches (Pal, 2006; Samui, 2011) showed that Support Vector Machine produced the best results in terms of liquefaction prediction. On the other hand, logistic regression is widely used for binary and linear classification problems and its ability in evaluating seismic liquefaction potential was studied by researchers, which manifests that this model can capture and describe the intrinsic, complex relationship between seismic parameters, soil parameters and the liquefaction potential (Zhang and Goh, 2016).

However, in the recent past ensemble learning methods are the most current state-of-the-art and dominant algorithms in the area of machine learning to obtain the maximum model performance and is quite useful in dealing with complex data, especially imbalanced, high-dimensional, noisy and multi-source data. The basic idea of ensemble models is to combine multiple ML algorithms to obtain better predictive performance than any of the constituent models. Substantial models have thus been developed and improved over the years and widely adopted ensemble strategies have been used in the field of liquefaction studies. For this study AdaBoost algorithm has also been selected for performance evaluation in addition to Logistic Regression and Support Vector Machine.

4.4.1 Machine Learning Algorithms

Logistic Regression

Logistic regression expresses the multiple linear regression equation in logarithmic terms (the logit), thereby overcoming the problem of violating the linearity assumption. Instead of predicting the value of the outcome variable from one or more predictor variables, the algorithms predict the probability of the outcome occurring, given known values of the predictors K-fold cross validation technique to split the data into multiple number of folds for splitting into testing and training sets. The available hyperparameters to be tuned for this algorithm were C value, solver and a penalty. Using random search cross-validation technique the best accuracy that can be achieved with this algorithm in correspondence to the best parameters used for achieving it was identified. The

logistic regression is basically a statistical model where the equation of linear regression is put through a sigmoid function. This makes the model give binary outputs i.e., predicts a value that can represent two different classes.

$$y = \beta_0 + \beta_1 x_1 + \beta_2 x_2 \dots \dots \dots \beta_n x_n$$

This equation above expresses a linear regression according to statistics, where β_0 is the intercept and x is the input feature. But in case of machine learning the intercept is considered as overall bias of the model and the coefficient of x expresses the weights assigned to the corresponding feature.

Therefore, the transformed equations are:

$$y = \sum_{i=1}^{m} w_i\, x_i$$

$$\emptyset(y) = \frac{1}{1 + e^{-y}}$$

Here, $\emptyset$ function represents the sigmoid function that was used for prediction in this machine learning model.

Support Vector Machine

The support vector machine (SVM) classifier uses statistical learning theory as its foundation (Vapnik, 1995) and searches for the best hyperplane to use as a decision function in high dimensional space (Cristianini et al., 2000). Instead of employing empirical risk minimization, the SVMs use structural risk minimization to get their results. Empirical risk reduces the probability of making a misclassification on the training set, whereas structural risk reduces the probability of making a misclassification on a data point that has never been seen before and is drawn at random from a probability distribution that is either fixed or unknown.

As a result of the fact that the samples from each of the dataset are already separated into liquefied cases and non-liquefied cases, the classification of the samples from the three sets of data is a problem of binary classification. The support vector machine (SVM) is a technique for automatic learning and is predicated on the statistical learning theory. When it comes to dealing with binary classification issues, the SVM has had a great degree of success for a significant amount of time

in the past. An ideal classification hyperplane must be determined from the outset in order to guarantee accurate classification. Once this is done, the blank area on both sides of the hyperplane must be maximized in order to meet this requirement (Zhou et al., 2018). So, two boundary conditions were applied to establish a hyperplane by which classification will be done on two kinds of samples.

$w^T \times x_i + b \geq +1$ for $y_i = +1 \rightarrow$ liquefaction

$w^T \times x_i + b \leq -1$ for $y_i = -1 \rightarrow$ no liquefaction

Around this defined hyperplane there will be many sample points. These points are known as support vectors. The sum of the distance from the hyperplane to the support vectors is called Margin which is expressed by the following equation:

$$Margin = \frac{2}{\|w\|}$$

Adaptive Boosting (AdaBoost)

AdaBoost stands out as one of the most widely used boosting algorithms. Introduced by Freund and Schapire (2009), this algorithm is efficient and excels at creating diverse models. It has found success in various scenarios, including solving problems with two-class, multi-class single-label, multi-class or multi-label setups, as well as single-label categories (Hastie et al., 2009). Operating through iterations, AdaBoost's goal is to construct a robust classifier using weak classifiers. These weak classifiers are strategically selected in each iteration to minimize errors during training. The ultimate aim is to create a strong classifier that significantly enhances the performance of the initial weak classification algorithm (Kim, 2010). This enhancement is achieved by combining the outputs of the set of weak classifiers.

4.4.2 Cross-Validation

Cross-validation is a crucial technique in machine learning for assessing the performance of models and mitigating overfitting. It involves partitioning a dataset into subsets to train and test a model on different data portions. This helps in evaluating the model's generalization ability and robustness. There are several types of cross-validation techniques such as hold-out validation, leave one out cross-validation, K-fold cross-validation etc.

The K-fold CV technique is frequently used in the areas of machine learning, even when there is only a small amount of data available to work with. This method is used to train and modify the model before it is put through its paces against the definitive testing set.

To find the optimal nos. of fold hyperparameter tuning was conducted using "Grid Search CV" based on cross-validation score of different folds. Grid Search employs a unique combination of each of the hyperparameters that have been specified and the values for those hyperparameters. It then assesses the performance of each combination and chooses the one that results in the best performance for the hyperparameters. In addition to the Grid Search operation, the cross-validation procedure is carried out using Grid Search CV. During the training of the model, cross-validation is performed. Because of this, the processing takes a significant amount of time and becomes prohibitively expensive due to the high number of hyperparameters involved. Before training the model with the data, the data are split into 'n' number of folds which includes one-fold for testing and the remaining 'n-1' folds are used for training. In this study, grid search technique was adopted for logistic regression, SVM as well as Adaboost which is an ensemble learning method.

According to the accuracy score for different algorithms, the decision was made to proceed with the optimal no. of folds in order to cross validate the output of the algorithms.
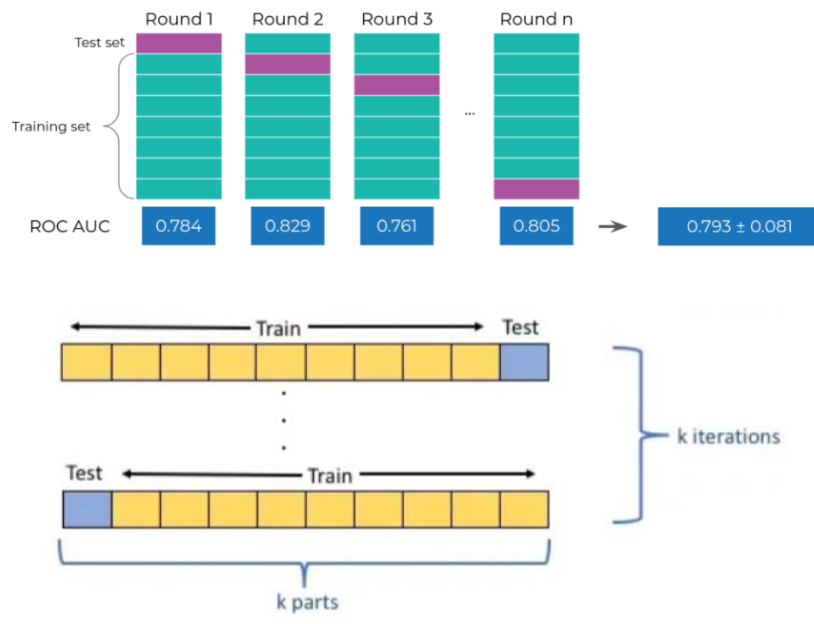
Fig. 4.5 Schematic diagram K-fold cross-validation with ROC score

This process is repeated with a variety of validation folds, and it was carried out in the absence of a testing set. The training and testing dataset were split using optimum number of folds.

4.4.3 Performance Metrics

In the evolving landscape of geotechnical engineering, the assessment of liquefaction susceptibility remains a critical concern. Various performance metrics have been employed to evaluate the efficacy of predictive models, including F1 score, precision, sensitivity, specificity, and overall accuracy. However, the Receiver Operating Characteristic (ROC) curve and its associated Area Under the Curve (AUC) score have emerged increasingly as a relevant tool for this purpose.

Application within the field of geotechnical engineering remains comparatively limited with recent initiatives taken by Maurer et al. (2017, 2019), Green et al. (2017), Upadhaya et al. (2021, 2023) etc. Specifically, ROC analysis proves invaluable in scenarios where the distributions of "positive" outcomes (e.g., instances of liquefaction) and "negative" outcomes (e.g., absence of liquefaction) exhibit overlap when graphically represented as a function of diagnostic test metrics.
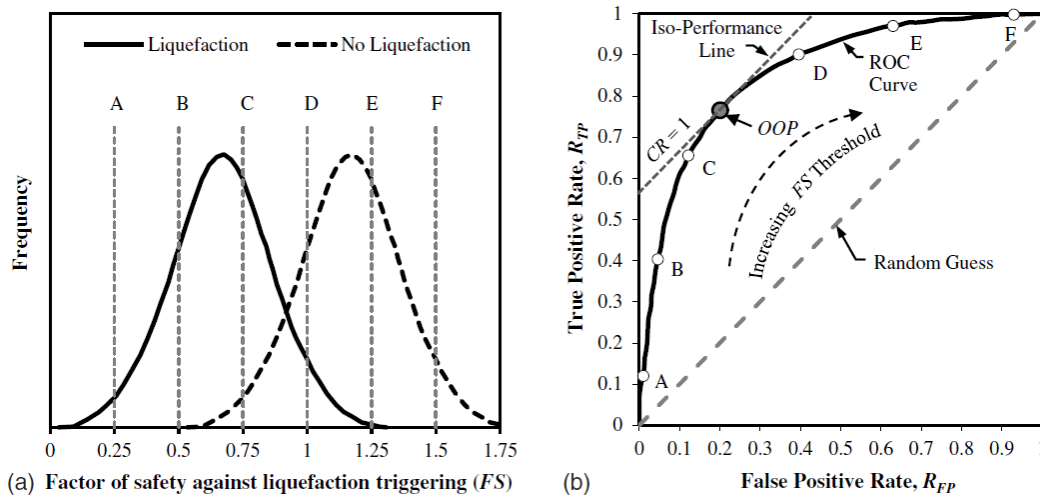
Fig. 4.6 Illustration of ROC curve considering FS as a threshold (Upadhaya et al., 2021)

For evaluating the performance of a model for classification, K- fold cross validation with ROC curve was utilized for this research. Mean AUC score was considered as the key performance indicator of liquefaction evaluation. Any AUC value of less than 0.5 suggests that the model has no discriminative power and is essentially performing at the level of random guessing. Range of

0.5 to 0.7 is considered to indicate poor to fair performance. Anything between 0.7 to 0.8 suggests that the model does have moderate discriminative capability. 0.8 to 0.9 is considered to be a good range and the outcome is considered to be reliable. Finally, any AUC score of greater than 0.9 suggests that the models have excellent prediction ability. The True positive rate (TPR) in an ROC curve is often referred as Sensitivity and the false positive rate (FPR) is referred as Specificity and can be expressed as a function of True Positive and Negative counts.

$$\text{Sensitivity} = \frac{\text{True Positive}}{\text{True Positive}+\text{False Negative}}$$

$$\text{Specificity} = \frac{\text{True Negative}}{\text{True Negative}+\text{False Positive}}$$

In addition, overall accuracy and F1 score also have considered for performance evaluation.

$$\text{Overall Accuracy} = \frac{\text{True Negative}+\text{True Positive}}{(\text{True Negative}+\text{False Positive}+\text{True Positive}+\text{False Negative})}$$

$$\text{F1 score} = \frac{2\text{True Positive}}{(\text{False Positive}+\text{True Positive}+\text{False Negative})}$$

For understanding these the parameters for calculating the indicators, the following table 4-2 expresses a typical confusion matrix:

Table 4. 2 Confusion matrix between cluster labels

Actual	Predicted	
	Positive	Negative
Positive	True Positive	False Negative
Negative	False Positive	True Negative

For the purpose of this study, the following considerations were made: '0' as a binary output for cases with no liquefaction prediction and '1' as binary output for cases with liquefaction prediction from the calculation based on Cetin et al. (2018) formulations. On the other hand, after fitting the data into machine learning algorithms if the prediction gives an output of '0' then the results are considered to be 'true negative' and if it gives an output of '1' then it is referred to as 'true positive'

counts. The results have been presented in the form of multiple confusion matrixes for different algorithms.

4.5   Geostatistical Analysis for Development of Hazard Maps

Existing soil data frequently falls short in furnishing the necessary information essential for the effective management of the environmental resources. A substantial volume of soil information and numerous cartographic representations remain underutilized for scholarly investigation due to their absence in digital formats.

Within this context, the Geographic Information System (GIS) emerges as a potent and commendable instrument for the estimation of the spatial dispersion of soil parameters (Shit et al., 2016). The prognosis of spatial patterns and the modeling of soil properties have evolved into prevalent focal points within the realm of soil science research (Brevik et al., 2016).

To find out the liquefaction susceptibility in the zones where borehole data is not available, special statistical analysis is being done. To perform this, Geo-statistical Analyst tool installed in GIS as an extension has been used for analysis. Geo-statistics is intimately related to interpolation methods but extends far beyond simple interpolation problems to prepare a continuous map. Different statistical and geostatistical approaches have been used in the past to estimate the spatial distribution of soil properties. Classical statistics could not make out the spatial allocation of soil properties at the unsampled locations. Geo-statistics is an efficient method for the study of spatial allocation of soil characteristics and their inconsistency and reducing the variance of assessment error and execution costs. Interpolation is an estimation of a variable at an unmeasured location from observed values at surrounding locations.

Interpolation can be undertaken utilizing a variety of mathematical models in the form of Kriging, Inverse Direct Weighted Method (IDW), Spline etc. In case of weak spatial dependency, or there is a limitation in the number of data, the Inverse Weighted Average method is a suitable alternative for other interpolation methods. (Lu and Wong, 2008). In case of Kriging the range of changes in the estimation based on interpolation is less than the range of changes in IDW as the large values of the parameter are estimated less than the real value and the small ones are estimated more than the real value causing the estimation range to become more limited. On the other hand, Splines produce good results with gently varying surfaces, and thus are often not appropriate when there

are large changes in the surface values within a short horizontal distance and hence leads to considerable interpolation error (Robinson and Metternicht, 2006).

Since, soil data obtained at different investigation point is highly variable and has weak spatial dependency hence Inverse Direct Weighted method has been adopted for development of hazard maps in the context of seismic hazard and liquefaction susceptibility mapping. To supplement to the fact it may be also mentioned, here that past researches carried out for similar studies (Bhunia et al., 2018) in a global platform also adopted Inverse Direct Weighted (IDW) method for development of similar maps.

Inverse Direct Weighted Method (IDW)

The IDW technique computes an average value for unsampled locations using values from nearby weighted locations. The weights are proportional to the proximity of the sampled points to the unsampled location and can be specified by the IDW power coefficient (Muhashi et al., 2018). Depending upon larger the power coefficient, the stronger the weight of nearby points as can be gleaned from the following equation 4.11 that estimates the value Z at an unsampled location j:

$$\widehat{Z}_J = \frac{\sum_i z_i/d_{ij}^n}{\sum_i 1/d_{ij}^n}$$
(Eq. 4.11)

The carat ^ above the variable z reminds the point location for estimating the value at j. The parameter n is the weight parameter that is applied as an exponent to the distance thus amplifying the irrelevance of a point at location i as distance to j increases. So, a large 'n' results in nearby points wielding a much greater influence on the unsampled location than a point further away resulting in an interpolated output looking like a Thiessen interpolation. On the other hand, a very small value of 'n' will give all points within the search radius equal weight such that all unsampled locations will represent nothing more than the mean values of all sampled points within the search radius.

CHAPTER 5: RESULTS AND DISCUSSIONS

5.1 General

This chapter aims to provide a brief overview of the analytical outcome of a comprehensive multi-disciplinary approach to liquefaction susceptibility assessment by integrating updated liquefaction susceptibility evaluation methods, machine learning algorithms and hazard mapping techniques.

5.2 Descriptive Statistics of Liquefaction Susceptibility Assessment

Descriptive statistics can also serve to elucidate the entire population under consideration. In essence, descriptive statistics aid in comprehending the attributes of a specific dataset by providing brief summaries of both the dataset's samples and measurements.

Parameters of centrality, including the mean, median and mode, represent the most familiar forms of descriptive statistics, and their application spans across educational levels in the fields of mathematics and statistics. To calculate the mean, commonly referred to as the average, the sum of all values within the dataset is initially calculated. Subsequently, this sum is divided by the total count of values in the dataset. The domain of descriptive statistics encompasses both measures of central tendency and measures of dispersion (spread). Among the measures of central tendency are the mean, median and mode. Conversely, measures of dispersion encompass elements like standard deviation, variance, as well as the minimum and maximum values.

In the present study, 3063 raw input variables were used to evaluate liquefaction potential for different magnitude scenario earthquakes in the form of 7.0, 7.5 and 8. The number of liquefaction cases predicted according to Cetin et al. (2018) SPT based deterministic calculation methodology was 272, 461 and 685 for respective moment magnitude of 7.0, 7.5 and 8.0 (visually represented in Figure 5.1, 5.2 and 5.3). On the other hand, the non-liquefied cases were 2791, 2602 and 2378 for the aforesaid scenario seismic events. The pair plots of different raw input parameters in the form of corrected SPT value $(N_1)_{60}$, Fines Content FC, depth, effective and total stress, stress reduction factor r_d and cyclic stress ration CSR have been plotted for 7, 7.5 and 8 magnitude earthquakes.
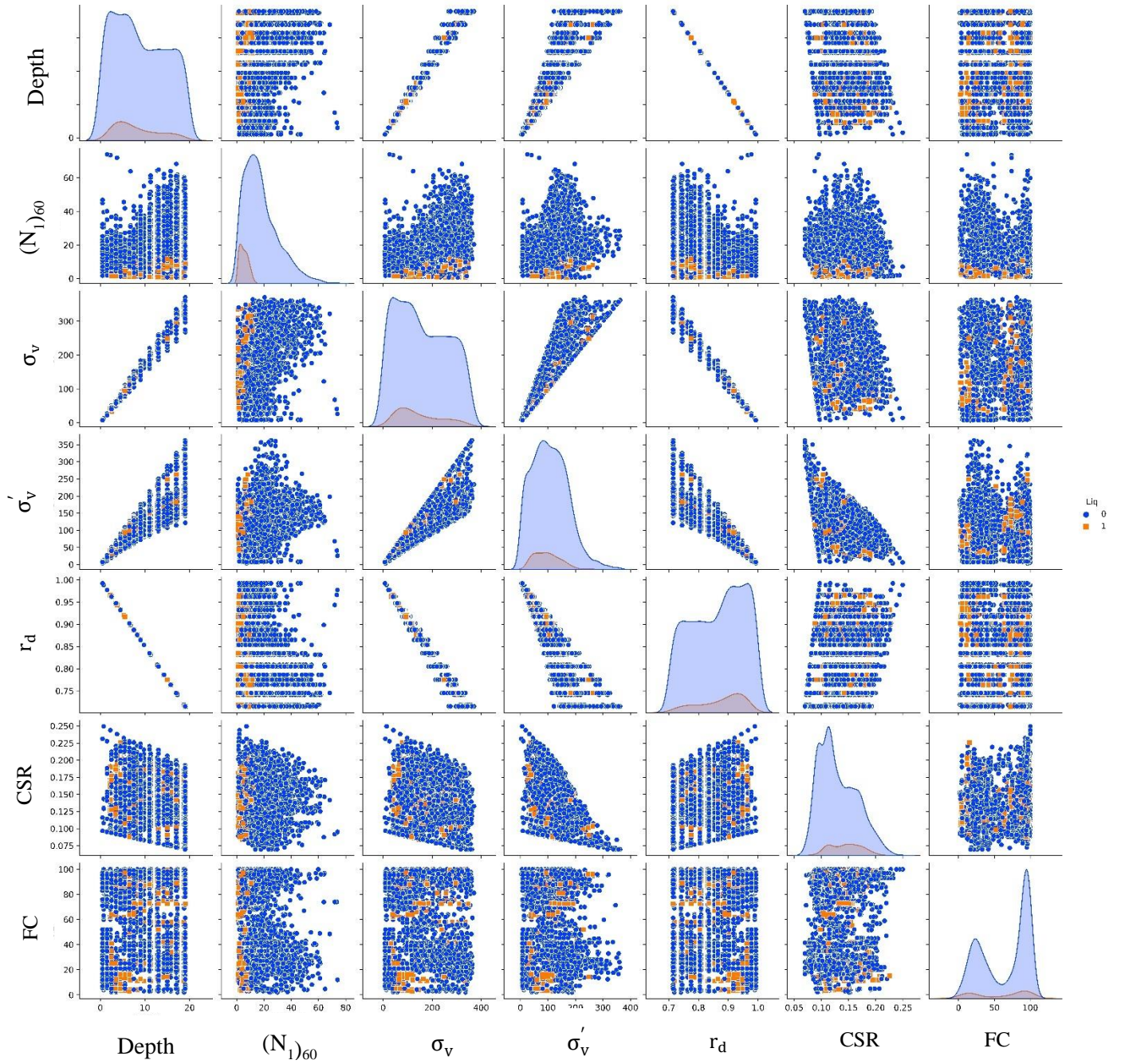
Fig. 5.1 Pair plot showing relation between features for 7 magnitude earthquake
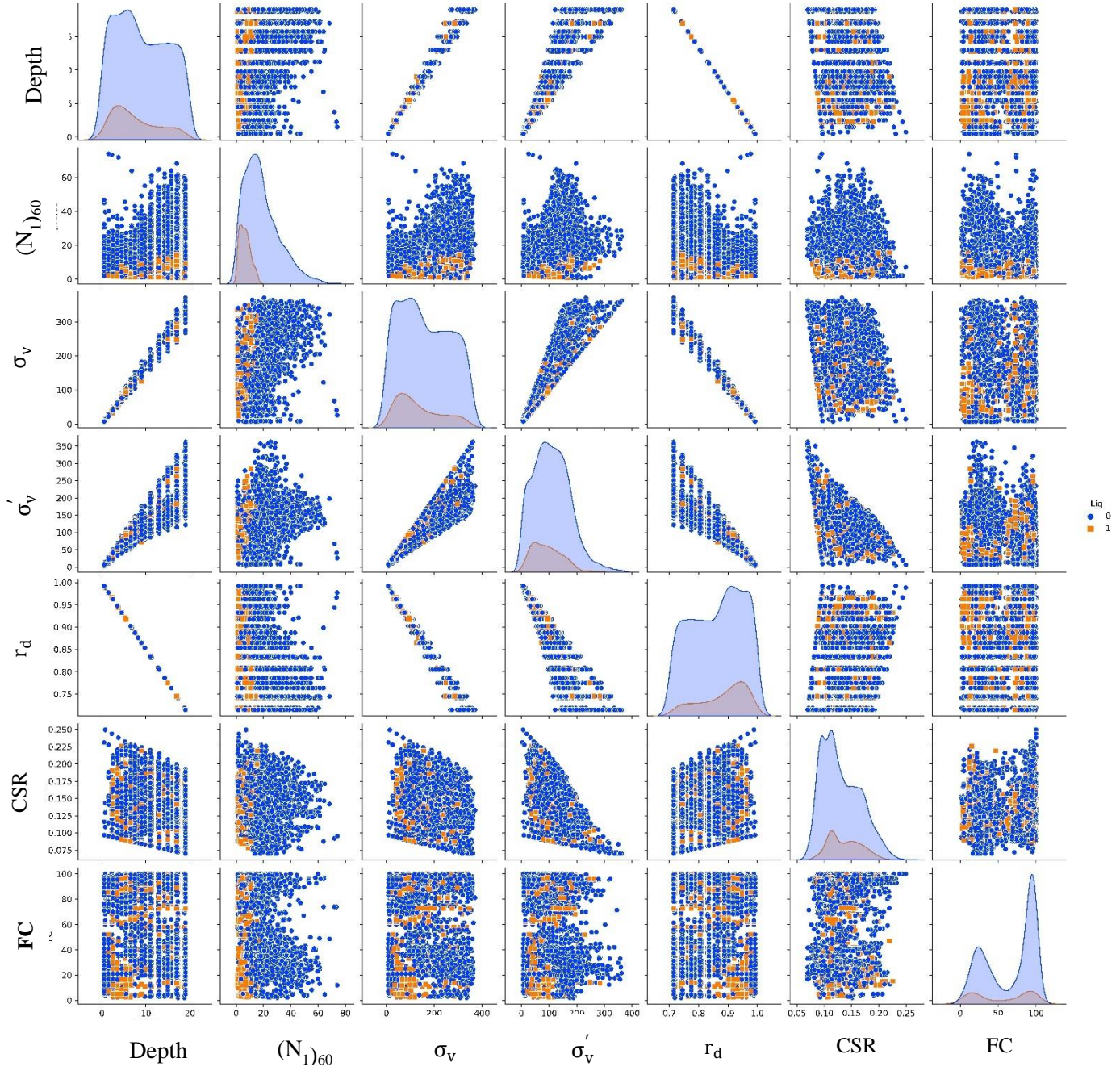
Fig. 5.2 Pair plot showing relation between features for 7.5 magnitude earthquake
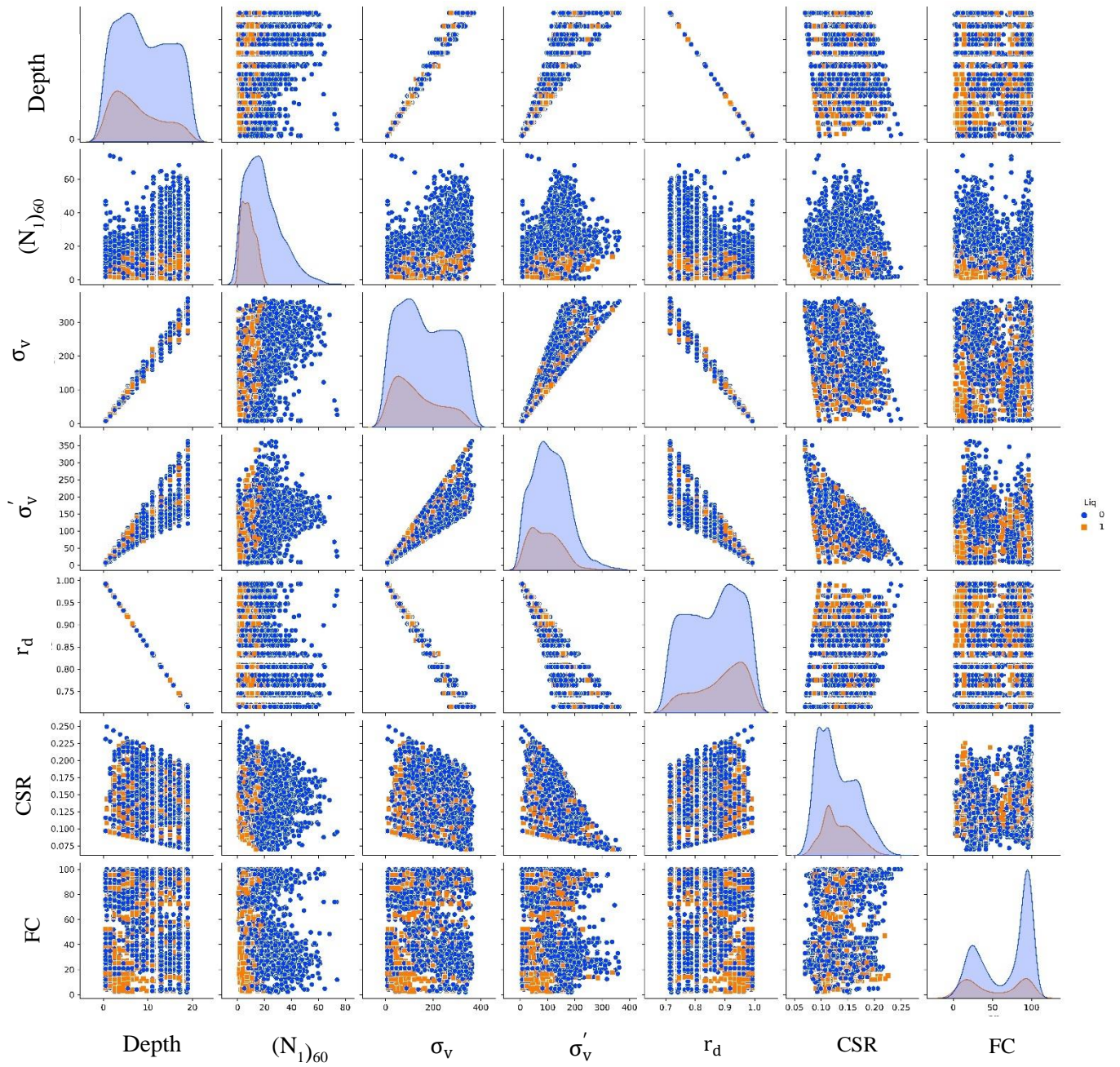
Fig. 5.3 Pair plot showing relation between features for 8 magnitude earthquake

Table 5.1 shows the various statistical parameters of all independent variables. The terms Q25% and Q75% represent the corresponding quartile values of the related variable. The statistical characteristics of each independent variable demonstrate the diversity of datasets at a suitable level.

Table 5. 1 Descriptive statistics of variables

Parameter	$N_{1(60)}$	FC	r_d	CSR
Count	3063	3063	3063	3063
Mean	16.7190	64.32	.8675	.1324
Standard Deviation	12.6078	33.3392	0.0856	0.07
Minimum	.78	2.00	.7150	0.07
Q_1	7.20	29.00	0.7862	0.11
Median	13.92	81.00	0.8762	0.13
Q_2	23.06	95.00	0.9437	0.16
Maximum	73.96	100.00	0.9925	0.37
Skewness	1.1511	-0.414	-.251	0.6809
Kurtosis	1.1873	-1.5235	-1.164	0.421

A positive skewness value indicates that the distribution of the data is skewed to the right (or positively skewed). In case of $N_{1(60)}$ since, in some of the projects such as surveys conducted by Geological Survey of Bangladesh (GSB) and Metro Rail Authority recorded SPT blow counts beyond 50 hence, some outliers were on the high end which has led to comparatively higher deviation from normal distribution. On the other hand, in the case of Fines Content (FC) more un-usual lower values than higher values illustrated by a negative skewness were observed. Since, in case of Dhaka City apart from artificially filled areas in most cases clay and silt layers within the upper 20m of soil exists. Hence, majority of the dataset contained higher percentage of fines content values. Apart from that, since stress reduction factor r_d and Cyclic Stress Ratio (CSR) are functions of depth and effective and total stresses hence, the values are much closer to normal distribution.

5.3   ROC Analysis and Confusion Matrix

As discussed in the methodology this research included the use three machine learning algorithms based on literature review of past researches in the form of Logistic Regression, Support Vector Classifier and Adaboost. Accordingly, hyperparameter tuning and K-fold cross-validation for the aforesaid machine learning algorithms were carried out. GridSearchCV was utilized to find the best hyperparameters for each algorithm and then a loop was used to test results of different numbers of folds. The cross-validation accuracy for each fold count was plotted for all three algorithms as shown in Figure 5.4, allowing us to visually identify the optimal number of folds for each.
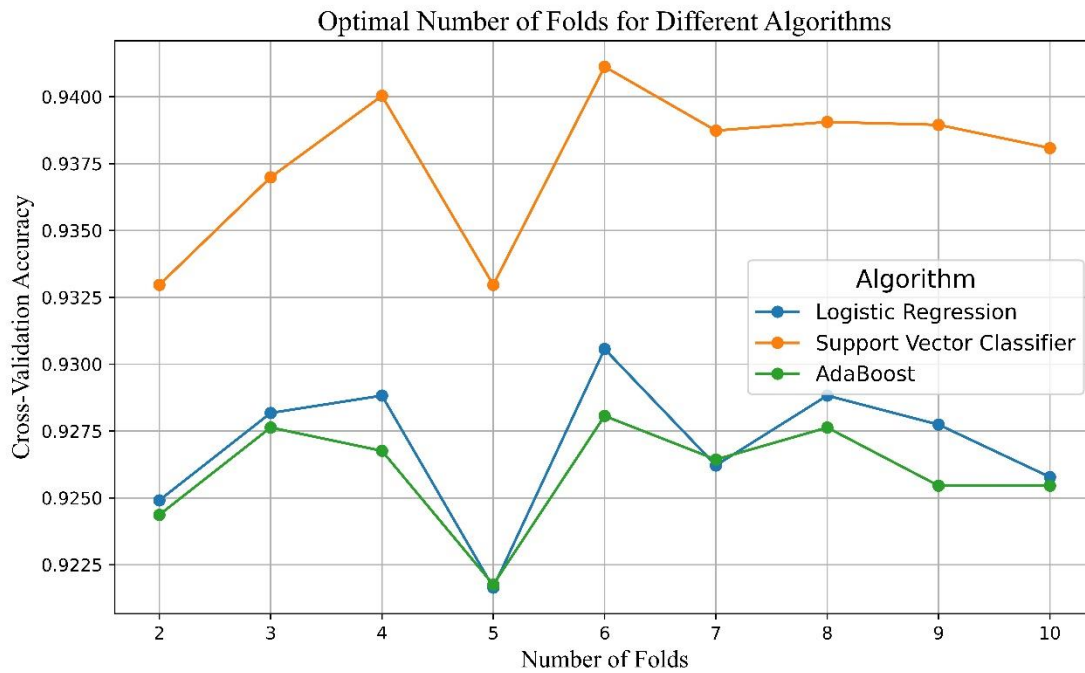
Fig. 5.4 Optimal fold number for K-fold cross validation

From the results it is evident that for the given dataset all the three algorithms follow a similar trend when compared with cross-validation score of the algorithms. Out of 10 folds, the results of considering 6 nos. of folds would yield the best results. Hence, 6 number of folds were considered as an input for K-fold cross validation as a part of determining ROC score for performance evaluation for the aforesaid algorithms.

The assessment produced certain outcomes in the form of Receiver Operating Characteristic (ROC) curve. The ROC curve demonstrates the relationship between sensitivity and false positive rate. The diagonal line on the graph signifies a 50 percent chance of accurate model prediction, while the Area Under the ROC Curve (AUC) lies between 0 and 1. The Area Under the ROC Curve (AUC) serves as a valuable quantitative measure for assessing the predictive efficacy of the model. A higher AUC value is indicative of superior predictive performance. A value closer to 1 indicates superior model performance. To summarize, the ROC curve plots sensitivity against false positive rate (Park et al., 2004). For performance evaluation purposes, an AUC value exceeding 0.7 is generally deemed acceptable.

In this study, the Logistic Regression model exhibited a mean AUC of 0.907, the mean accuracy score, F1 score and precision for the 6 folds of the cross validation were respectively 0.875, 0.512 and 0.709.
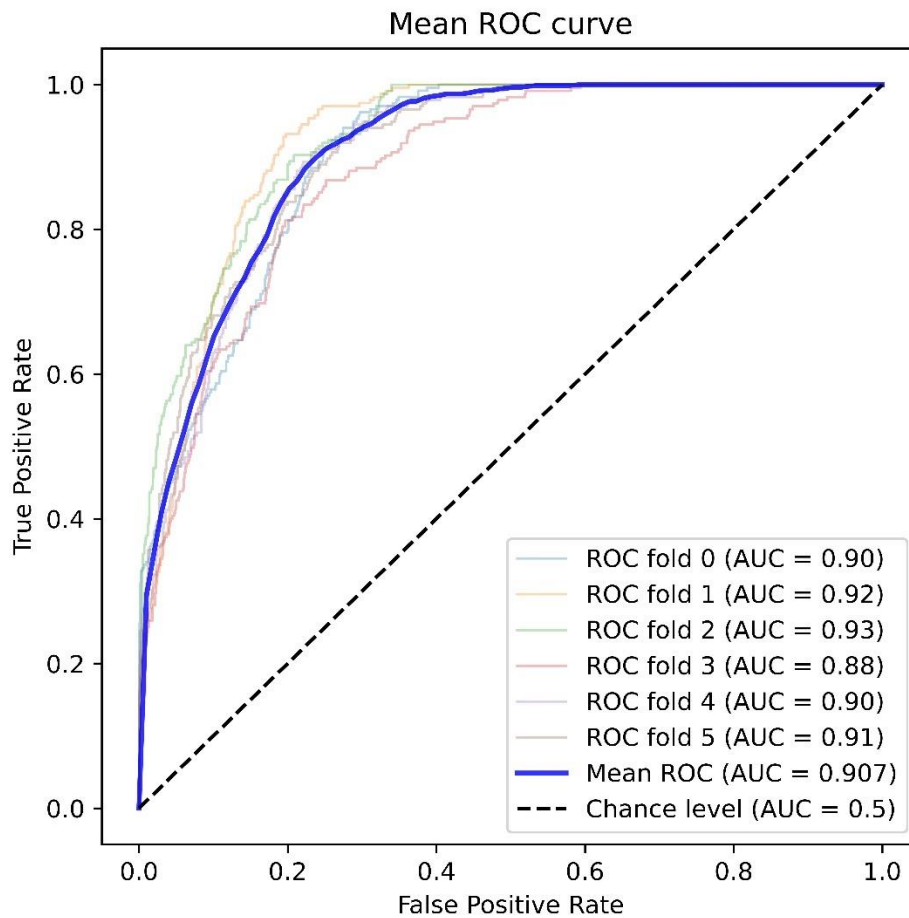
Fig. 5.5 Mean ROC curve for logistic regression

To supplement the results of the K-fold cross validation, confusion matrix for the respective folds were generated where the prediction was made based on randomly selected test train data. Since, in this study, 6 folds of test train data was used, 6 nos. of confusion matrix were generated for each algorithm.

Confusion Matrix for fold 1

	Predicted 0	Predicted 1
True 0	1295	2
True 1	169	66

Confusion Matrix for fold 2

	Predicted 0	Predicted 1
True 0	1281	15
True 1	177	59

Confusion Matrix for fold 3

	Predicted 0	Predicted 1
True 0	1237	59
True 1	100	136

Confusion Matrix for fold 4

	Predicted 0	Predicted 1
True 0	1266	30
True 1	163	72

Confusion Matrix for fold 5

	Predicted 0	Predicted 1
True 0	1109	187
True 1	61	174

Confusion Matrix for fold 6

	Predicted 0	Predicted 1
True 0	1198	98
True 1	87	148

Fig. 5.6 Confusion matrix for logistic regression

Here, in Figure 5.6, '0' denotes instances where liquefaction did not occur and '1' denotes events where liquefaction has occurred.

The SVM model achieved a mean AUC value of 0.913. The mean accuracy, F1 score and precision for the 6 folds of the cross validation were respectively 0.882, 0.530 and 0.697.
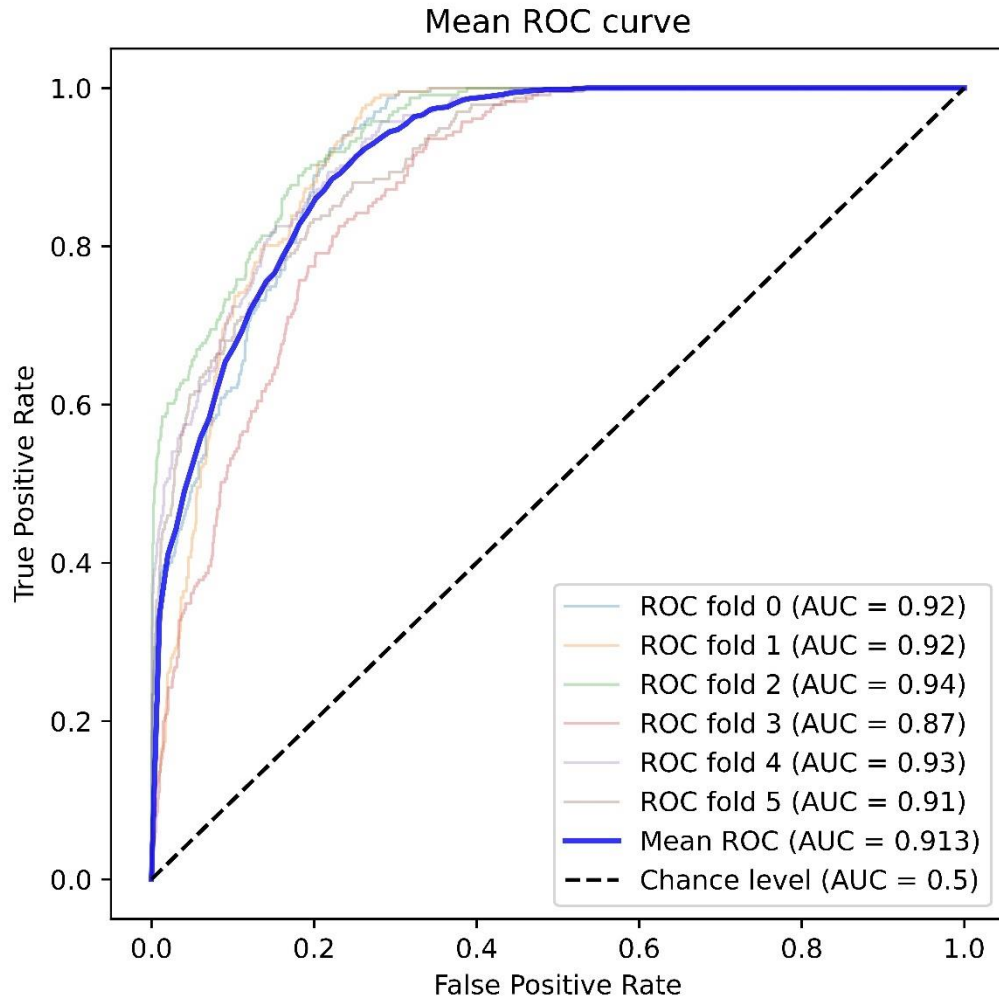
Fig. 5.7 Mean ROC curve for support vector classifier

Similarly in case of Support Vector Classifier algorithm to complement the outcomes of K-fold cross validation, confusion matrices were constructed for each fold. These matrices depicted predictions made using randomly chosen training and test datasets. Given that this analysis comprised 6 folds of such datasets, a total of 6 confusion matrices were generated for each algorithm under consideration.
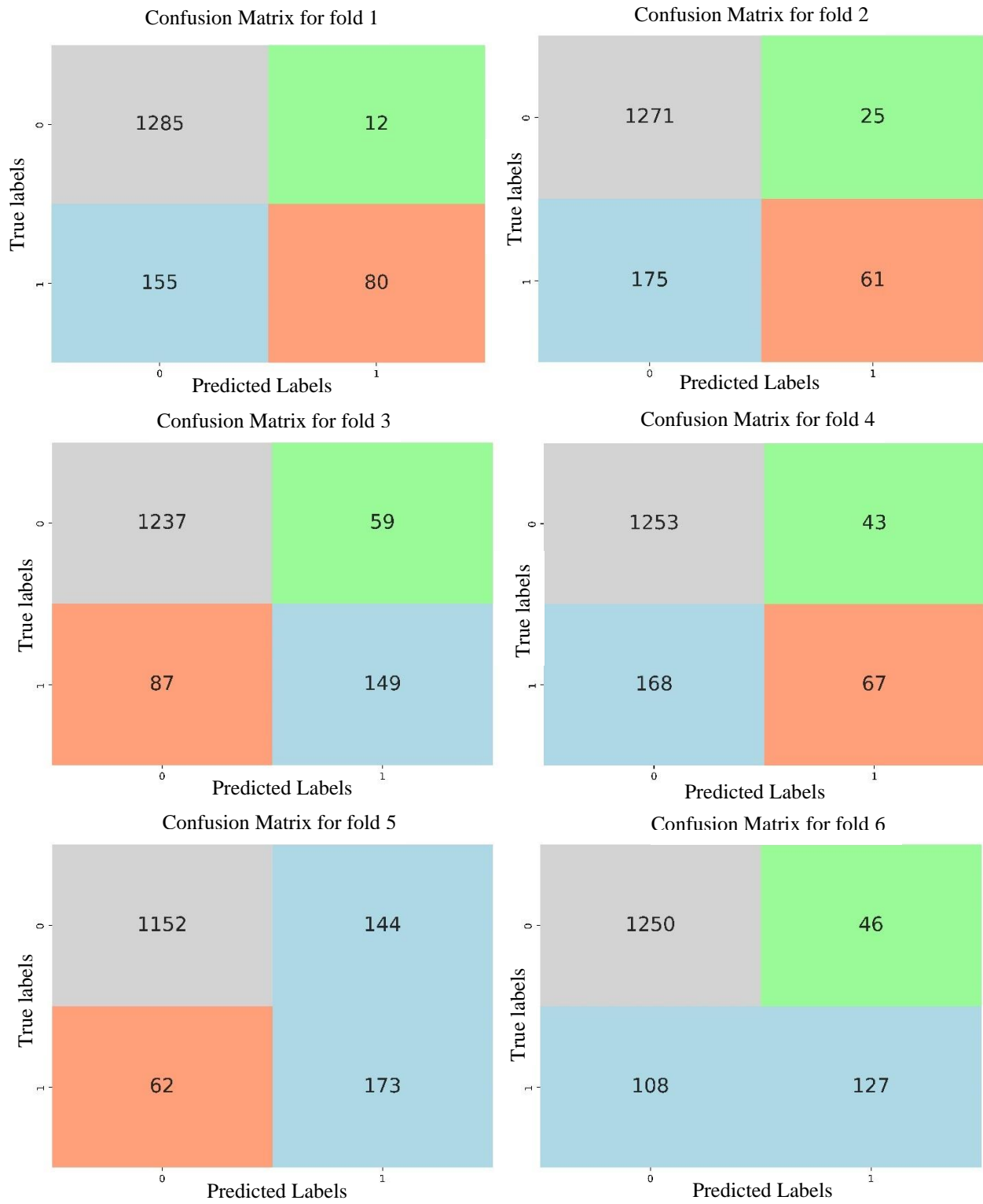
Fig. 5.8 Confusion matrix for support vector classifier

Conversely, the Adaboost model demonstrated a mean AUC score of 0.923. The average accuracy score, F1 score, and precision is respectively 0.886, 0.538 and 0.744.

The ROC curve and Confusion matrix for Adaboost algorithm is illustrated in Fig.5.9 and 5.10 respectively.
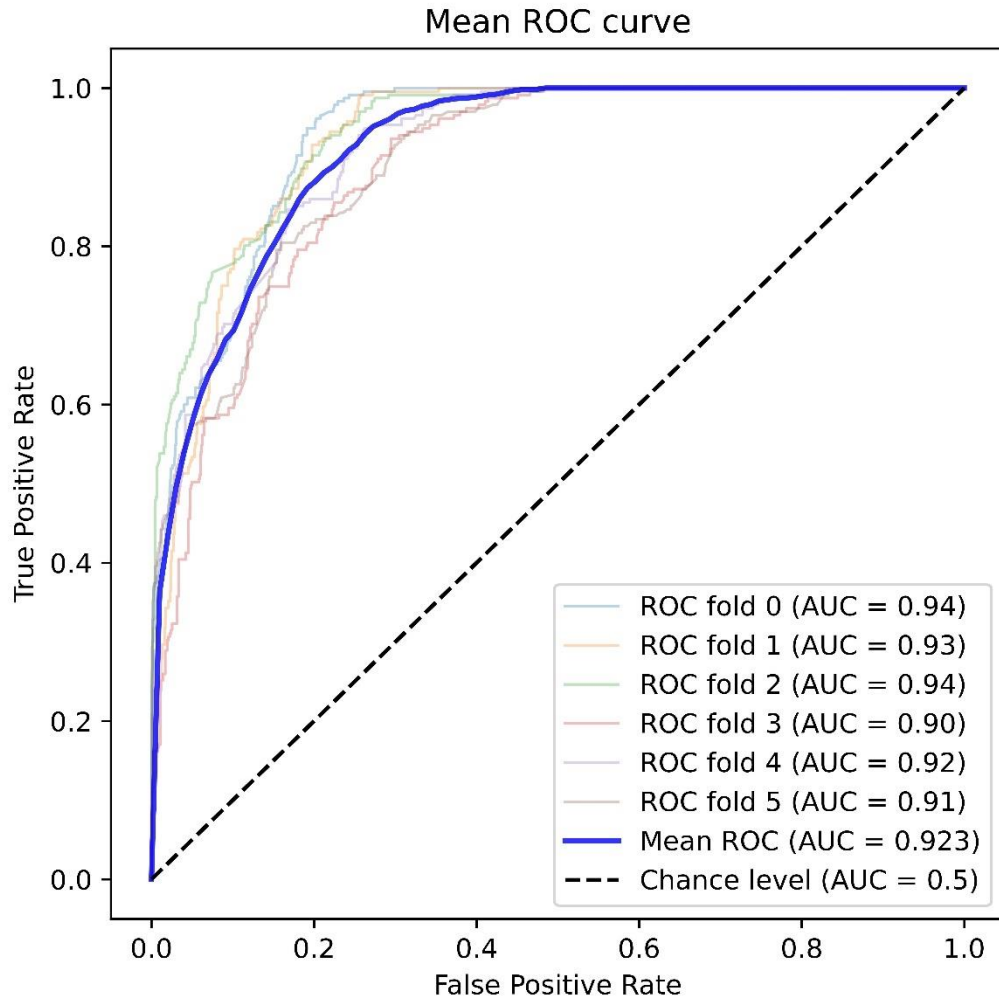
Fig. 5.9 Mean ROC curve for adaboost

Likewise, in the context of the Adaboost algorithm, development corresponding confusion matrices for each fold of the K-fold cross validation was carried out. These matrices illustrated predictions derived from randomly selected training and test datasets. Given this study involved six folds of such datasets, a collective total of 6 confusion matrices were produced for each algorithm being examined.
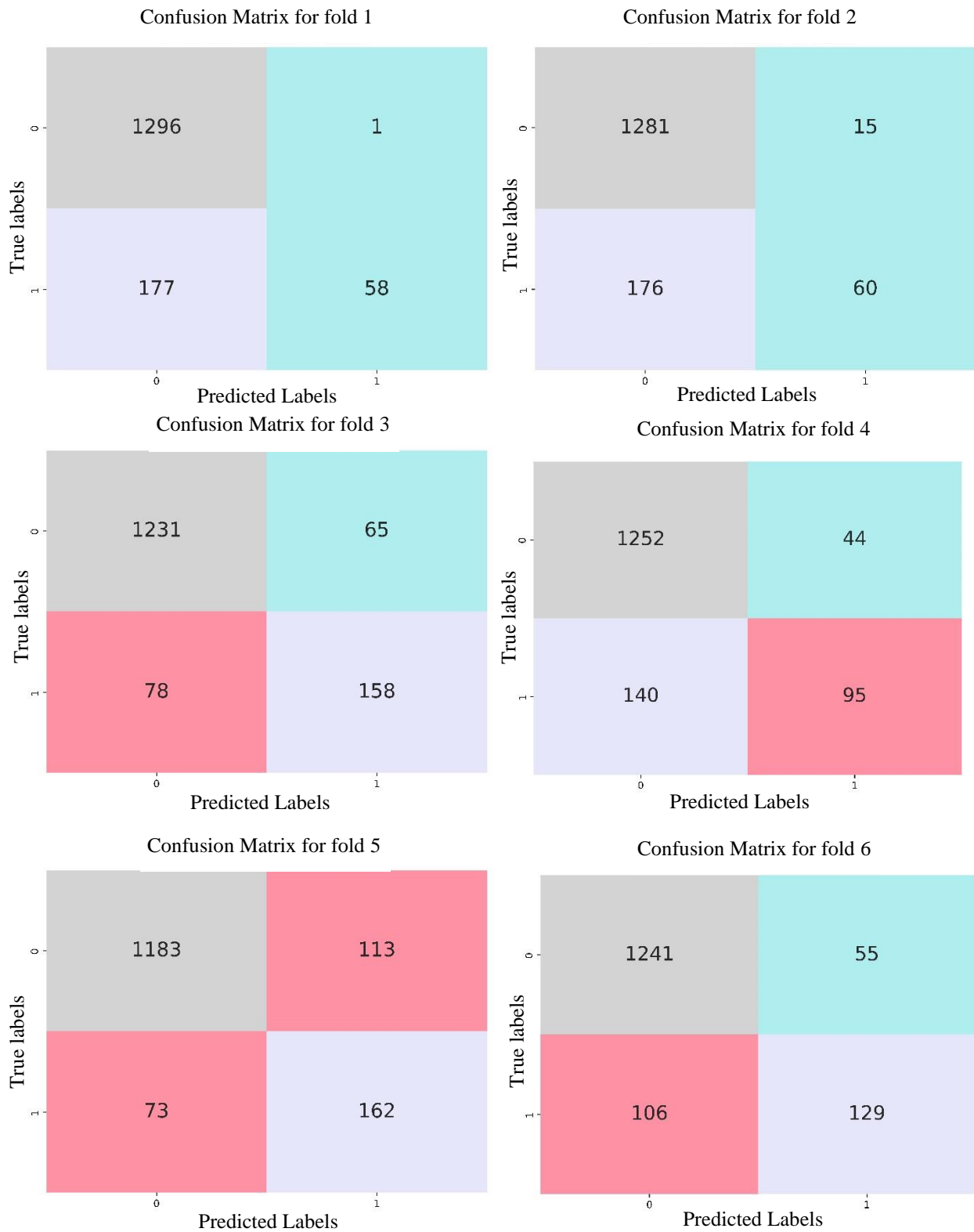
Fig. 5.10 Confusion matrix for adaboost

In the context of a Receiver Operating Characteristic (ROC) curve, an Area Under the Curve (AUC) value greater than 0.9 signifies a high level of classification accuracy for the model. An AUC value in this range suggests that the model has a strong ability to differentiate between the positive and negative classes, and it is effective at correctly ranking instances in terms of their predicted probabilities. In other words, an AUC value above 0.9 indicates that the model has a high probability of distinguishing true positives from true negatives, leading to reliable and robust predictions. In this case of all three machine learning algorithms, predicted AUC values were more than 0.9. AdaBoost yielded the best performance amongst other algorithms.

5.4   Hazard Maps

The characterization and understanding of seismic site conditions are paramount in ensuring the resilience and safety of civil infrastructure and urban environments against seismic events. Seismic site classification plays a crucial role in this endeavor, as it provides a systematic approach to categorize and depict the potential ground response to earthquakes. The primary focus of this section is twofold: the creation of seismic site classification maps predicated based on shear wave velocity of upper 30m of soil layer, and the concurrent development of liquefaction susceptibility maps based on the liquefaction potential index (LPI). Furthermore, within this section, this study emphasized the importance of taking into account varying moment magnitudes, recognizing that seismic hazards are not uniform across all scenarios. By accounting for different moment magnitudes, the liquefaction susceptibility map encompasses a broader spectrum of potential seismic scenarios, offering a more nuanced depiction of the potential risks associated with liquefaction.

Vs_{30} distribution map (Figure – 5.11) yielding in a seismic site characterization map of Dhaka City using Vs_{30} following provisions of BNBC (2020) was prepared based on the most updated database containing pertinent geotechnical information to date. The boundaries were delineated considering the Vs_{30} range specified in BNBC (2020). The current map (Figure – 5.11) supersedes the study carried out in the past (Rahman et al., 2018), which was developed according to NEHRP (National Earthquake Hazards Reduction Program, the USA) guidelines and provisions of Eurocode 8 in the absence of local mandates. The new map, in contrast, is constructed with a firm foundation in the pertinent local guidelines as defined by BNBC (2020). This transition represents a significant

advancement in seismic site characterization methodologies, leading to guidelines in following regional codes in the context of seismic site classification.
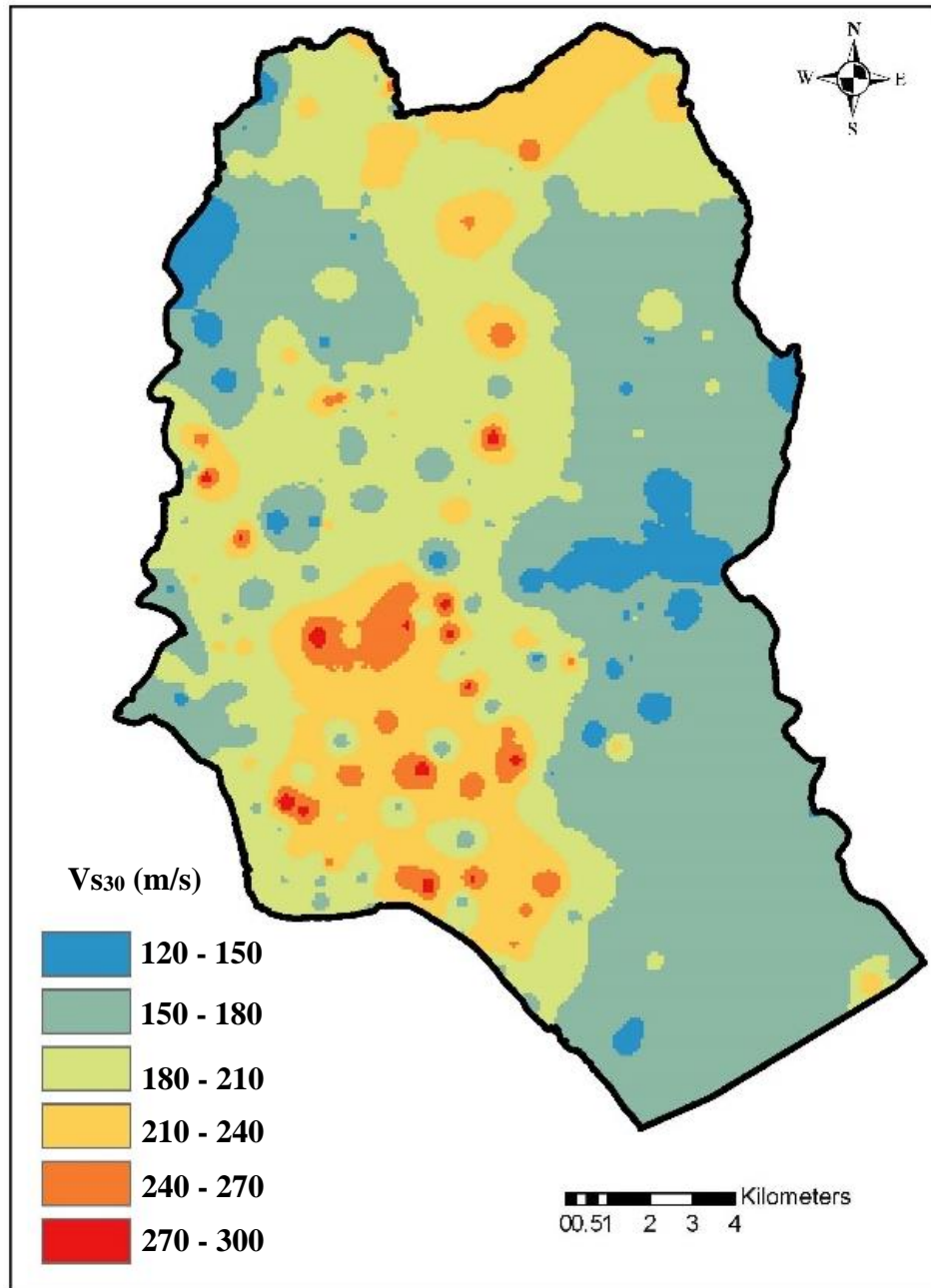
Fig. 5.11 Vs30 Distribution map of Dhaka city

In addition, a cumulative frequency distribution curve was plotted considering geotechnical investigation points lying within zones classified as Artificial Fill, Holocene Deposition and Pleistocene Deposition. (Figure – 5.12)
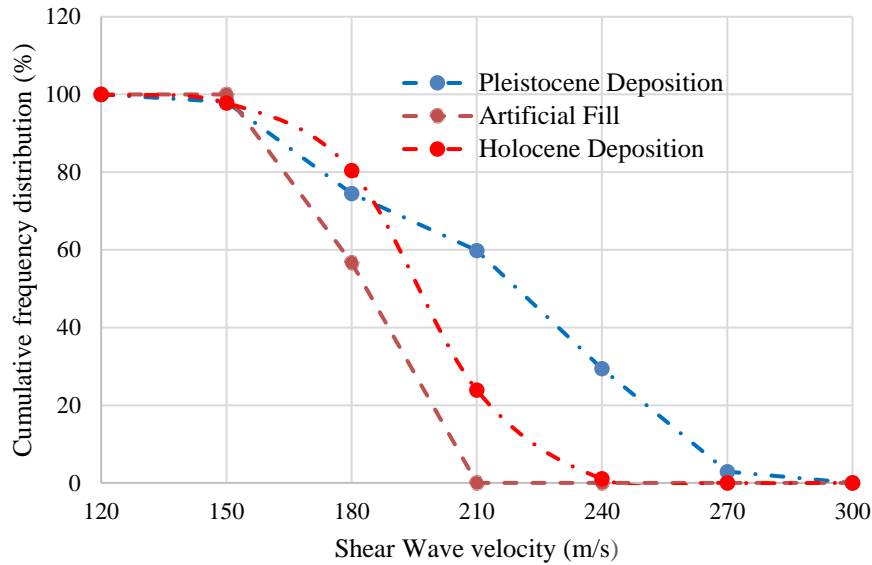
Fig. 5.12 Cumulative distribution plots for Vs_{30}

According to the results of cumilitative distribution plot for different classified geological units it has been observed that around 25%, 20% and 45% of the boreholes located within units classified as Pleistocene, Holocene and Artificial Fill have Vs_{30} values of less than 180 m/s which falls under seismic site class 'SD'. The remainder of the areas lie within seismic site class 'SC' having a range of Vs_{30} value from 180 m/s to 360 m/s according of BNBC 2020.

From the study, it has been observed that the entire study area either falls under seismic site class "SC" or "SD". According to BNBC (2020), seismic site class "SD" should be considered in the design of infrastructures in the absence of adequate site-specific information yielding in surface PGA value of 0.18 according to free field assessment conditions.

A seismic site class map generated based on Vs_{30} distribution along different stretches of the city area is shown in Figure 5.13.
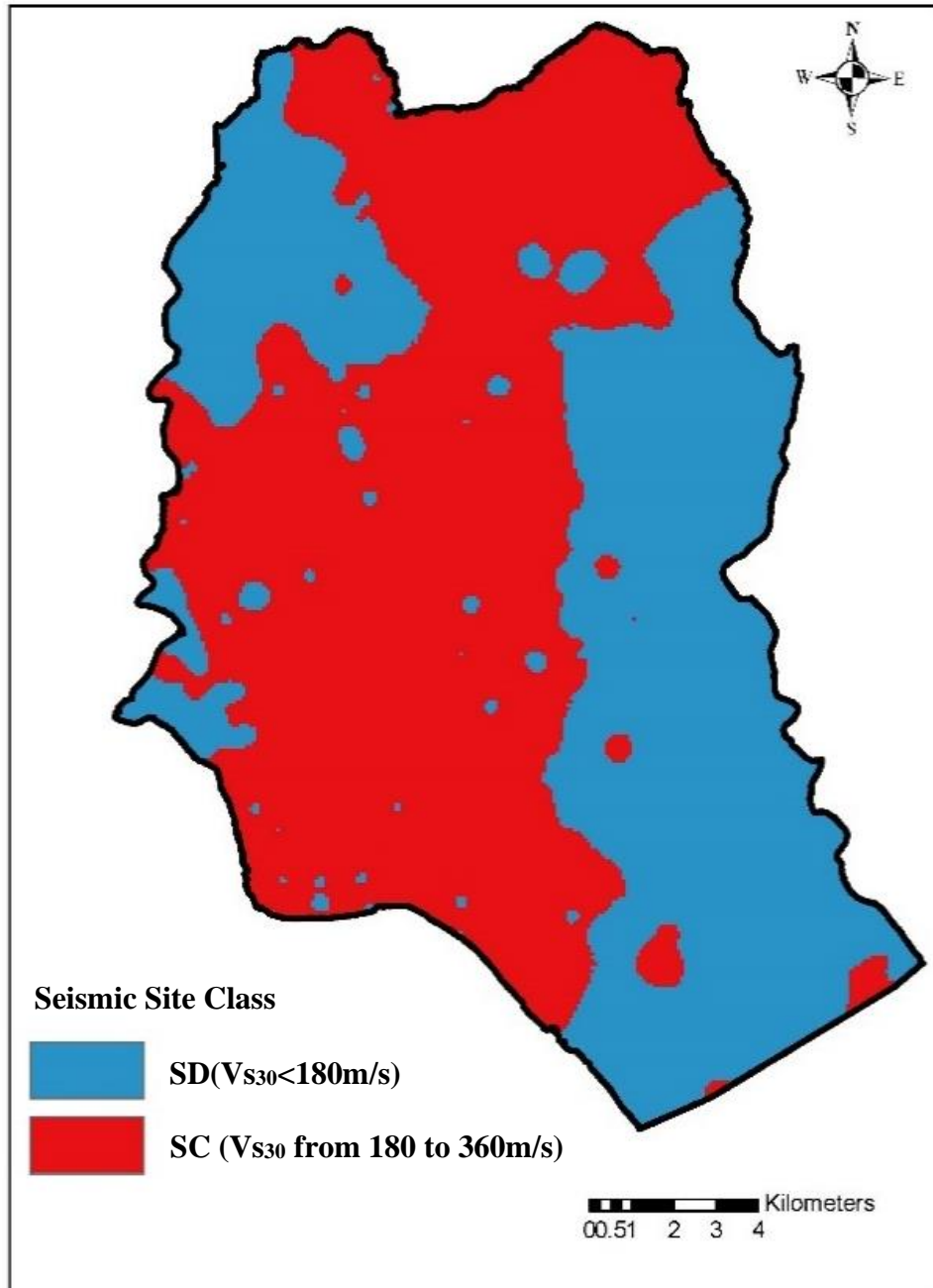
Fig. 5.13 Seismic site class map of Dhaka city according to BNBC (2020)

The seismic site class map (Figure – 5.13) showed that a significant amount of area falls under seismic site class "SD" in the south-eastern parts of the city, which was previously classified as seismic site class "D" as per NEHRP guidelines which is equivalent to site class "SC" according to BNBC (2020) which is expected to address major changes in the seismic design considertation

for the aforementioned region. Apart from that, the map also supplements liquefaction susceptibility calculation for addressing PGA value in absence of site specific data.

Based on the liquefaction potential index (LPI) evaluated at each drill-hole location, maps (Figure 5.14, 5.16, 5.18) for delineating LPI in unsampled locations within the domain of Dhaka City boundary was generated for different seismic scenerios in the form of 7, 7.5 and 8 magnitude earthquakes.
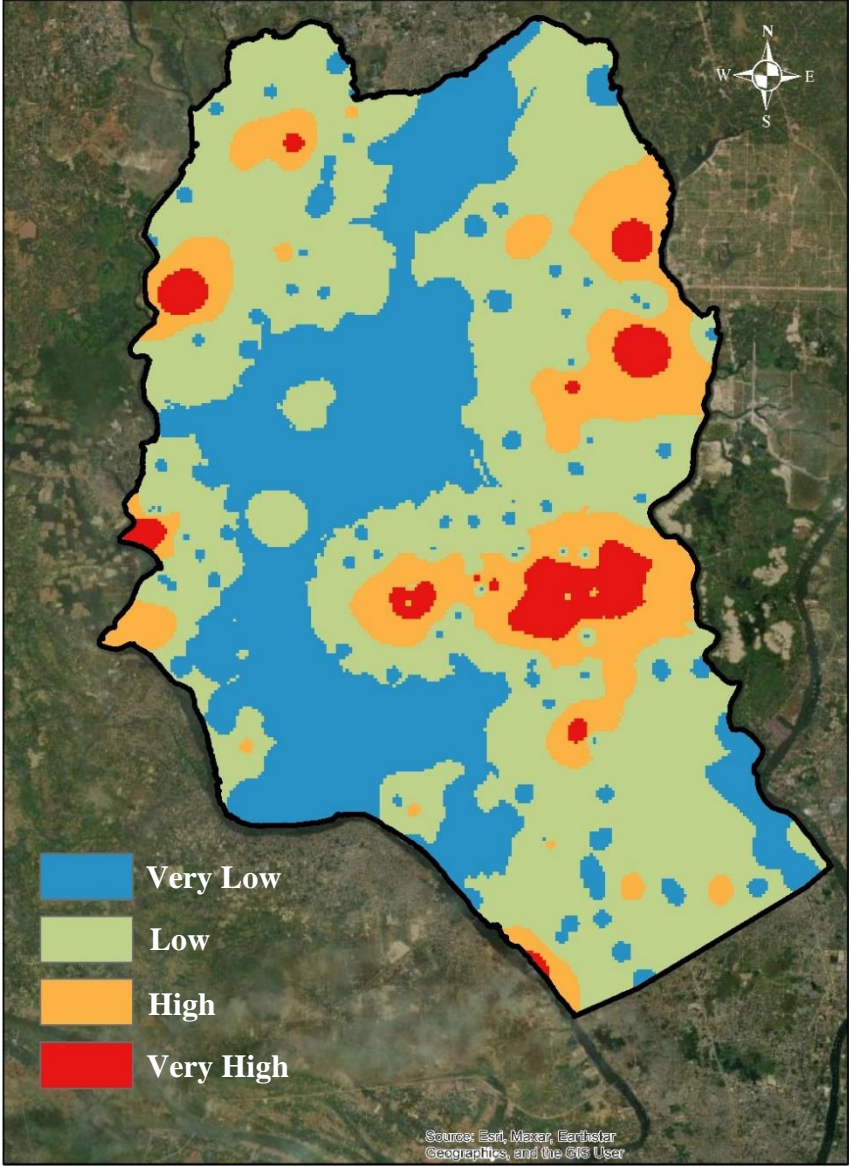
Fig. 5.14 Liquefaction susceptibility map of Dhaka city for Mw 7.0

Subsequently, based on Iwasaki's (1982) proposed range for very low , low , high and very high susceptibility, boundaries were outlined for each respective zone within the city area. The following map shows liquefaction suscptibility of Dhaka City for moment magnitude of 7.0.

The results for a moment magnitude of 7.0 showed that around 4% of the areas within the city boundary lie in a very highly susceptible zone. On the other hand, high, low and very low susceptible zones cover around 15%, 50% and 31% of the city area. Most of the areas underlain by Pleistocene deposition lie within low to very low susceptible areas.

Cumulative distribution plots for Liquefaction Potential Index were also plotted for different geological conditions which is shown in Figure – 5.15, 5.17 and 5.19 for different scenerio earthquake conditions.
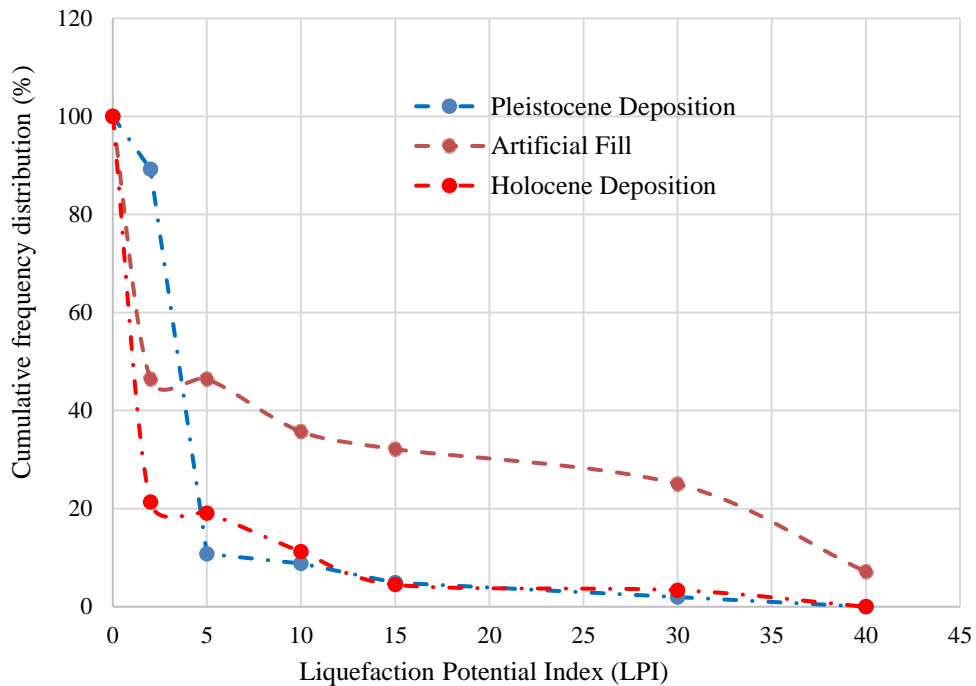
Fig. 5.15 Cumulative distribution plots for LPI considering Mw 7.0

According to Holzer (2006, 2008) threshold value for the surface manifestation of liquefaction based on the liquefaction potential index (LPI) is considered 5. The cumulative distribution curve illustrates that 46% of the sites located within the Artificially filled areas have LPI values higher than 5. On the other, the percentage is 19% and 10%, respectively, for Holocene and Pliestocene

depositions. The investigation points for Artificial Fill, Holocene Deposition and Pleistocene Deposition were 30, 92 and 102 numbers. It is to be mentioned here that according to Iwasaki (1982), zones susceptible to very high liquefaction is considered to have an LPI value of 15 or more. Considering that as a threshold limit for high susceptibility, the percentage of Artificial Fill, Holocene Deposition and Pleistocene Deposition were respectively 32%, 5% and 5%.
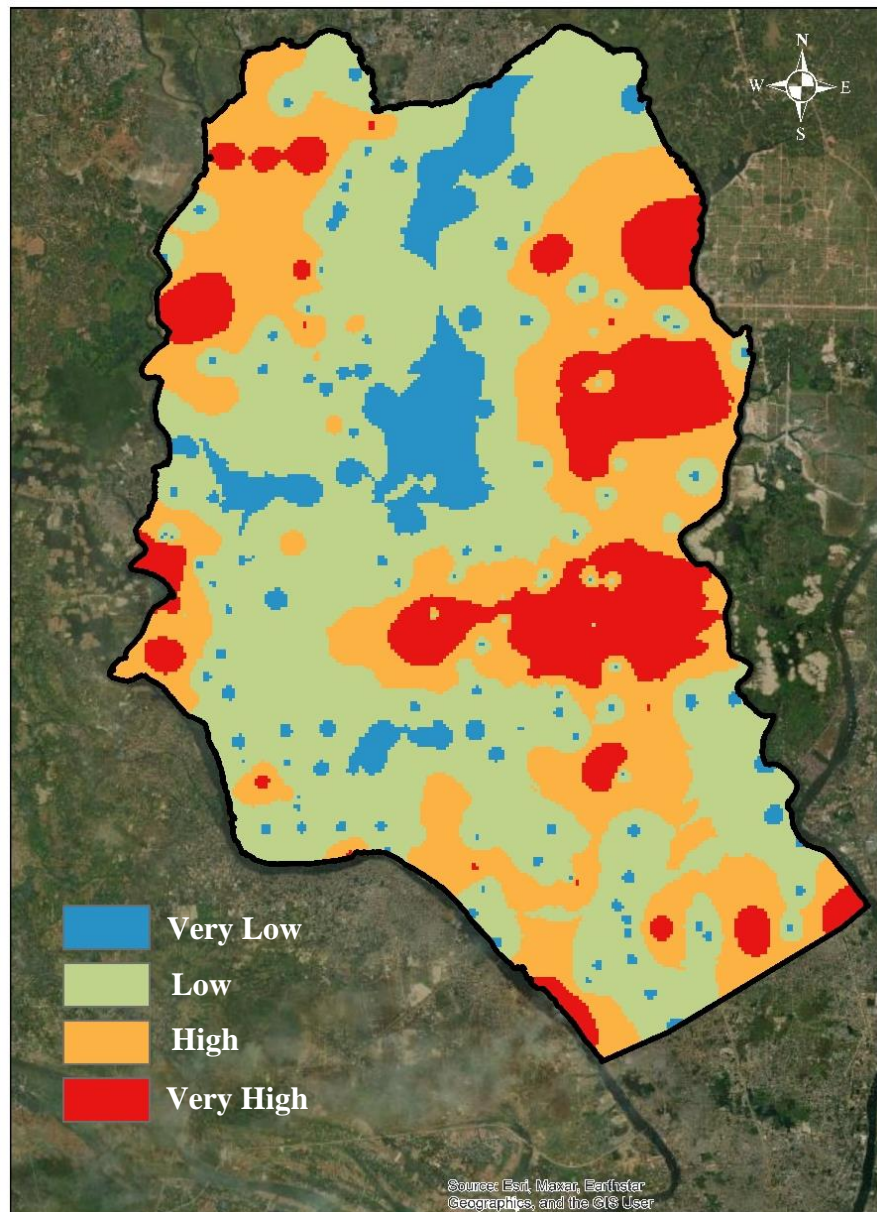
Fig. 5.16 Liquefaction susceptibility map of Dhaka City for Mw 7.5

On the other hand the results, for 7.5 magnitude earthquake illustrated in Figure 5.16 depicits around 9% of the areas within the city boundary lie in a highly susceptible zone. Subsequently, high, low and very low susceptible zones cover around 32%, 50% and 9% of the city area. Most of the areas underlain by Pleistocene deposition lie within low to very low susceptible areas. At the same time, the areas composed of Artificial fill and Holocene alluvium lie with high to very highly susceptible liquefaction-prone regions.

Cumulative distribution plots for 7.5 magnitude earthquake prepared on the basis of Liquefaction Potential Index for different geological conditions is shown in Figure – 5.17.
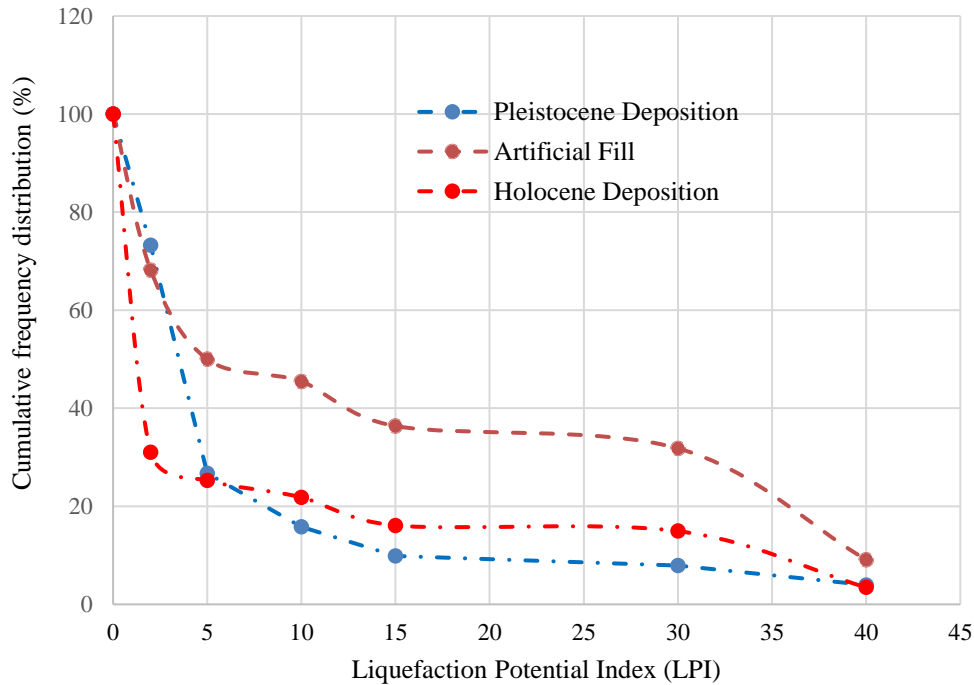
Fig. 5.17 Cumulative distribution plots for LPI considering Mw 7.5

The cumulative distribution curve demonstrates that 50% of the sites situated within artificially filled zones exhibit LPI values surpassing the threshold of 5. Conversely, this percentage amounts to 27% and 23% for sites characterized by Pleistocene and Holocene depositional contexts, respectively. On the other hand, employing LPI value of 15 as a threshold criterion for very high susceptibility the percentage of Artificial Fill, Holocene Deposition and Pleistocene Deposition were respectively 36%, 16% and 10%.
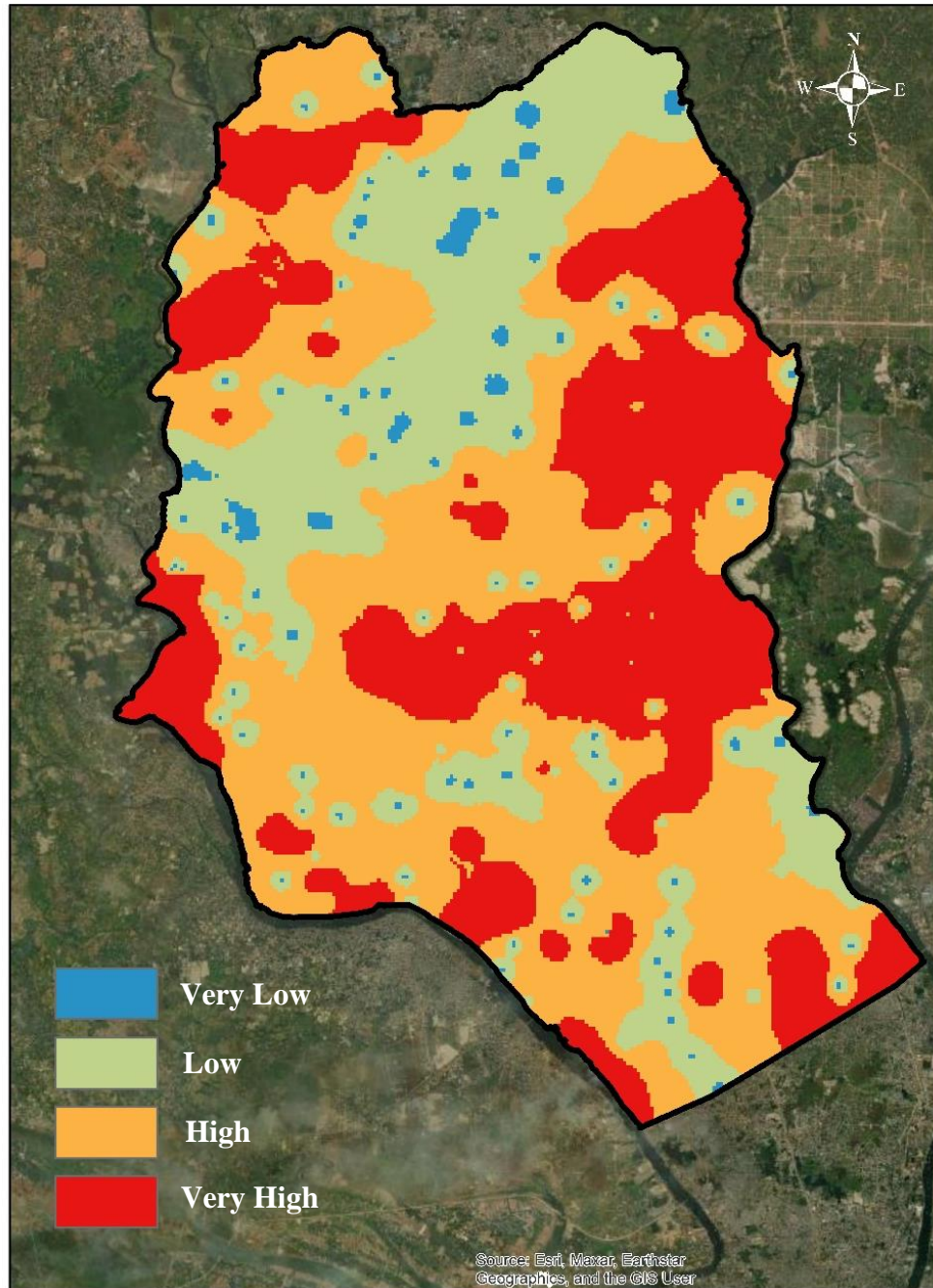
Fig. 5.18 Liquefaction susceptibility map of Dhaka city for Mw 8

In contrast, the outcomes pertaining to a seismic event of magnitude 8.0, as depicted in Figure 5.18, reveal that approximately 30% of the geographical expanse within the city's periphery occupies a highly vulnerable classification. Conversely, zones characterized by high, low, and very low susceptibility encompass approximately 42%, 26%, and 2% of the urban landscape, respectively. It is noteworthy that the majority of the zones characterized by artificial fill

73

predominantly reside within the ambit of high to very highly susceptible categories within liquefaction-prone regions.
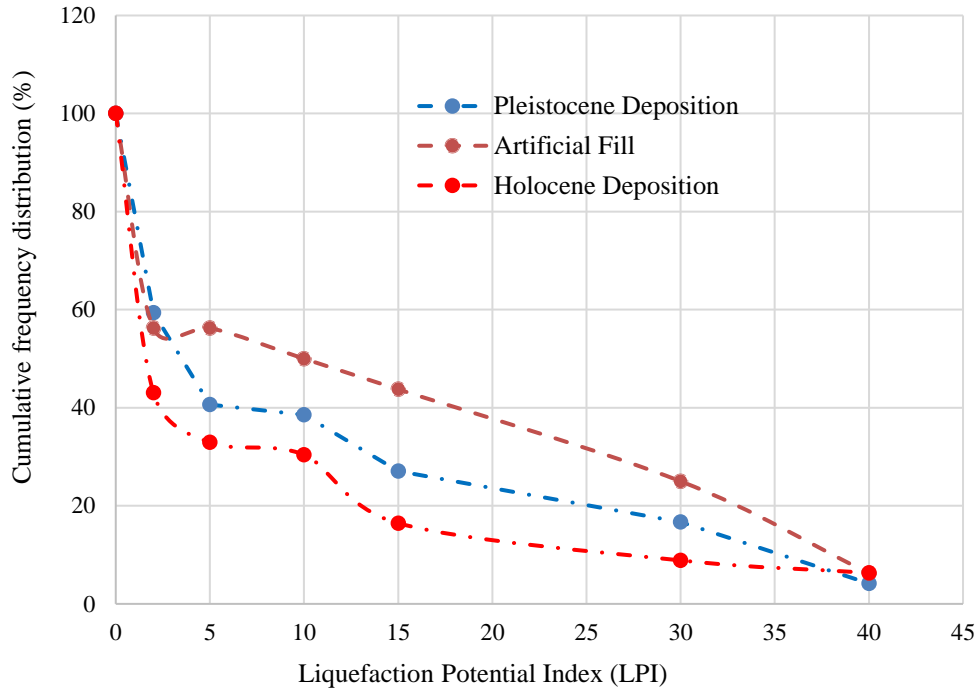
Fig. 5.19 Cumulative distribution plots for LPI considering Mw 8

The cumilative distribution curve provides a graphical representation illustrating that 56% of the sites positioned within areas with artificially filled deposits manifest LPI values that exceed the established threshold of 5. Conversely, these proportions translate to 40% and 33% for sites encompassing Pleistocene and Holocene depositional contexts, respectively. In parallel, employing an LPI value of 15 as a threshold criterion indicative of very high susceptibility, the corresponding proportions for Artificial fill, Holocene deposition, and Pleistocene deposition were determined as 44%, 16%, and 27%, respectively. In contrast to the results, of 7.0 and 7.5 magnitude earthquake it is to be mentioned here is that higher percentage of boreholes lying within Pleistocene depistion is likely to liquefy for a ground shaking of 8.0 magnitude earthquake compared to the results of boreholes lying within Holocene deposition.

CHAPTER 6: CONCLUSIONS AND RECOMMENDATIONS

6.1   General

In this comprehensive exploration of Dhaka City's susceptibility to liquefaction, the research delved deep into the city's geological and seismological intricacies. From identifying vulnerable zones to evaluating the city's geological performance, the findings shed light on the pressing need for proactive measures. As the conclusion navigates through the key findings, framework and recommendations, the aim is to provide a roadmap that not only addresses the current challenges but also paves the way for a safer, more resilient Dhaka.

6.2   Key Findings

In an attempt to unveil the seismic vulnerabilities associated with soil liquefaction the following are the findings that have been outlined under the current study which not only will identify the threats associated with soil liquefaction but also propel the discourse towards strategic planning, informed policymaking, and the adoption of robust assessment methodologies to navigate through the seismic challenges ahead.

    i.   **Vulnerable Areas:** The results of the current study show that areas near the eastern fringes of the city area which is also the cross-passage of some major ongoing projects such as Dhaka Metro Rail (Line – 1 and Line – 5), Dhaka Amula Demra Expressway, as well as residential development projects in Bashundhara and Aftabnagar, have a liquefaction potential index of more than 15 coupled with a shear wave velocity of less than 180 m/s which may trigger amplification of surface PGA value. On the other hand, compared to past studies, the coverage area of seismic site class "SD" is substantially higher within the city boundary, which requires special moment resisting frames for infrastructural development as per BNBC (2020).

    ii.   **Performance Evaluation:** In this study, it was observed that the classification performance evaluation cannot be done using only performance indicators. Techniques like ROC curves and confusion matrices are also better ways to assess the classification capability and model

validation in the field of liquefaction susceptibility prediction. Also, selection of appropriate number of folds for the cross validation is a must as a measure of deviation from the prediction based on outcome of different algorithms.

iii. **Effects of Geological Age:** A number of researchers have observed that liquefaction potential tends to decrease as age increases. Based on the observations the liquefaction susceptibility of sediments placed in the last hundred years are more susceptible to liquefaction than early Holocene sediments, hence Pleistocene sediments are significantly more resistant. Pre-Pleistocene sediments are considered to present a low liquefaction risk. According to the current study, the oldest deposition type was of Pleistocene age which even though is lesser susceptible compared to Holocene and Artificial fill type deposition however, the likelihood of potentiality to liquefaction still exists as illustrated in the results of cumulative distribution plots for 8 magnitude earthquakes. This can be also supplemented by the historical events such as Assam Earthquake 1897 (Oldham, 1899), San Fransisco earthquake 1906 (Youd, 1971), Bihar – Nepal earthquake 1934 (Roy, 1934) etc.

iv. **Over estimation of stress Reduction factor:** In reality earthquake induced stresses tend to denude with respect to depth depending upon the dynamic properties of soil. In absence of relevant geotechnical information related to dynamic properties of soil, BNBC (2020) have adopted a very conservative linear equation for evaluation of stress reduction factor, r_d which has been developed based on researches conducted in Japan. Even though the current study provides a guideline to integrate latest liquefaction assessment techniques with BNBC (2020) specified stress reduction parameters however, further studies are necessary for developing such factors in regional perspective.

v. **Policies for Framework:** The research primarily aimed to devise a comprehensive framework for evaluating the liquefaction susceptibility of the study area through an integrated approach, which encompassed utilizing current geotechnical data, calculating seismic site class per BNBC(2020), characterizing seismic site class and evaluating PGA value accordingly, assessing Cyclic Stress and Resistance Ratios using seismic and geotechnical data, categorizing liquefaction susceptibility outcomes, evaluating performance

via machine learning indicators, and employing geostatistical interpolation to formulate vulnerability maps. Based on the processes adopted for development of liquefaction hazard map for Dhaka city the following recommendations can be made for regulatory adoption at policy level

1. **Mandatory Assessment:** Make it mandatory to conduct site specific seismic assessment for regions identified as high-risk areas to undergo liquefaction susceptibility assessment before any major construction or infrastructure development. In addition, prioritization of assessments based on the potential impact on human settlements, critical infrastructure, and economic hubs is necessary.

2. **Regular Updates:** Ensure that the hazard maps and geotechnical database is updated regularly, especially after major seismic events or when new geotechnical data becomes available. A five-year scheme may be adopted for periodic upgradation of the geotechnical data.

3. **Public Awareness:** Educate the public, real estate organizations and practitioners about the risks associated with liquefaction and the importance of adhering to the guidelines and recommendations of the regional building codes.

4. **Collaboration:** Collaborate with international bodies and experts to stay updated with the latest methodologies and best practices in liquefaction susceptibility assessment and stay up to date for any latest upgradation process associated with evaluation of liquefaction susceptibility.

5. **Training:** Provide training to local engineers, geologists, and urban planners on the methodologies and tools used in the assessment.

Adopting these policies for liquefaction susceptibility assessment on a regulatory basis will ensure that regions are well-prepared and resilient against the risks associated with seismic activities. It will also provide a comprehensive, data-driven, and scientifically robust approach in understanding and mitigating the potential impacts of liquefaction.

6.3   Limitations and Recommendations for Future Studies

The research undertaken provides a comprehensive and in-depth analysis of the liquefaction susceptibility, with a particular focus on Dhaka City. Several key findings in the form of vulnerable

hotspots, potential areas of improvement in the newly published BNBC (2020) provisions (particularly concerning the linear equation for evaluating stress reduction factor), effects of geological age etc. have been addressed under the study. However, in absence of dynamic properties of soil in the context of Dhaka City it was not possible to conduct seismic site response analysis for the investigation points. Hence, for future studies it is necessary to establish region specific shear modulus reduction and damping curves according to soil type by means of conduction of adequate amount of cyclic tri-axial tests which will feed as an input parameter for site response analysis and development of region-specific stress reduction factor. In addition, water table was also reported from the borehole data which is usually measured at an interval 24 hours after completion of drilling which may not represent the ground realities. Also, application of artificial intelligence in the form of different machine learning algorithms is a data driven procedure which may lead to different outcome for different datasets. Hence, further research on application of such algorithms using different types of datasets including observed liquefaction case history record is essential to produce better outcome. It may also be mentioned that the current research uses a deterministic evaluation technique for liquefaction mapping. Further studies are recommended to be carried out based on probabilistic boundaries defined by different researchers.

Nevertheless, the proposed framework, which integrates regional factors, up-to-date geotechnical data and historical seismotectonic information, offers a holistic approach to evaluating liquefaction susceptibility. The use of machine learning algorithms further enhances the accuracy and reliability of the assessment. The subsequent development of a liquefaction hazard map for Dhaka City, based on this framework is a testament to its effectiveness. By following the proposed regulatory guidelines Dhaka can become a highly disaster resilient city from being a highly vulnerable disaster-prone city.

REFERENCES

Andrus, R.D. and Stokoe II, K.H., 2000. Liquefaction resistance of soils from shear-wave velocity. *Journal of geotechnical and geoenvironmental engineering*, *126*(11), pp.1015-1025.

Andrus, R.D. and Stokoe, K.H., 1999. Liquefaction resistance based on shear wave velocity.

Andrus, R.D., Chung, R.M., Juang, C.H. and Stokoe, K.H., 2003. *Guidelines for evaluating liquefaction resistance using shear wave velocity measurement and simplified procedures*. US Department of Commerce, National Institute of Standards and Technology.

Andrus, R.D., Fairbanks, C.D., Zhang, J., Camp III, W.M., Casey, T.J., Cleary, T.J. and Wright, W.B., 2006. Shear-wave velocity and seismic response of near-surface sediments in Charleston, South Carolina. *Bulletin of the Seismological Society of America*, *96*(5), pp.1897-1914.

Andrus, R.D., Mohanan, N.P., Piratheepan, P., Ellis, B.S. and Holzer, T.L., 2007, June. Predicting shear-wave velocity from cone penetration resistance. In *Proceedings of the 4th international conference on earthquake geotechnical engineering, Thessaloniki, Greece* (Vol. 2528).

Anbazhagan, P., Basavaraj, S. and Premalatha, K.V., 2011. Liquefaction hazard mapping of Chennai, India using SPT data.

Ansari, A., Zahoor, F., Rao, K.S. and Jain, A.K., 2023. Seismic response and vulnerability evaluation of Jammu Region (Jammu and Kashmir). *Indian Geotechnical Journal*, *53*(3), pp.509-522.

Ansary, M.A. and Rashid, M.A., 2000, July. Generation of liquefaction potential map for Dhaka, Bangladesh. In *8th ASCE Specialty Conference on Probabilistic Mechanics and Structural Reliability* (pp. 24-26).

Ashikuzzaman, M., Hossain, A. and Salan, M.S.A., 2023. Liquefaction Assessment of Rajshahi City Corporation, Bangladesh. *Indian Geotechnical Journal*, *53*(2), pp.455-464.

Arulmoli, K., Arulanandan, K. and Seed, H.B., 1985. New method for evaluating liquefaction potential. *Journal of Geotechnical Engineering*, *111*(1), pp.95-114.

Al-Hussaini, T.M., Hossain, T.R. and Al-Noman, M.N., 2012. Proposed changes to the geotechnical earthquake engineering provisions of the Bangladesh National Building Code. *Geotechnical Engineering Journal of the SEAGS & AGSSEA*, *43*(2), pp.1-7.

AASHTO., 2017. LRFD Bridge Design Specifications, Seventh Edition, American Association of State Highway and Transportation Officials, Washington, DC

Asaduzzaman, A.T.M., Nasreen, N. and Olsen, H., 1999. Urban geology of Dhaka, Bangladesh. *Atlas of urban geology*, *11*.

Akhter, S.H., 2010. Earthquakes of dhaka. *Environment of Capital Dhaka—Plants wildlife gardens parks air water and earthquake. Asiatic Society of Bangladesh*, pp.401-426.

Anderson, J.G., Lee, Y., Zeng, Y. and Day, S., 1996. Control of strong motion by the upper 30 meters. *Bulletin of the Seismological Society of America*, *86*(6), pp.1749-1759.

An, T.K. and Kim, M.H., 2010, October. A new diverse AdaBoost classifier. In *2010 International conference on artificial intelligence and computational intelligence* (Vol. 1, pp. 359-363). IEEE.

Boulanger, R.W. and Idriss, I.M., 2016. CPT-based liquefaction triggering procedure. *Journal of Geotechnical and Geoenvironmental Engineering*, *142*(2), p.04015065.

Brankman, C.M. and Baise, L.G., 2008. Liquefaction susceptibility mapping in Boston, Massachusetts. *Environmental & Engineering Geoscience*, *14*(1), pp.1-16.

Boulanger, R.W. and Idriss, I.M., 2014. CPT and SPT based liquefaction triggering procedures. *Report No. UCD/CGM.-14*, *1*.

Bolt, B.A., 1987. Site specific study of seismic intensity and ground motion parameters for proposed Jamuna river bridge. *Bangladesh: a report on Jamuna Bridge Study*.

Bilham, R. and England, P., 2001. Plateau 'pop-up'in the great 1897 Assam earthquake. *Nature*, *410*(6830), pp.806-809.

Bhunia, G.S., Shit, P.K. and Maiti, R., 2018. Comparison of GIS-based interpolation methods for

spatial distribution of soil organic carbon (SOC). *Journal of the Saudi Society of Agricultural Sciences*, *17*(2), pp.114-126.

Borcherdt, R.D., 1994. Estimates of site-dependent response spectra for design (methodology and justification). *Earthquake spectra*, *10*(4), pp.617-653.

Brevik, E.C., Calzolari, C., Miller, B.A., Pereira, P., Kabala, C., Baumgarten, A. and Jordán, A., 2016. Soil mapping, classification, and pedologic modeling: History and future directions. *Geoderma*, *264*, pp.256-274.Eurocode 8 (Part 5, 1998): "Design provisions for earthquake resistance of structures-foundation, retaining structures and geotechnical aspects", European Committee for   Standardization, Brussels.

Cao, Z., Youd, T.L. and Yuan, X., 2013. Chinese dynamic penetration test for liquefaction evaluation in gravelly soils. *Journal of Geotechnical and Geoenvironmental Engineering*, *139*(8), pp.1320-1333.

Ceryan, S. and Ceryan, N., 2021. A new index for microzonation of earthquake prone settlement area by considering liquefaction potential and fault avoidance zone: an example case from Edremit (Balikesir, Turkey). *Arabian Journal of Geosciences*, *14*(21), p.2216.

Chung, J.W. and Rogers, J.D., 2012. Seismic site classifications for the St. Louis urban area. *Bulletin of the Seismological Society of America*, *102*(3), pp.980-990.

Cetin, K.O., Seed, R.B., Kayen, R.E., Moss, R.E., Bilge, H.T., Ilgac, M. and Chowdhury, K., 2018. The use of the SPT-based seismic soil liquefaction triggering evaluation methodology in engineering hazard assessments. *MethodsX*, *5*, pp.1556-1575.

Cetin, K.O., Seed, R.B., Kayen, R.E., Moss, R.E., Bilge, H.T., Ilgac, M. and Chowdhury, K., 2016. *Summary of SPT based field case history data of cetin (2016) database* (No. METU/GTENG 08/16-01). Middle East Technical University.

Cetin, K.O., Youd, T.L., Seed, R.B., Bray, J.D., Stewart, J.P., Durgunoglu, H.T., Lettis, W. and Yilmaz, M.T., 2004. Liquefaction-induced lateral spreading at Izmit Bay during the Kocaeli (Izmit)-Turkey earthquake. *Journal of Geotechnical and Geoenvironmental Engineering*, *130*(12), pp.1300-1313.

Comprehensive Disaster Management Program, 2009, Seismic hazard and vulnerability

assessment of Dhaka, Chittagong, and Sylhet city corporation areas. Final report, Comprehensive Disaster Management Program, pp. 1-106.

Council, B.S.S., 2009. NEHRP recommended seismic provisions for new buildings and other structures. *Rep. FEMA P*, *750*.

Council, B.S.S., 1998. 1997 Edition NEHRP Recommended Provisions for the Development of Seismic Regulations for New Buildings and Other Structures. *FEMA*, *302*.

Chen, B.S. and Mayne, P.W., 1996. Statistical relationships between piezocone measurements and stress history of clays. *Canadian Geotechnical Journal*, *33*(3), pp.488-498.

Chen, Q., Wang, C. and Juang, C.H., 2016. Probabilistic and spatial assessment of liquefaction-induced settlements through multiscale random field models. *Engineering Geology*, *211*, pp.135-149.

Cummins, P.R., 2007. The potential for giant tsunamigenic earthquakes in the northern Bay of Bengal. *Nature*, *449*(7158), pp.75-78.

Chowdhury, I.N., 2016. Neo-deterministic studies for seismic hazard assessment of Bangladesh.

Demir, S. and Şahin, E.K., 2022. Liquefaction prediction with robust machine learning algorithms (SVM, RF, and XGBoost) supported by genetic algorithm-based feature selection and parameter optimization from the perspective of data processing. *Environmental Earth Sciences*, *81*(18), p.459.

Dobry, R., Borcherdt, R.D., Crouse, C.B., Idriss, I.M., Joyner, W.B., Martin, G.R., Power, M.S., Rinne, E.E. and Seed, R.B., 2000. New site coefficients and site classification system used in recent building seismic code provisions. *Earthquake spectra*, *16*(1), pp.41-67.

Drucker, H., Burges, C.J., Kaufman, L., Smola, A. and Vapnik, V., 1996. Support vector regression machines. Advances in neural information processing systems, 9.

Engdahl, E.R., Di Giacomo, D., Sakarya, B., Gkarlaouni, C.G., Harris, J. and Storchak, D.A., 2020. ISC-EHB 1964–2016, an improved data set for studies of Earth structure and global seismicity. *Earth and Space Science*, *7*(1), p.e2019EA000897.F

Fabbrocino, S., Lanzano, G., Forte, G., de Magistris, F.S. and Fabbrocino, G., 2015. SPT blow

count vs. shear wave velocity relationship in the structurally complex formations of the Molise Region (Italy). *Engineering Geology*, 187, pp.84-97.

Freund Y, Schapire RE (1997) A decision-theoretic generalization of on-line learning and an application to boosting. *J Comput Syst Sci* 55(1):119–139.

Gurung, L. and Chatterjee, K., 2023. Evaluation of Liquefaction Potential of Kolkata City, India: A Deterministic Approach. *Pure and Applied Geophysics*, *180*(1), pp.439-474.

Gurung, D., McHugh, C.M., Mondal, D.R., Seeber, L., Steckler, M.S., Bastas-Hernandez, A., Akhter, S.H., Mustaque, S. and Goodbred Jr, S.L., 2014, December. Evidence for a tsunami generated by the 1762 Great Arakan earthquake, Southeastern Bangladesh. In *AGU Fall Meeting Abstracts* (Vol. 2014, pp. T43B-4732).

Green, R.A., Upadhyaya, S., Wood, C.M., Maurer, B.W., Cox, B.R., Wotherspoon, L., Bradley, B.A. and Cubrinovski, M., 2017, September. Relative efficacy of CPT-versus Vs-based simplified liquefaction evaluation procedures. In *Proc. 19th Intern. Conf. on Soil Mechanics and Geotechnical Engineering* (pp. 1521-1524).

Goh, A.T. and Goh, S.H., 2007. Support vector machines: their use in geotechnical engineering as illustrated using seismic liquefaction data. *Computers and Geotechnics*, *34*(5), pp.410-421.

Haque, D.M.E., Khan, N.W., Selim, M., Kamal, A.M. and Chowdhury, S.H., 2020. Towards improved probabilistic seismic hazard assessment for Bangladesh. *Pure and Applied Geophysics*, *177*, pp.3089-3118.

Hastie, T., Rosset, S., Zhu, J. and Zou, H., 2009. Multi-class adaboost. *Statistics and its Interface*, *2*(3), pp.349-360.

House Building Research Institute, Bangladesh National Building Code 2006, 2006.

House Building Research Institute, Bangladesh National Building Code 2020, 2021.

Holzer, T.L., Toprak, S. and Bennett, M.J., 2002, July. Liquefaction potential index and seismic hazard mapping in the San Francisco Bay area, California. In *7th National Conference on Earthquake Engineering, Boston, USA*.

Holzer, T.L., 2008. Probabilistic liquefaction hazard mapping. In *Geotechnical earthquake*

engineering and soil dynamics IV (pp. 1-32).

Holzer, T.L., Bennett, M.J., Noce, T.E., Padovani, A.C. and Tinsley III, J.C., 2006. Liquefaction hazard mapping with LPI in the greater Oakland, California, area. *Earthquake Spectra*, *22*(3), pp.693-708.

Hossain, M.B., Roknuzzaman, M. and Rahman, M.M., 2022. Liquefaction Potential Evaluation by Deterministic and Probabilistic Approaches. *Civil Engineering Journal*, *8*(7), pp.1459-1481.

Hwang, J.H., Chen, C.H. and Juang, C.H., 2005. Liquefaction hazard analysis: A fully probabilistic method. In *Earthquake engineering and soil dynamics* (pp. 1-15).

Hu, J., 2021. A new approach for constructing two Bayesian network models for predicting the liquefaction of gravelly soil. *Computers and Geotechnics*, *137*, p.104304.

Islam, M.S., Sharif, T.B. and Akter, F., Assessing Disaster Resilience Planning Approaches and Policy Framework for the Mega City Dhaka of Bangladesh.

Idriss, I.M. and Boulanger, R.W., 2010. SPT-based liquefaction triggering procedures. *Rep. UCD/CGM-10*, *2*, pp.4-13.

Iai, S., Tsuchida, H. and Koizumi, K., 1989. A liquefaction criterion based on field performances around seismograph stations. *Soils and Foundations*, *29*(2), pp.52-68.

Iwasaki, T., 1978. A practical method for assessing soil liquefaction potential based on case studies at various sites in Japan. In *Proc. of 2nd Int. National Conf. on Microzonation, 1978* (Vol. 2, pp. 885-896).

Iwasaki, T., Tokida, K.I., Tatsuoka, F., Watanabe, S., Yasuda, S. and Sato, H., 1982, June. Microzonation for soil liquefaction potential using simplified methods. In *Proceedings of the 3rd international conference on microzonation, Seattle* (Vol. 3, No. 2, pp. 1310-1330).

Japan Road Association, 1996. Specifications for highway bridges, Part V. *Earthquake resistant design*, *228*.

Jena, R., Pradhan, B., Almazroui, M., Assiri, M. and Park, H.J., 2023. Earthquake-induced liquefaction hazard mapping at national-scale in Australia using deep learning

techniques. *Geoscience Frontiers*, *14*(1), p.101460.

Juang, C.H. and Jiang, T., 2000. Assessing probabilistic methods for liquefaction potential evaluation. In *Soil dynamics and liquefaction 2000* (pp. 148-162).

Kayen, R., Moss, R.E.S., Thompson, E.M., Seed, R.B., Cetin, K.O., Kiureghian, A.D., Tanaka, Y. and Tokimatsu, K., 2013. Shear-wave velocity–based probabilistic and deterministic assessment of seismic soil liquefaction potential. *Journal of Geotechnical and Geoenvironmental Engineering*, *139*(3), pp.407-419.

Karim, S., Akther, K.M., Khatun, M. and Ali, R.M.E., 2019. Geomorphology and geology of the Dhaka city corporation area-an approach of remote sensing and GIS technique. *Int J Astron Astrophys Space Sci*, *6*(2), pp.7-16.

Khaleda, S., Mowla, Q.A. and Murayama, Y., 2017. Dhaka metropolitan area. *Urban Development in Asia and Africa: Geospatial Analysis of Metropolises*, pp.195-215.

Knudsen, K.L., Sowers, J.M., Witter, R.C., Wentworth, C.M. and Helley, E.J., 2000. Description of mapping of quaternary deposits and liquefaction susceptibility, nine-county San Francisco Bay Region, California. *Rep. No. United States Geologic Survey Open-File Report 00*, *444*.

Lee, C.Y. and Chern, S.G., 2013. Application of a support vector machine for liquefaction assessment. *Journal of Marine Science and Technology*, *21*(3), p.10.

Lu, G.Y. and Wong, D.W., 2008. An adaptive inverse-distance weighting spatial interpolation technique. *Computers & geosciences*, *34*(9), pp.1044-1055.

Maurer, B.W., 2017, July. Assessing liquefaction susceptibility using the CPT soil behavior type index. In Proc. 3rd Intern. Conf. on Performance-Based Design in Earthquake Geotechnical Engineering (PBDIII).

Maurer, B.W., Green, R.A., Van Ballegooy, S. and Wotherspoon, L., 2019. Development of region-specific soil behavior type index correlations for evaluating liquefaction hazard in Christchurch, New Zealand. *Soil Dynamics and Earthquake Engineering*, *117*, pp.96-105.

Martin, G.R. and Dobry, R., 1994. Earthquake site response and seismic code provisions. *NCEER*

Bulletin, *8*(4), pp.1-6.

Mazumder, R.K., Utsob, M.T.U. and Bhuiyan, M.R., 2018. Seismic vulnerability assessment of medical facilities: A GIS based application for Chittagong, Bangladesh. *Malaysian Journal of Civil Engineering*, *30*(1), pp.97-112.

Maheswari, R.U., Boominathan, A. and Dodagoudar, G.R., 2010. Seismic site classification and site period mapping of Chennai City using geophysical and geotechnical data. *Journal of Applied Geophysics*, *72*(3), pp.152-168.

Martin, S. and Szeliga, W., 2010. A catalog of felt intensity data for 570 earthquakes in India from 1636 to 2009. *Bulletin of the Seismological Society of America*, *100*(2), pp.562-569.

Mhaske, S.Y. and Choudhury, D., 2010. GIS-based soil liquefaction susceptibility map of Mumbai city for earthquake events. *Journal of Applied Geophysics*, *70*(3), pp.216-225.

Monaco, P., Marchetti, S., Totani, G. and Calabrese, M., 2005. Sand liquefiability assessment by flat dilatometer test (DMT). In *Proceedings of the 16th International Conference on Soil Mechanics and Geotechnical Engineering* (pp. 2693-2698). IOS Press.

Musashi, J.P., Pramoedyo, H. and Fitriani, R., 2018. Comparison of inverse distance weighted and natural neighbor interpolation method at air temperature data in Malang region. *CAUCHY: Jurnal Matematika Murni dan Aplikasi*, *5*(2), pp.48-54.

Mohammady, M., Pourghasemi, H.R. and Amiri, M., 2019. Land subsidence susceptibility assessment using random forest machine learning algorithm. *Environmental Earth Sciences*, *78*, pp.1-12.

Meisina, C., Bonì, R., Bozzoni, F., Conca, D., Perotti, C., Persichillo, P. and Lai, C.G., 2022. Mapping soil liquefaction susceptibility across Europe using the analytic hierarchy process. *Bulletin of Earthquake Engineering*, *20*(11), pp.5601-5632.

Naji, D.M., Akin, M.K. and Cabalar, A.F., 2021. Evaluation of seismic site classification for Kahramanmaras City, Turkey. *Environmental Earth Sciences*, *80*(3), p.97.

Nath, S. K., M. D. Adhikari, S. K. Maiti, N. Devaraj, N. Srivastava, and L. D. Mohapatra. "Earthquake scenario in West Bengal with emphasis on seismic hazard microzonation of

the city of Kolkata, India." *Natural Hazards and Earth System Sciences* 14, no. 9 (2014): 2549-2575.

Nath, S.K., Srivastava, N., Ghatak, C., Adhikari, M.D., Ghosh, A. and Sinha Ray, S.P., 2018. Earthquake induced liquefaction hazard, probability and risk assessment in the city of Kolkata, India: its historical perspective and deterministic scenario. *Journal of Seismology*, *22*, pp.35-68.

National Earthquake Hazards Reduction Program (US) and Building Seismic Safety Council (US), 2001. *NEHRP Recommended Provisions (National Earthquake Hazards Reduction Program) for Seismic Regulations for New Buildings and Other Structures*. Building Seismic Safety Council.

Ohta, Y. and Goto, N., 1978. Empirical shear wave velocity equations in terms of characteristic soil indexes. *Earthquake engineering & structural dynamics*, *6*(2), pp.167-187.

Oldham T (1882) The Cachar earthquake of 10 January 1869. In: Oldham RD (ed) Mem. Geological Survey of India, vol 19, pt.1, pp 1–88

Pal, M., 2006. Support vector machines-based modelling of seismic liquefaction potential. *International Journal for Numerical and Analytical Methods in Geomechanics*, *30*(10), pp.983-996.

Papathanassiou, G., Valkaniotis, S., Chaztipetros, A. and Pavlides, S., 2010. Liquefaction susceptibility map of Greece. *Bulletin of the Geological Society of Greece*, *43*(3), pp.1383-1392.

Pirhadi, N., Hu, J., Fang, Y., Jairi, I., Wan, X. and Lu, J., 2021. Seismic gravelly soil liquefaction assessment based on dynamic penetration test using expanded case history dataset. *Bulletin of Engineering Geology and the Environment*, *80*, pp.8159-8170.

Pokhrel, R.M., Kuwano, J. and Tachibana, S., 2012. Geostatistical analysis for spatial evaluation of liquefaction potential in Saitama City. *Lowland Technology International*, *14*(1, June), pp.45-51.

Pokhrel, R.M., Gilder, C.E., Vardanega, P.J., De Luca, F., De Risi, R., Werner, M.J. and Sextos, A., 2022. Liquefaction potential for the Kathmandu Valley, Nepal: a sensitivity

study. *Bulletin of Earthquake Engineering*, *20*(1), pp.25-51.

Pitilakis, K., Gazepis, C. and Anastasiadis, A., 2004, August. Design response spectra and soil classification for seismic code provisions. In *Proceedings of the 13th world conference on earthquake engineering, Vancouver, BC, Canada.*

Rahman, M.A., Wiegand, B.A., Badruzzaman, M. and Ptak, T., 2013. Hydrogeological analysis of the upper Dupi Tila Aquifer, towards the implementation of a managed aquifer-recharge project in Dhaka City, Bangladesh. *Hydrogeology Journal*, *21*(5), p.1071.

Rahman, M.Z., Kamal, A.M. and Siddiqua, S., 2018. Near-surface shear wave velocity estimation and V s 30 mapping for Dhaka City, Bangladesh. *Natural Hazards*, *92*, pp.1687-1715.

Rahman, M.Z. and Siddiqua, S., 2017. Evaluation of liquefaction-resistance of soils using standard penetration test, cone penetration test, and shear-wave velocity data for Dhaka, Chittagong, and Sylhet cities in Bangladesh. *Environmental Earth Sciences*, *76*, pp.1-14.

Rahman, M.Z. and Karim, M.F., 2005. Geological advantages for construction of underground metro railway transit system in Dhaka city. *Bangladesh J Geol*, *24*, pp.19-37.

Rahman, M.Z., Siddiqua, S. and Kamal, A.M., 2020. Seismic source modeling and probabilistic seismic hazard analysis for Bangladesh. *Natural Hazards*, *103*, pp.2489-2532.

Rahman, M.Z., Siddiqua, S. and Kamal, A.M., 2015. Liquefaction hazard mapping by liquefaction potential index for Dhaka City, Bangladesh. *Engineering geology*, *188*, pp.137-147.

Robinson, T.P. and Metternicht, G., 2006. Testing the performance of spatial interpolation techniques for mapping soil properties. *Computers and electronics in agriculture*, *50*(2), pp.97-108.

Robertson, P.K., 2009. Performance based earthquake design using the CPT. *Proc. IS-Tokyo*, pp.3-20.

Robertson, P.K., 2016. Cone penetration test (CPT)-based soil behaviour type (SBT) classification system—an update. *Canadian Geotechnical Journal*, *53*(12), pp.1910-1927.

Samui, P. and Sitharam, T.G., 2011. Machine learning modelling for predicting soil liquefaction susceptibility. *Natural Hazards and Earth System Sciences*, *11*(1), pp.1-9.

Samui, P. and Karthikeyan, J., 2013. Determination of liquefaction susceptibility of soil: a least square support vector machine approach. *International Journal for Numerical and Analytical Methods in Geomechanics*, *37*(9), pp.1154-1161.

Sarker, J.K., Ansary, M.A., Islam, M.R. and Safiullah, A.M.M., 2010. Potential losses for Sylhet, Bangladesh in a repeat of the 1918 Srimangal earthquake. *Environmental economics*, (1, Iss. 1), pp.12-31.

Shawe-Taylor, J. and Cristianini, N., 2000. Support vector machines (Vol. 2). Cambridge: Cambridge university press.

Sharma, B. and Chetia, M., 2016. Deterministic and probabilistic liquefaction potential evaluation of Guwahati city. *Japanese Geotechnical Society Special Publication*, *2*(22), pp.823-828.

Seismic hazard and vulnerability assessment of Dhaka, Chittagong, and Sylhet city corporation areas. Final report, Comprehensive Disaster Management Program (CDMP2009). Dhaka, Bangladesh

Seed, H.B. and Idriss, I.M., 1971. Simplified procedure for evaluating soil liquefaction potential. *Journal of the Soil Mechanics and Foundations division*, *97*(9), pp.1249-1273.

Seed, H.B., 1982. Ground motions and soil liquefaction during earthquakes. *Earthquake engineering research insititue*.

Seed, H.B., 1979. Soil liquefaction and cyclic mobility evaluation for level ground during earthquakes. *Journal of the geotechnical engineering division*, *105*(2), pp.201-255.

Seed, R.B., Cetin, K.O., Moss, R.E., Kammerer, A.M., Wu, J., Pestana, J.M., Riemer, M.F., Sancio, R.B., Bray, J.D., Kayen, R.E. and Faris, A., 2003. Recent advances in soil liquefaction engineering: a unified and consistent framework. In *Proceedings of the 26th Annual ASCE Los Angeles Geotechnical Spring Seminar: Long Beach, CA*.

Sreejaya, K.P., Raghukanth, S.T.G., Gupta, I.D., Murty, C.V.R. and Srinagesh, D., 2022. Seismic hazard map of India and neighbouring regions. *Soil Dynamics and Earthquake Engineering*, *163*, p.107505.

Shit, P.K., Bhunia, G.S. and Maiti, R., 2016. Spatial analysis of soil properties using GIS based

geostatistics models. *Modeling Earth Systems and Environment*, *2*, pp.1-6.

Tinsley, J.C., Youd, T.L., Perkins, D.M. and Chen, A.T.F., 1985. IMPROVING PREDICTIONS OF LIQUEFACTION POTENTIAL. FUTURE DIRECTIONS IN EVALUATING EARTHQUAKE HAZARDS OF SOUTHERN CALIFORNIA, p.293.

Tunusluoglu, M.C. and Karaca, O., 2018. Liquefaction severity mapping based on SPT data: a case study in Canakkale city (NW Turkey). *Environmental earth sciences*, *77*, pp.1-29.

Toprak, S. and Holzer, T.L., 2003. Liquefaction potential index: field assessment. *Journal of Geotechnical and Geoenvironmental Engineering*, *129*(4), pp.315-322.

Tokimatsu, K. and Yoshimi, Y., 1983. Empirical correlation of soil liquefaction based on SPT N-value and fines content. *Soils and Foundations*, *23*(4), pp.56-74.

Upadhyaya, S., Maurer, B.W., Green, R.A. and Rodriguez-Marek, A., 2021. Selecting the optimal factor of safety or probability of liquefaction triggering for engineering projects based on misprediction costs. *Journal of Geotechnical and Geoenvironmental Engineering*, *147*(6), p.04021026.

Upadhyaya, S., Green, R.A., Rodriguez-Marek, A. and Maurer, B.W., 2023. True liquefaction triggering curve. *Journal of Geotechnical and Geoenvironmental Engineering*, *149*(3), p.04023005.

Wair, B.R., DeJong, J.T. and Shantz, T., 2012. Pacific Earthquake Engineering Research Center.

Whitman, R.V., 1971. Resistance of soil to liquefaction and settlement. *Soils and Foundations*, *11*(4), pp.59-68.

Wang, M.X., Huang, D., Wang, G. and Li, D.Q., 2020. SS-XGBoost: a machine learning framework for predicting newmark sliding displacements of slopes. *Journal of Geotechnical and Geoenvironmental Engineering*, *146*(9), p.04020074.

Xia, J., Miller, R.D. and Park, C.B., 1999. Estimation of near-surface shear-wave velocity by inversion of Rayleigh waves. *Geophysics*, *64*(3), pp.691-700.

Xie, Y., Ebad Sichani, M., Padgett, J.E. and DesRoches, R., 2020. The promise of implementing machine learning in earthquake engineering: A state-of-the-art review. *Earthquake*

Spectra, *36*(4), pp.1769-1801.

Yegian, M.K. and Vitelli, B.M., 1981. Analysis for liquefaction: empirical approach.

Youd, T.L. and Idriss, I.M., 2001. Liquefaction resistance of soils: summary report from the 1996 NCEER and 1998 NCEER/NSF workshops on evaluation of liquefaction resistance of soils. *Journal of geotechnical and geoenvironmental engineering*, *127*(4), pp.297-313.

Youd, T.L. and Perkins, D.M., 1978. Mapping liquefaction-induced ground failure potential. *Journal of the Geotechnical Engineering Division*, *104*(4), pp.433-446.

Youd, T.L. and Perkins, D.M., 1987. Mapping of liquefaction severity index. *Journal of Geotechnical Engineering*, *113*(11), pp.1374-1392.

Zhang, W. and Goh, A.T., 2016. Evaluating seismic liquefaction potential using multivariate adaptive regression splines and logistic regression. *Geomech. Eng*, *10*(3), pp.269-284.

Zhou, Y., Zhang, H., Li, F. and Qi, P., 2018. Local focus support vector machine algorithm. *Journal of Computer Applications*, 38(4), p.945.

Zhang, Y., Xie, Y., Zhang, Y., Qiu, J. and Wu, S., 2021. The adoption of deep neural network (DNN) to the prediction of soil liquefaction based on shear wave velocity. *Bulletin of Engineering Geology and the Environment*, 80, pp.5053-5060.

Zhou, J., Huang, S., Wang, M. and Qiu, Y., 2021. Performance evaluation of hybrid GA–SVM and GWO–SVM models to predict earthquake-induced liquefaction potential of soil: a multi-dataset investigation. *Engineering with Computers*, pp.1-19.

Zhang, W. and Goh, A.T., 2016. Evaluating seismic liquefaction potential using multivariate adaptive regression splines and logistic regression. *Geomech. Eng*, 10(3), pp.269-284.

APPENDIX – A : EARTHQUAKE EVENT CATAOGUE

Table A – 1: Earthquake event catalogue (1762 to 2023)

Year	Latitude	Longitude	Depth (km)	Moment Magnitude	Reference*
1762	22	92		7.5	1
1764	24	88		6	1
1822	23.5	91		6	1
1826	28	85		6	1
1826	27	85		6	1
1828	24.5	94.5		5	1
1830	22	91		5	1
1833	27.5	86.5		7.5	1
1833	27	85		6.5	1
1833	27	84		6	1
1833	27.7	85.3		5	1
1834	25.8	89.4		6.3	1
1834	25.8	89.4		6	1
1839	27.8	95.6		5	1
1839	25.3	86.5		5	1
1841	26.2	91.8		5.6	1
1842	25	87		5.5	1
1842	26.2	91.8		5	1
1842	25	90		6.5	1
1843	28	95		5.7	1
1843	27	94.7		5	1
1843	27.2	95.4		5.7	1
1843	27	94.7		5.7	1
1843	27	88.3		5.5	1
1843	26	93		5	1
1843	26	93		5	1
1843	26.2	91.8		5.7	1
1845	24.8	91.8		6.5	1
1845	26.2	91.8		5.7	1
1845	26.2	91.8		5	1
1846	24.8	90.4		6.3	1
1846	24	90		6	1
1846	27	94		6	1
1846	26.3	92.7		6.3	1
1849	26	92		5.7	1

Year	Latitude	Longitude	Depth (km)	Moment Magnitude	Reference*
1849	26.3	91		5	1
1849	26.3	91		5	1
1849	27	88.3		6	1
1851	22.3	91.8		5.5	1
1851	22.6	88.4		5.7	1
1851	25.3	91.7		5	1
1852	27	88		6.5	1
1852	27	88.3		7	1
1852	23.7	90.4		5.7	1
1858	19	95		7.5	1
1861	22.6	88.4		5.7	1
1862	27	88.3		5	1
1863	27	88.3		5.7	1
1863	27	88.3		5	1
1863	27	88.3		5	1
1865	27	88.3		5	1
1865	22.2	92.5		6	1
1866	21.8	87.8		5	1
1866	27	85		7	1
1868	24.9	91.9		5.5	1
1868	24	85		5	1
1869	26	92.7		7.5	1
1869	25.6	91.9		5	1
1869	27	85		6.5	1
1869	27	88.3		5.7	1
1869	27	88.3		5.7	1
1875	26.5	93		5.7	1
1880	24.5	94		6.3	1
1882	24.8	92.8		5	1
1885	24.8	89.7		7	1
1885	24	90		5.7	1
1885	25	89.2		5.7	1
1897	26	91		8.1	1
1897	19.4	84.9		5.5	1
1898	24.8	92.8		6.3	1
1899	27	88.3		6	1
1901	29.5	90.1	0	6.8	2
1902	30	85		6.7	1
1903	19.5	95		6.5	1

Year	Latitude	Longitude	Depth (km)	Moment Magnitude	Reference*
1905	26	96	0	7.1	2, 1
1906	27	97	100	7	2
1906	22.6	88.4		5	1
1908	26.95	96.77	15	7	2, 3
1909	27	87		5	1
1909	28.8	90.5	0	6.5	2
1911	23	88		5	1
1912	21.04	96.74	15	7.5	2, 3
1915	29.5	91.5		7.1	1
1915	26	92		5	1
1915	27.7	91.64	15	6.5	2, 3
1915	26	92		5	1
1918	29.6	87.8		6	1
1918	24.3	90.71	15	7.6	2, 3, 5
1920	22.2	93.2		6	1
1923	29.6	87.8		5.5	1
1923	22.6	93.4		6	1
1923	24.94	90.72	15	7.1	2, 3, 1
1924	25	93		6	1
1924	26	96		5.5	1
1924	26	96		5.5	1
1924	29.5	90	35	5.8	2, 1
1924	23	95		5.5	1
1924	30.88	89.65	15	6.5	2 , 1
1925	30	85.8		5.5	1
1926	26	97	80	6.2	2
1926	26	96		5.5	1
1926	24.5	94.5		5.5	1
1926	23	95		5.5	1
1926	25	93		5.5	1
1926	29.6	87.8		6	1
1927	24.5	95	130	6.5	2 , 1
1927	24.5	94.5		5.5	1
1927	27	96		5.5	1
1927	22	90		5.5	1
1928	27	96		5.5	1
1928	27	96		5.5	1
1928	23	95		5.5	1
1929	29	94.5	35	5.6	2 , 1

Year	Latitude	Longitude	Depth (km)	Moment Magnitude	Reference*
1929	19.4	96.4		5.5	1
1929	19.32	95.84	15	6.6	2, 3
1929	26	96		5.5	1
1930	17.86	96.43	35	7.5	2, 3, 1
1930	25.93	90.18	15	7.2	2, 3, 5
1930	25.8	90.2		5.5	1
1930	25.8	90.2		5.5	1
1930	25.8	90.8		5.5	1
1930	25.8	90.8		5.5	1
1930	25.8	90.8		5.5	1
1930	25	93.5		5.5	1
1930	25.8	90.8		5.5	1
1930	23	96		5.5	1
1930	25	94	35	6.3	2, 5
1930	17.3	96.5		5.5	1
1930	18.23	96.3	10	7.5	2, 3, 7
1931	25.85	96.79	15	7.6	2, 3, 1
1931	25.5	96	35	5.8	2, 1
1931	18.5	96	35	5.6	2 , 1
1932	25.5	92.5	35	5.6	2 , 1
1932	25	90	35	5.6	2 , 1
1932	30	89.2		5.5	1
1932	24.5	92	35	5.6	2 , 1,7
1932	25.84	95.64	110	7	2 , 1
1932	22	95.5		5.5	1
1932	26.5	92	35	5.6	2 , 1
1933	26	90.5	35	5.6	2 , 1,7
1933	19	97	35	5.6	2
1933	25.8	95.7		5.2	1
1934	26.88	86.59	15	8.3	2, 3, 1
1934	28	86		5.6	1
1934	24.5	95	130	6.5	2 , 7, 1
1934	25.8	89.4		5.5	1
1935	24.25	89.5	80	6.2	2 , 1, 7
1935	27	85		5.5	1
1935	24	94.75	110	6.2	2 , 7, 1
1935	28.75	89.25	140	6.2	2 , 7, 1
1936	27.5	87	50	5.6	2 , 1
1936	23	96	35	5.8	2, 1

Year	Latitude	Longitude	Depth (km)	Moment Magnitude	Reference*
1936	25.7	90.5		5.3	1
1936	27.5	87		5.5	1
1936	26.6	90.3		5.8	1
1936	27.5	87		5.7	1
1937	27	92		5.7	1
1937	25.5	94		5.9	1
1937	30	90		5.8	1
1937	26.01	96.71	15	6.6	2, 3
1937	24.9	94.7		5.7	1
1938	27.5	87	35	5.8	2, 1
1938	28	90.5		5.7	1
1938	26	91		5.2	1
1938	23.23	94.46	105	6.8	2, 7
1938	24.5	95	100	5.8	2 , 1
1938	24.5	95		5.8	7
1938	22.75	93.92	75	7.2	2, 3, 7
1938	30	95	35	6.1	2, 1
1939	24.4	94.08	66	6.8	2, 3, 5,7
1939	28.5	86.5		5.7	1
1939	23.5	94	35	5.8	2, 1
1940	27	92		5.7	1
1940	23.75	94.25	80	6.5	2 , 1
1940	28	90.5		5.2	1
1940	30	92	35	6.1	2, 1
1941	27.17	91.86	15	6.8	2, 3, 5
1941	26.5	92.5	180	6.5	2 , 1,7
1941	28	96	90	5.5	2 , 7
1941	27.5	93	35	5.6	2 , 1,7
1941	27	92		5.8	1
1942	24	90.3		5.9	1
1942	18	96		6	1
1942	29.8	95.3		5.9	1
1943	27	92		6	1
1943	26.64	93.85	15	7.2	2, 3, 5
1944	24.7	92.2		5.9	1
1945	25.1	90.9		6.1	1
1945	29.5	84		5.5	1
1946	19.5	95		5.9	1
1946	27.5	96.4		5.9	1

Year	Latitude	Longitude	Depth (km)	Moment Magnitude	Reference*
1946	26.4	92.6		5.6	1
1946	23	96		5.4	1
1946	30	92		5.7	1
1946	24.05	95.67	15	8	2, 3, 1
1946	23.31	95.52	15	7.8	2 , 1,7
1947	24.9	94.7		5.5	1
1947	23.8	94.8		6.2	1
1947	28.58	93.63	20	7.8	2, 3, 1,7
1947	23.8	94.8		6.2	1
1947	23.8	94.8		6	1
1947	23.9	96.2		6	1
1947	23.9	96.2		5.9	1
1947	27.9	91.9		5.9	1
1948	23.8	94.8		6	1
1948	26.8	94		5.5	1
1948	22.3	94.1		6	1
1948	27.9	91.9		5.5	1
1948	26.8	94		6	1
1949	24	93		6	1
1949	21	95		5.5	1
1949	26	89		6	1
1950	29.8	95.3		5.5	1
1950	29.8	95.3		6	1
1950	27.22	90.82	15	6	3, 1
1950	28.36	96.45	15	8.6	2, 3, 5
1950	28.52	95.73	25	6.2	2, 3
1950	27.34	96.78	25	5.8	3
1950	25.34	92.94	25	6	2, 3, 1
1950	28.5	95.13	25	5.8	3
1950	28.66	96.75	25	5.8	2, 3
1950	28.38	95.89	25	6.2	2, 3
1950	27.5	96.4		6	1
1950	27.9	91.9		5.5	1
1950	29.06	94.87	25	6.6	2, 3, 1
1950	28.18	94.97	25	6	3, 1
1950	27.49	92.8	15	6.7	2, 3, 1
1950	28.72	95.96	25	6.4	2, 3, 1
1950	29.2	95.1		6	1
1950	26.86	96.97	25	5.7	2, 3

Year	Latitude	Longitude	Depth (km)	Moment Magnitude	Reference*
1950	28.43	94.84	25	6.5	2, 3, 1
1950	29.2	95.1		5.5	1
1950	29.62	94.77	25	6.2	2, 3, 1
1950	29.2	95.1		6	1
1950	27.9	91.9		6	1
1950	29.21	95.81	20	6.4	2, 3
1950	29.2	95.1		6	1
1950	29.72	96.56	25	6.1	2, 3
1950	29.47	95.06	25	6.4	2, 3, 1
1950	29.2	95.1		5.5	1
1950	33.04	91.48	15	5.8	2
1950	29.2	95.1		6.1	1
1950	28.8	93.7		6	1
1950	29.93	95.51	25	6	2, 3, 1
1950	28.97	94.58	25	6.3	2, 3, 1
1950	29.2	95.1		6	1
1950	29.21	95.02	25	6	2, 3, 1
1950	28.5	96.48	25	5.9	2, 3
1950	28.25	96.67	25	6.3	2, 3, 1
1950	29.2	95.1		5.5	1
1950	29.2	95.1		6	1
1950	27.23	94.96	25	7	2, 3, 1
1950	29.2	95.1		6	1
1950	29.18	94.6	25	6.2	3, 1
1950	29.2	95.1		6	1
1950	27.5	96.4		5.5	1
1950	28.61	95.33	25	6.1	2, 3, 1
1950	29.69	95.3	25	6	3, 1
1950	29.59	95.23	25	5.5	3, 1
1950	29.76	96.75	25	5.9	2, 3
1950	28.7	94.2		6	1
1950	29.2	95.1		6	1
1950	29.71	96.73	25	5.7	3
1950	29.3	92		5.5	1
1950	29.2	95.1		5.5	1
1950	26.8	95		6	1
1950	28.61	94.16	25	6	2, 3, 1
1950	27.6	95.13	25	7	2, 3, 1
1950	29.2	95.1		6	1

Year	Latitude	Longitude	Depth (km)	Moment Magnitude	Reference*
1950	24	93		5.5	1
1950	28.87	94.41	20	6.7	2, 3, 1
1950	28.55	94.4	25	6.6	2, 3, 1
1950	28.22	95.46	25	6.2	3, 1
1950	27.42	95.35	25	6.4	3, 1
1950	26.1	96.81	25	5.7	3
1950	27.23	94.81	25	6.4	3, 1
1950	25.38	96.9	15	5.7	3, 1
1950	24.9	94.7		6.7	1
1950	29	96		6	1
1950	28.77	95.69	25	6.6	2, 3, 1
1950	23.85	91.84	15	6.3	2, 3, 1
1951	29	96		5.5	1
1951	28.7	94.2		6.6	1
1951	28.7	94.2		5.6	1
1951	27.5	95.5		5.8	1
1951	28.7	94.2		5.8	1
1951	28.66	95.43	15	6.4	2, 3, 1
1951	27.99	94.67	25	6.5	2, 3, 1
1951	25.95	90.58	15	6.8	3, 1
1951	28.28	93.86	15	6.5	2, 3, 1
1951	28.84	94.58	25	6.5	2, 3, 1
1951	28.93	86.68	15	6	2, 3, 1
1951	21	95		5.5	1
1951	27.5	96.4		5.5	1
1951	28.62	96.53	25	5.8	2, 3
1951	22.3	94.1		6	1
1951	28.8	93.7		6	1
1951	29	96		5.5	1
1951	31.06	91.26	30	7.7	2
1951	30	92		5.5	1
1952	23.8	94.8		6	1
1952	29.43	95.92	15	5.5	3, 1
1952	29.88	90.77	15	5.5	3, 1
1952	30	92		5.5	1
1952	26.62	95.07	35	6	3, 1
1952	28.4	94.49	20	6	2, 3, 1
1952	18.3	95.4		6	1
1952	30.65	91.6	25	7.5	2

Year	Latitude	Longitude	Depth (km)	Moment Magnitude	Reference*
1952	28.14	93.91	15	6	2, 3, 1
1952	30	92		5.5	1
1952	27.8	85.7		5.5	1
1952	25.5	94		6	1
1952	29.68	86.51	15	6	2, 3, 1
1952	25	95.2		6	1
1954	27.67	91.6	15	6.5	2, 3, 1
1954	24.45	95.06	184	7.4	2 , 1
1955	29.67	90.17	15	6.2	2, 3, 1
1955	27.05	96.93	15	5.8	2, 3
1955	30.67	86.43	15	5.4	2
1955	23.98	95.84	15	6	2, 3, 1
1955	25	95	150	5.7	2
1955	27.5	90		5.6	1
1955	27.5	90		5.7	2
1955	26.5	90		5.1	5
1955	26.5	90		5	2
1955	21.82	92.66	35	6.5	2, 3, 5
1955	29.85	90.19	15	5.9	2, 3
1956	23.5	93.5		6.1	5
1956	23	94		6.1	2
1956	23.3	94.28	53	6.2	2, 3, 1
1956	23.42	93.97	50	6.4	2, 3, 1, 8
1956	23.38	94.22	52	6	2, 3, 1
1956	25.2	90.8		5	5
1956	30	90		5	1
1956	25.03	90.85	15	6	2, 3, 1
1956	22.65	94.05	90	6.3	2, 5
1956	22.18	95.78	34	7	2, 3, 1
1956	27.97	95.21	15	5.8	2, 3, 1
1956	23.74	94.7	115	6.1	2 , 1
1956	26.61	96.21	15	6	2, 3, 1
1956	23.38	94.12	50	6	2, 3, 1
1956	23	94		5.2	2 , 1
1957	30.52	84.35	15	6.5	2
1957	25.4	95		6	1
1957	25.53	95.06	80	5.2	2
1957	24.5	93.5		6.8	5
1957	24.31	93.89	65	6.2	2, 3

Year	Latitude	Longitude	Depth (km)	Moment Magnitude	Reference*
1957	24.5	93		5.5	1
1958	27	92		5	1
1958	25.65	96.8	15	5.8	2, 3
1958	30.62	84.13	15	5.9	2
1958	24.75	90.69	25	5	2 , 1, 1
1958	27.5	92		5.5	1
1958	27.7	92.56	15	5.5	2
1958	23.51	93.84	50	6.4	2, 3, 5
1958	25.22	96.19	35	6	3, 1
1958	30.44	84.54	15	5.2	2
1958	28.79	86.94		5.5	1
1959	27.6	96.46	15	6	2, 3, 1
1959	28.95	91.93	20	5.7	2 , 1
1959	25.65	94.74	60	5.2	2, 1
1959	22	93.3		5.9	5
1959	25.3	96.17	35	5	2 , 1
1959	26.15	90.19	20	5.4	2, 3
1959	24	94		5.4	1
1959	30	91		5.7	1
1959	25.09	96.13	35	5.7	2, 3, 1
1959	28	93		5	1
1959	21.54	92.43	35	5.7	2, 3, 1
1960	26.82	92.68	0	5	2 , 1
1960	26.49	90.3	15	6.5	2, 3, 1
1960	27	88.5	29	5.5	2 , 1
1960	23.65	94.32		5.5	1
1961	24.86	95.34	141	5.8	2 , 1
1961	24.55	94.69	91	5.8	2 , 1
1961	28	87		5.5	1
1961	26.7	91.9		5	1
1961	27	90		5.5	1
1962	28.05	84.99	0	5.5	2
1962	26.1	97	35	6.3	2, 3
1962	16.67	93.86	42	5	2
1962	26.33	96.92	25	6.1	2, 3
1962	26.6	93.3		5.5	1
1963	27	88		5.2	2
1963	22.5	84.5		5.2	1
1963	25	92.03	45	6.2	2, 3

Year	Latitude	Longitude	Depth (km)	Moment Magnitude	Reference*
1963	24.8	90.9		6.2	1
1963	24.9	92.17	51	5.7	2, 3, 1
1963	24.8	92.1		6.4	5,10
1963	22.9	94.5		5.9	6
1963	23	94		5.6	2
1963	25.2	95.3		5.3	1
1964	22.33	93.58	60	6.2	2, 3
1964	27.4	91.18	22	5.3	2
1964	21.65	94.4	91	6	2, 3
1964	18.28	94.44	46	5	2
1964	23.47	94.39	94	5.1	2
1964	25.82	95.71	115	5.2	2
1964	27.13	89.36	29	5	2
1964	27.52	90.17	1	5.3	2
1964	21.6	88.07	6	5.2	2
1964	25.88	95.69	121	5.6	2, 3
1964	23	93.95	60	5.2	2
1964	24.88	95.31	152	5.6	2, 3
1964	23.51	94.67	110	5.4	2
1964	27.36	88.21	21	5.1	2
1964	27.12	92.26	33	5.8	2, 3
1964	28.04	93.75	37	6.8	2, 3
1964	29.53	86.04	33	5.1	2
1964	26.39	96.13	108	5	2
1965	27.4	87.84	23	5.9	2, 3
1965	27.31	87.68	18	5.2	2
1965	19.96	94.44	80	5.1	2
1965	24.97	94.21	45	5.6	2, 3
1965	23.63	94.64	94	5.1	2
1965	26.82	92.33	70	5	2
1965	25.93	95.8	101	5.3	2
1965	20.13	94.83	81	5.3	2
1965	19.9	94.7	33	5.1	2
1965	24.68	95.33	149	5	2
1965	29.67	95.51	30	5.3	2
1965	24.94	93.67	48	5.3	2
1965	17.54	94.79	44	5.1	2
1965	23.34	94.46	97	5.1	2
1965	27.43	92.51	4	5.2	2

Year	Latitude	Longitude	Depth (km)	Moment Magnitude	Reference*
1965	26.7	92.5	8	5.3	2
1965	22	94.47	109	5.2	2
1965	22	94.5	114	5.1	2
1966	26.14	92.84	74	5	2
1966	27.49	92.61	20	5.9	2, 3
1966	24.28	94.87	86	5.1	2
1966	23.04	94.28	72	5.1	2
1966	18.35	95.32	79	5.2	2
1966	21.51	94.43	84	5.7	2, 3
1966	28	89	33	5.2	2
1967	23.55	94.19	54	5.2	2
1967	30	86	33	5.2	2
1967	26.1	96.14	39	5.6	2, 3
1967	23.13	93.8	51	5.1	2
1967	20.33	93.99	51	5.3	2
1967	28.7	86.38	20	5.2	2
1967	28.45	94.39	15	5.1	2
1967	28.41	94.29	20	5.7	2, 3
1967	27	87	33	5.2	2
1967	27.42	91.86	19	5.8	2, 3
1967	22.49	94.88	153	5	2
1968	29.8	92.2	25	5.1	2
1968	24.83	91.94	39	5.3	2
1968	26.42	90.62	22	5.1	2
1968	24.12	91.61	27	5.1	2
1969	22.98	92.4	49	5.2	2
1969	27.46	94.14	33	5	2
1969	41.42	79.24	3	5.8	2
1969	27.9	85.4	33	5	2
1969	27.9	85.6	33	5.2	2
1969	25.93	95.2	68	5	2
1969	26.93	92.71	44	5	2
1969	26.35	96.06	72	5.2	2
1969	23.09	94.7	124	6.3	2, 3
1969	27.66	90.24	13	5	2
1969	26.6	91.8	33	5	2
1970	27.4	93.96	12	5.4	2
1970	27.62	85.7	96	5	2
1970	26.83	96.98	24	5.2	2

Year	Latitude	Longitude	Depth (km)	Moment Magnitude	Reference*
1970	26.45	96.34	98	5	2
1970	23.96	94.06	49	5.1	2
1970	25.72	88.58	32	5.1	2
1970	26.02	95.37	68	7	2, 3
1970	26.04	95.33	33	5	2
1970	26.24	95.1	52	5.3	2
1970	26.16	95.61	47	5.1	2
1971	23.71	91.66	37	5.4	2
1971	28.72	94.9	35	5	2
1971	25.22	96.43	44	5	2
1971	25.2	96.41	40	6.3	2, 3
1971	25.22	96.51	22	6.1	2, 3
1971	24.6	94.78	74	5	2
1971	26.41	93.15	52	5.5	2, 3
1971	23.06	95.86	47	5.1	2
1971	21.44	93.88	55	5	2
1971	27.93	87.95	29	5.2	2
1971	25.17	94.73	46	5.7	2, 3
1972	16.99	94.85	28	5.3	2
1972	27.23	88.02	33	5.1	2
1972	26.44	96.37	94	5.2	2
1972	25.09	96.25	0	5	2
1972	21.25	94.35	76	5	2
1973	28.12	87.15	33	5.2	2, 3
1973	24.31	93.52	1	5.9	2, 3
1973	27.49	92.6	30	5.2	2, 3
1973	23.6	94.86	126	5.2	2, 3
1973	23.28	94.49	60	5.4	2, 3
1973	28.36	82.99	34	5	2
1973	22.43	93.38	31	5.1	2, 3
1974	27.66	86	20	5.7	2, 3
1974	21.33	93.68	47	5	2, 3
1974	25.82	96.43	30	5.2	2
1974	28.59	85.51	20	5.6	2, 3
1974	19.99	94.99	78	5.1	2, 3
1975	28.09	84.77	19	5.4	2, 3
1975	17.65	97.84	6	5.5	2
1975	24.11	93.5	42	5	2, 3
1975	19.69	93.97	0	5.2	2

Year	Latitude	Longitude	Depth (km)	Moment Magnitude	Reference*
1975	27.44	87.04	26	5.1	2, 3
1975	23.86	94.09	51	5.3	2, 3
1975	26.55	96.92	53	5.7	2
1975	26.59	96.91	43	5.2	2, 3
1975	26.59	96.95	10	5.4	2
1975	28.19	95.91	30	5.1	2, 3
1975	26.71	93.27	65	5.4	2
1975	27.74	87.5	33	5.2	2, 3
1975	29.06	95.56	48	5	2, 3
1975	22.64	94.89	137	5.1	2, 3
1975	21.42	94.62	112	6.5	2, 3
1975	26.58	96.36	22	5.2	2, 3
1975	18.24	96.4	11	5.2	2, 3
1975	24.09	95.11	98	5.2	2
1975	28.15	87.8	33	5.1	2, 3
1975	23.62	94.27	62	5.2	2, 3
1975	18.15	96.52	23	5.2	2, 3
1976	21.89	95.3	69	5.5	2, 3
1976	21.18	88.62	50	5.3	2, 3
1976	26.7	97.04	31	6.2	2
1976	29.81	89.57	75	5.5	2, 3
1976	28.63	86.24	81	5.1	2, 3
1976	23.1	94.61	103	5	2, 3
1977	31.25	87.98	25	5	2
1977	21.6	92.77	40	5.9	4, 2, 3
1977	23.27	93.16	61	5.4	4, 2, 3
1977	26.51	93	52	5.1	2, 3
1977	32.65	88.39	24	5.7	2
1977	23.71	92.31	33	5.1	2, 3
1978	24.73	95.2	98	5.1	2, 3
1978	23.02	94.7	92	5.1	2, 3
1978	28.03	84.7	0	5.3	2, 3
1978	23.3	94.13	83	5	2, 3
1978	23.16	94.93	122	5.1	4, 2, 3
1978	26.46	96.94	38	5.1	2, 3
1978	16.6	95.88	7	5.5	2
1978	27.82	85.93	19	5.2	2, 3
1978	14.58	96.43	3	5	2
1978	16.69	95.94	12	5	2

Year	Latitude	Longitude	Depth (km)	Moment Magnitude	Reference*
1979	20.51	93.59	95	5.3	4, 2, 3
1979	23.04	95.98	43	5.1	2, 3
1979	24.92	95.05	109	5.3	4, 2, 3
1979	26.29	87.57	24	5.2	4, 2, 3
1979	25.13	95.59	117	5	4, 2, 3
1979	24.2	94.93	113	5	2, 3
1979	29.04	95.8	35	5.1	2, 3
1979	18.11	94.94	54	5.6	4, 2, 3
1979	25.21	96.32	10	5.2	4, 2, 3
1979	30.05	95.48	12	5.2	2, 3
1980	27.83	101.24	22	5.1	2
1980	30.55	88.65	14	5.7	2
1980	21.3	93.76	64	5.2	2, 3
1980	30.13	81.77	29	5.1	2
1980	33	88.55	3	5.1	2
1980	24.81	94.62	52	5.1	2, 3
1980	31.43	87.72	34	5	2
1980	23.9	91.46	30	5	2, 3
1980	29.55	85.18	24	5	2, 3
1980	27.42	89.05	44	6.2	4, 2, 3
1980	22.69	94.49	20	5.3	4, 2, 3
1981	27.2	89.76	16	5.1	2, 3
1981	24.99	95.52	153	5.7	4, 2, 3
1981	23.32	94.64	99	5	4, 2, 3
1981	32.58	82.36	18	5	2
1981	23	95.45	10	5.1	4, 2, 3
1981	25.13	97.9	42	5	2
1981	25.15	97.96	38	5.2	2
1981	25.52	96.63	38	5.1	2, 3
1981	26.7	96.06	82	5.2	2, 3
1981	29.89	94.93	0	5.1	2, 3
1982	30.89	89.87	3	5.3	2
1982	31.68	82.28	25	6	2
1982	31.56	82.21	31	5.3	2
1982	21.41	94.67	120	5.4	2, 3
1982	31.58	82.25	33	5.1	2
1982	23.56	95.58	42	5	2, 3
1982	27.38	88.84	9	5.1	2, 3
1982	18.01	85.84	32	5.5	4, 2, 3

Year	Latitude	Longitude	Depth (km)	Moment Magnitude	Reference*
1982	29.94	95	14	5.1	2, 3
1982	19.56	90.65	29	5.6	4, 2, 3
1982	25.88	90.31	8	5.1	2, 3
1982	25.38	91.46	32	5	2, 3
1982	25.93	95.31	88	5	2, 3
1982	27.78	94.87	29	5.1	2, 3
1982	22.4	100.99	7	5.2	2
1982	26.01	91.69	61	5	2, 3
1983	24.23	94.45	84	5.1	2, 3
1983	26.9	97	31	5	2
1983	24.67	95.03	109	5.4	2, 3
1983	24.72	95.04	70	5	2, 3
1983	26.9	92.87	42	5.2	2, 3
1983	28.63	96.05	40	5.1	2, 3
1983	21.86	94.19	112	5.1	4, 2, 3
1983	23.06	93.87	81	5	2, 3
1983	24.48	94.69	148	5.2	4, 2, 3
1983	25.34	94.9	69	5.7	4, 2, 3
1983	20.58	93.09	43	5.1	2, 3
1983	24.77	95.12	115	5.2	2, 3
1983	28.05	92.52	38	5	2, 3
1983	21.87	94.37	92	5.3	4, 2, 3
1983	26.58	96.38	144	5.4	4, 2, 3
1984	19.68	94.61	60	5.2	2, 3
1984	28.65	96.36	28	5	2, 3
1984	13.01	95.72	37	5	2
1984	24.99	94.79	51	5	2, 3
1984	24.85	95.49	96	5.5	4, 2, 3
1984	26.76	93.3	15	5	2, 3
1984	26.03	95.7	109	5	2, 3
1984	24.33	93.42	61	6	4, 2, 3
1984	29.52	81.79	0	5.6	2
1984	23.66	91.51	13	5.3	2, 3
1984	26.49	92.15	29	5.2	2, 3
1984	25.44	91.51	34	5.1	2, 3
1984	28.67	83.32	0	5.4	2, 3
1984	26.52	96.96	16	5.7	4
1984	27.41	96.84	84	5.3	2, 3
1984	24.75	92.99	102	6	4, 2, 3

Year	Latitude	Longitude	Depth (km)	Moment Magnitude	Reference*
1985	27.14	91.96	12	5.6	2, 3
1985	24.7	94.38	94	5	2, 3
1985	28.35	96.04	15	5.4	2, 3
1985	25.83	95.97	56	5.3	4, 2, 3
1985	18.4	87.43	10	5.5	4, 2, 3
1985	19.25	97.3	19	5	2
1985	29.24	95.53	40	5.7	4, 2, 3
1985	25.45	97.68	14	5	2
1985	25.4	97.71	20	5	2
1985	27.11	92.52	14	5.3	2, 3
1985	27.09	92.07	11	5	2, 3
1986	27.38	88.43	42	5	2, 3
1986	28.6	87.09	81	5.5	4, 2, 3
1986	21.1	95.56	22	5.2	2, 3
1986	23.79	93.09	33	5.4	4, 2, 3
1986	24.89	91.18	18	5.3	4, 2, 3
1986	24.43	94.74	86	5	2, 3
1986	23.31	94.92	129	5.1	4, 2, 3
1986	31.22	86.82	33	5.9	2
1986	26.25	96.89	32	5	2, 3
1986	31.18	86.86	17	5.1	2
1986	26.75	95.54	68	5.4	2, 3
1986	23.86	94.19	65	5.5	4, 2, 3
1986	25.38	92.15	47	5.3	2, 3
1986	25.53	96.91	70	5.4	4, 2, 3
1986	32.61	92.84	33	5.1	2
1986	26.47	92.91	46	5.1	2, 3
1987	27.63	92.69	24	5	2, 3
1987	28.67	95.85	17	5.1	2, 3
1987	22.6	93.73	48	5.3	2, 3
1987	24.07	94.64	107	5.1	2, 3
1987	24.58	93.94	75	6.3	4, 2, 3
1987	29.47	83.74	74	5.5	2
1987	23.04	94.53	127	5.3	4, 2, 3
1987	26.64	93.41	58	5.2	2, 3
1987	30.35	94.83	4	5	2
1987	29.47	90.34	15	5.1	4, 2, 3
1987	29.9	90.42	10	5	2, 3
1988	20.33	96.01	26	5.2	2, 3

Year	Latitude	Longitude	Depth (km)	Moment Magnitude	Reference*
1988	29.8	94.87	33	5.4	4, 2
1988	24.05	91.66	31	5.9	4, 2, 3
1988	18.62	95.57	66	5.3	4, 2, 3
1988	27.02	86.72	55	5.4	2, 3
1988	29.02	94.77	20	5.1	2, 3
1988	29.04	94.78	23	5	2, 3
1988	22.22	94.36	86	5.2	4, 2, 3
1988	25.19	94.89	101	7.3	4, 2, 3
1988	24.94	95.24	126	5.1	4, 2, 3
1988	26.52	86.64	35	6.9	4, 2, 3
1988	24.94	95.89	94	5.2	4, 2, 3
1988	27.19	88.37	28	5	2, 3
1988	20.74	94.67	46	5.1	4, 2, 3
1988	27.39	85.73	18	5.5	4, 2, 3
1988	23.23	99.45	8	5.1	2
1988	23.52	93.72	33	5.2	2, 3
1988	27.66	91.12	39	5	2, 3
1988	23.25	94.74	124	5.1	2, 3
1989	30.18	100.21	28	5.1	2
1989	18.29	94.13	33	5.2	2, 3
1989	29.74	90.13	15	5.4	4
1989	26.18	96.83	33	5.3	4, 2, 3
1989	26.94	92.77	59	5.1	2, 3
1989	25.15	94.81	85	5.6	4, 2, 3
1989	28.74	89.94	15	5.2	4, 2, 3
1989	24.25	91.71	33	5.5	4, 2, 3
1989	30.04	99.53	1	5.8	2
1989	30.01	99.53	20	5	2
1989	23.54	99.54	33	5.4	2
1989	27.38	87.86	5	5	2, 3
1989	22.13	89.88	15	5.8	4, 2, 3
1989	23.79	94.37	66	5	2, 3
1989	22.91	93.94	139	5.6	4, 2, 3
1989	24.51	94.55	80	5.2	2, 3
1989	20.22	94.75	144	5.4	4, 2, 3
1989	21.62	93.89	45	5.3	4, 2, 3
1989	21.54	93.78	15	5.6	4, 2, 3
1990	28.15	88.11	36	5.7	2, 3
1990	24.42	94.95	130	6.3	4, 2, 3

Year	Latitude	Longitude	Depth (km)	Moment Magnitude	Reference*
1990	24.46	94.63	87	5.3	2, 3
1990	29.14	90.02	54	5	2, 3
1990	24.95	93.13	52	5.1	2, 3
1990	23.02	94.01	93	5	2, 3
1990	25.11	96.61	57	5.2	4, 2, 3
1990	26.54	95.23	150	5.3	2, 3
1990	26.58	92.67	57	5.2	2, 3
1990	23.81	93	26	5.2	2, 3
1990	24.37	94.64	82	5	2, 3
1990	26.68	92.59	27	5	2, 3
1991	23.61	96.18	21	7	4, 2, 3
1991	23.97	96.04	43	5.2	2, 3
1991	24.72	95.22	118	5.4	2, 3
1991	26.08	95.39	0	5	2, 3
1991	25.51	91.17	26	5	2, 3
1991	25.81	94.74	33	5	2
1991	23.42	93.25	74	5.4	4, 2, 3
1991	26.59	93.19	46	5.4	2, 3
1991	21.52	94.02	58	5	2, 3
1991	25.27	88.66	10	5	2, 3
1991	24.19	93.83	70	5.5	4, 2, 3
1991	24	93.83	52	5.1	2, 3
1991	24.47	93.08	101	5.4	4, 2, 3
1992	29.61	95.64	15	5.6	2, 3
1992	29.64	95.68	10	5.1	2, 3
1992	25.17	92.23	33	5	2, 3
1992	24.18	95.2	120	5.2	4, 2, 3
1992	21.12	94.52	86	5.6	4, 2, 3
1992	23.96	94.57	143	5.7	4, 2, 3
1992	22.43	98.88	10	5.7	2
1992	28.94	81.9	56	5.2	2
1992	23.95	96.03	23	6.3	4, 2, 3
1992	21.07	93.51	79	5.4	4, 2, 3
1992	20.96	90.2	30	5.3	4, 2, 3
1992	29.46	90.3	15	6.1	4, 2, 3
1992	30.12	92.09	30	5	2
1992	18.88	96.29	49	5.5	4, 2, 3
1992	20.43	94.51	71	5.3	4, 2, 3
1992	25.48	91.39	41	5	2, 3

Year	Latitude	Longitude	Depth (km)	Moment Magnitude	Reference*
1993	25.89	87.51	30	5	2, 3
1993	28.87	87.64	15	6.2	4, 2, 3
1993	29.03	87.35	27	5.2	4, 2, 3
1993	24.64	95.02	109	5	2, 3
1993	29.1	87.33	16	5.1	2, 3
1993	23.55	94	107	5.3	4, 2, 3
1993	28.91	96.18	43	5	2, 3
1994	26.16	96.84	9	5.9	2, 3
1994	24.63	94.81	102	5.1	2, 3
1994	24.98	95.58	192	5	2, 3
1994	24.78	94.44	60	5	2, 3
1994	25.62	95.3	108	5.1	2
1994	20.45	94.17	49	6.5	4, 2, 3
1994	21.51	93.98	34	5.8	3
1994	21.61	93.88	65	5.7	4, 2
1994	24.76	94.97	146	6.1	4, 2, 3
1994	17.96	96.58	15	5.8	4, 2, 3
1994	25.37	96.83	43	5.9	4, 2, 3
1995	19.26	96.08	3	5.1	2, 3
1995	18.61	93.8	21	5	2, 3
1995	27.48	92.62	35	5.5	4, 2, 3
1995	24.83	95.02	148	6.4	4, 2, 3
1995	25	94.94	124	5.2	4, 2, 3
1995	17.89	96.49	11	6.1	2, 3
1995	26.87	96.07	33	5.1	2, 3
1996	27.84	87.8	25	5	2, 3
1996	28.71	92.58	83	5.2	4, 2, 3
1996	29.77	88.32	15	5.6	4, 2
1996	29.92	88.19	33	5	4, 2, 3
1996	21.33	94.77	120	5.1	2, 3
1996	24.68	96.53	68	5.4	4, 2, 3
1996	20.8	94.85	129	5.2	4, 2, 3
1996	29.74	88.67	15	5.4	4, 2
1996	30.1	88.13	33	5	2
1996	27.6	88.8	32	5	2, 3
1996	19.27	95.05	86	6	4, 2, 3
1996	24.05	93.38	53	5.4	4, 2, 3
1996	28.86	95.95	29	5	2, 3
1996	27.49	86.77	33	5	2, 3

Year	Latitude	Longitude	Depth (km)	Moment Magnitude	Reference*
1997	27.99	85.21	7	5.2	2, 3
1997	22.55	94.18	110	5.3	4, 2, 3
1997	24.51	92.36	35	6	4, 2, 3
1997	21.41	94.64	150	5.4	4, 2, 3
1997	26.83	91.8	46	5	2, 3
1997	23.8	93.43	42	5.3	4, 2, 3
1997	29.54	89.73	45	5.3	2, 3
1997	28.6	85.39	33	5.5	4, 2, 3
1997	22.21	92.7	54	6.1	4, 2, 3
1997	27.56	87.31	33	5.1	2, 3
1997	27.5	87.27	33	5	2, 3
1997	25.01	96.52	54	5.8	4, 2, 3
1998	24.84	95.09	127	5.5	4, 2, 3
1998	27.32	91.07	33	5.2	2, 3
1998	29.83	88.47	15	5.7	4
1998	29.93	88.5	16	5	4, 2
1998	27.65	91.1	35	5.2	2, 3
1998	29.86	88.31	15	5.8	4
1998	27.86	86.95	3	5.6	2, 3
1998	27.87	93.6	33	5.5	4, 2, 3
1998	29.64	88.25	33	5.2	4, 2, 3
1998	29.89	88.6	33	5.2	4
1998	23.82	94.74	112	5.4	4, 2, 3
1998	11.06	92.49	33	5.1	2
1998	27.69	87.86	35	5.1	2, 3
1998	26.4	93.5	10	5	2, 3
1999	23.15	93.99	51	5.1	4, 2, 3
1999	24.5	93.96	65	5.6	4, 2, 3
1999	25	93.51	33	5.5	2
1999	21.53	92.02	10	5.2	2, 3
1999	21.62	91.9	10	5.2	2
1999	25.77	93.23	11	5	2
1999	28.37	86.79	40	5.2	2, 3
1999	28.55	86.75	87	5	2
1999	18.46	96.23	39	5.2	4, 2, 3
1999	18.38	96.38	47	5	2
1999	27.24	87.98	23	5	2
1999	25.88	91.89	33	5.2	4, 2, 3
1999	26.26	91.93	33	5.3	2

Year	Latitude	Longitude	Depth (km)	Moment Magnitude	Reference*
2000	27.6	92.57	6	5.1	2, 3
2000	27.68	88.36	32	5	2
2000	27.68	92.65	4	5.3	2, 3
2000	23.03	94.13	39	5.1	2, 3
2000	26.8	97.19	33	6.2	2
2000	24.45	94.67	103	5.2	4, 2, 3
2000	24.38	97.8	33	5.1	2
2000	23.58	94.63	122	5.6	4, 2, 3
2000	21.94	93.04	74	5.5	4, 2, 3
2001	23.99	93.43	64	5.3	4, 2, 3
2001	25.35	94.91	149	5.3	4, 2, 3
2001	28.77	87.13	25	5.2	2, 3
2001	22.6	93.32	33	5	2
2001	28.15	84.87	4	5	2, 3
2001	24.43	94.99	142	5.1	4, 2, 3
2001	18.93	92.28	10	5.3	2
2001	18.69	91.8	15	5.2	4, 2, 3
2001	18.95	92.3	8	5.4	2
2001	21.08	93.69	47	5	2, 3
2001	19.73	92.68	12	5.3	2
2001	19.06	92.44	10	5.2	2
2001	18.84	92.18	10	5.6	2
2001	27.39	91.97	21	5.2	2, 3
2001	23.89	92.88	10	5	2
2001	19.57	92.81	150	5.2	2
2001	19.65	92.62	10	5.3	2
2001	19.7	92.73	19	5.2	2
2001	19.02	92.31	21	5.1	2
2001	27.22	88.18	25	5.1	2, 3
2001	22.01	94.14	10	5.6	2
2001	20.76	93.35	10	5.3	2
2002	23.75	93.53	33	5.4	2
2002	21.54	92.27	145	5	2
2002	13.04	93.57	24	5	2
2002	21.21	94.24	87	5.3	2
2002	25.53	96.11	33	5.1	2
2002	20.97	94.35	99	5.2	2
2002	22.36	94.51	132	5.9	2
2002	29.88	88.06	16	5	2, 3

Year	Latitude	Longitude	Depth (km)	Moment Magnitude	Reference*
2002	24.85	95.27	159	5.9	2, 3
2002	21.16	93.16	46	5.1	4, 2, 3
2002	23.33	93.88	93	5.7	2
2002	17.26	93.56	42	5.1	4, 2, 3
2002	28.62	95.07	31	5.1	2, 3
2002	19.57	94.86	49	5.7	4, 2, 3
2002	23.52	93.66	69	6	2
2003	29.96	88.11	12	5.1	2, 3
2003	19.68	95.13	114	5	4, 2, 3
2003	26.92	89.82	56	5.5	4, 2, 3
2003	22.9	92.31	15	5.7	4, 2, 3
2003	22.83	92.34	15	5.5	4, 2, 3
2003	29.26	95.91	33	5.5	4, 2, 3
2003	19.86	95.72	16	6.6	4, 2, 3
2003	19.82	95.73	15	5.3	4, 2, 3
2003	19.85	95.91	10	5.1	2, 3
2003	19.65	95.8	15	5.5	4, 2, 3
2004	17.4	94.31	33	5	2, 3
2004	29.78	95.7	31	5.2	4, 2, 3
2004	24.66	92.72	39	5.4	4, 2, 3
2004	19.86	95.85	42	5	2, 3
2005	26.04	95.58	79	5	4, 2, 3
2005	19.61	96.05	16	5.1	4, 2, 3
2005	24.52	92.61	27	5.1	4, 2, 3
2005	24.4	94.62	60	5.2	4, 2, 3
2005	25.54	94.92	83	5.2	4, 2, 3
2005	28.81	94.72	19	5.9	4, 2, 3
2005	20.8	95.09	122	5	4, 2, 3
2005	24.48	94.71	105	5.7	4, 2, 3
2005	25.86	96.66	10	5	2, 3
2005	17.58	92.68	19	5	4, 2, 3
2005	28.38	84.88	23	5	4, 2, 3
2005	24.74	96.29	19	5.1	4, 2, 3
2006	27.22	88.64	19	5.3	4, 2, 3
2006	26.91	91.94	12	5.8	4, 2, 3
2006	26.9	91.62	1	5.2	2, 3
2006	21.15	94.44	121	5.2	2, 3
2006	23.33	93.91	46	5.1	4, 2, 3
2006	23.31	94.3	34	5.7	4, 2, 3

Year	Latitude	Longitude	Depth (km)	Moment Magnitude	Reference*
2006	24.59	92.86	33	5	4, 2, 3
2006	21.99	93.26	35	5	4, 2, 3
2007	19.13	95.35	98	5.1	4, 2, 3
2007	23.02	94.58	97	5	4, 2, 3
2007	25.4	96.79	14	5.2	4, 2, 3
2007	19.06	95.77	12	5.9	4, 2, 3
2007	19.05	95.79	14	5.2	4, 2, 3
2007	27.39	87.73	22	5	2, 3
2007	-22.24	-179.5	608	5.3	2
2007	19.95	93.64	35	5.1	2, 3
2007	23.94	94.54	42	5.1	2, 3
2007	22.15	92.5	25	5.5	4, 2, 3
2007	29.39	95.44	28	5	2, 3
2007	23.37	94.49	116	5.1	2, 3
2007	23.46	94.66	109	5	4, 2, 3
2008	23.89	90.04	49	5.1	2
2008	23.6	94.63	114	5.2	2, 3
2008	26.31	101.89	2	5.6	2
2008	29.66	90.5	12	6.3	4, 2, 3
2008	29.81	90.38	10	5	2, 3
2008	29.79	90.31	10	5.1	2, 3
2008	29.56	90.53	14	5.2	4, 2, 3
2008	29.76	90.57	15	5.5	4, 2, 3
2008	28.16	85.32	31	5	2
2008	27.32	87.97	24	5.2	2, 3
2008	29.99	82.09	15	5.3	2
2008	22.65	96.09	15	5.3	4, 2, 3
2009	22.41	85.87	10	5.1	2, 3
2009	31.17	85.96	13	5.8	2
2009	24.25	94.77	115	5.5	4, 2, 3
2009	26.51	92.45	46	5	2, 3
2009	25.13	95.06	78	5.3	4, 2, 3
2009	24.29	94.73	116	5.9	4, 2, 3
2009	19.61	95.03	10	5	2
2009	27.2	91.63	12	6.1	4, 2, 3
2009	20.14	94.87	74	5.7	4, 2, 3
2009	27.2	91.62	15	5.2	4, 2, 3
2009	29.31	86.28	19	5.6	4, 2, 3
2009	27.95	92.9	35	5	2

Year	Latitude	Longitude	Depth (km)	Moment Magnitude	Reference*
2009	21.87	91.74	12	5.1	4, 2, 3
2009	24.31	94.84	125	5.6	4, 2, 3
2009	27.33	91.48	19	5.5	2, 3
2010	28.41	86.77	85	5.5	4, 2, 3
2010	22.99	94.62	115	5.5	4, 2, 3
2010	19.18	93.01	31	5.3	4, 2, 3
2010	23.29	90.74	18	5.1	4, 2, 3
2010	29.78	90.53	21	5.4	4, 2, 3
2010	30.88	86.52	14	5.2	2
2011	24.46	94.68	104	6.4	4, 2, 3
2011	27.9	87.31	50	5.4	2
2011	27.45	87.84	30	5	2, 3
2011	26.88	97.25	10	5.3	2
2011	27.44	88.35	46	6.9	4, 2, 3
2011	24.82	95.19	129	5.8	4, 2, 3
2011	25.17	97.57	10	5.1	2
2012	26.01	87.7	31	5	2, 3
2012	26.18	93.03	46	5.4	4, 2, 3
2012	25.6	94.73	50	5.6	4, 2, 3
2012	25.29	96.66	12	5.1	4, 2, 3
2012	25.4	94.45	41	5.3	4, 2, 3
2012	24.86	96.43	18	5.1	4, 2, 3
2012	29.93	88.32	25	5	4, 2, 3
2012	22.83	94.32	72	5.8	4, 2, 3
2012	26.13	96.24	35	5.1	2, 3
2012	26.78	92.95	36	5.2	4, 2, 3
2012	22.73	96.03	17	6.8	4, 2, 3
2012	22.6	96.05	12	5.9	4, 2, 3
2012	23.06	96.07	20	5.6	4, 2, 3
2012	22.83	95.98	16	5	4, 2, 3
2012	22.29	94.8	142	5.5	4, 2, 3
2012	22.77	95.87	27	5	4, 2, 3
2013	25.09	94.95	106	5.8	4, 2, 3
2013	24.56	92.28	45	5.5	4, 2, 3
2013	22.94	96.07	12	5.2	4, 2, 3
2013	19.13	95.79	12	5.8	4, 2, 3
2013	19.08	95.77	12	5.6	4, 2, 3
2013	19.04	95.83	12	5.5	4, 2, 3
2013	28.67	95.12	40	5.2	4, 2, 3

Year	Latitude	Longitude	Depth (km)	Moment Magnitude	Reference*
2013	23.74	94.82	93	5	4, 2, 3
2013	22.91	96.05	23	5.2	4, 2, 3
2013	22.81	96.04	12	5	4, 2, 3
2013	22.88	96.04	12	5.7	4, 2, 3
2013	22.91	95.74	74	5.6	2
2013	26.92	89.52	10	5.5	2
2013	27.17	88.79	27	5.3	4, 2, 3
2013	27.3	87.45	10	5.5	2
2013	26.56	94.51	15	5.9	2
2013	20	96.92	10	5.3	2
2013	20.17	95.04	10	6.1	2
2013	27.46	92.35	10	5.7	2
2013	26.39	93.74	36	5.4	4, 2, 3
2013	28.91	95.85	10	5	2, 3
2013	22.2	91.56	10	5.7	2
2014	22.78	96.01	20	5.2	4, 2, 3
2014	23.71	94.08	54	5.1	4, 2, 3
2014	19.24	95.69	0	5.1	2, 3
2014	29.79	91.62	10	5.1	2
2014	18.1	88.09	58	6.1	4, 2, 3
2014	25.03	97.78	10	6	2
2014	29	85.57	19	6	4, 2, 3
2014	29.3	85.54	31	5.3	2
2014	24.66	94.76	94	5	4, 2, 3
2014	21.98	93.14	16	5.4	4, 2, 3
2014	20.78	94.44	90	5.3	4, 2, 3
2014	23.49	93.46	35	5.7	4, 2, 3
2014	27.46	86.56	30	5	4, 2, 3
2014	24.3	94.76	93	5.1	4, 2, 3
2015	23.97	93.93	96	5	4, 2, 3
2015	22.76	88.39	33	5.6	2
2015	27.91	85.33	12	7.9	4, 2, 3
2015	27.44	85.07	0	6.1	2, 3
2015	28.18	84.82	30	6	2
2015	27.64	85.76	0	5.6	2, 3
2015	27.85	86.1	0	5.4	2
2015	28.02	84.41	0	5.4	2, 3
2015	28.08	85.03	10	5.8	2
2015	27.81	85.13	10	5.2	2, 3

Year	Latitude	Longitude	Depth (km)	Moment Magnitude	Reference*
2015	27.76	85.08	0	5	2
2015	27.8	85.44	0	5.1	2
2015	27.32	85.34	0	5	2, 3
2015	27.81	85.11	0	5.1	2, 3
2015	27.86	84.93	21	6.7	4, 2, 3
2015	28.39	84.83		7.1	2, 3
2015	27.7	85.31	10	5	2, 3
2015	27.72	84.91	0	5.5	2, 3
2015	27.74	85.78	0	5.2	2
2015	27.68	86	0	5.1	2, 3
2015	27.82	85.64	0	5	2, 3
2015	27.77	85.81	12	5	2, 3
2015	28.05	84.73	11	5.1	2, 3
2015	27.75	85.24	10	5.2	2, 3
2015	27.46	85.67	0	5.3	2, 3
2015	28.44	87.35	10	5.7	2, 3
2015	27.68	85.98	10	5	2, 3
2015	27.97	85.47	10	5.1	2, 3
2015	27.9	85.53	10	5.2	2, 3
2015	28.1	85.44	10	5	2, 3
2015	28.04	85.41	10	5	2
2015	28.06	84.67	0	5.2	2, 3
2015	27.89	85.66	19	5	2, 3
2015	28.06	85.89	21	5.3	4, 2, 3
2015	28.26	85.88	10	5	2, 3
2015	27.61	84.96	15	5.5	4, 2, 3
2015	27.56	85.95	21	6.8	4, 2, 3
2015	27.78	85.96	10	5	2
2015	27.81	85.98	10	5.1	2
2015	27.66	85.9	10	5	2, 3
2015	27.56	85.9	20	5.2	4, 2, 3
2015	26.66	88.27	27	5.1	4, 2, 3
2015	27.8	85.11	10	5	2, 3
2015	27.67	86.08	12	7.3	4, 2, 3
2015	27.74	86.26	25	5.7	2
2015	27.32	86.16	0	5.5	2, 3
2015	27.82	86.16	10	5.7	2
2015	27.62	86.33	0	5	2, 3
2015	27.7	86.01	0	5.4	2, 3

Year	Latitude	Longitude	Depth (km)	Moment Magnitude	Reference*
2015	27.37	86.35	20	6.3	4, 2, 3
2015	27.63	86.09	0	5	2, 3
2015	27.91	85.83	10	5.2	2, 3
2015	27.79	86.16	10	5.2	2, 3
2015	27.78	84.7	0	5.2	2, 3
2015	27.61	86.11	0	5	2, 3
2015	27.37	86.26	12	5.5	4, 2, 3
2015	27.91	85.5	10	5.3	2
2015	26.38	90.59	40	5.3	4, 2, 3
2015	19.15	96.25	19	5	4, 2, 3
2015	27.75	86.15	0	5	2, 3
2015	27.76	85.64	0	5	2, 3
2015	22.38	94.99	17	5.4	4, 2, 3
2017	23.98	92.03	24.5	5.6	4, 2
2018	26.22	90.26	27.4	5.4	4, 2
2018	23.93	93.5	35.3	5.1	4, 2
2019	22.7414	95.522	10	5.4	4, 2
2019	24.0196	93.858	63.4	5	4, 2
2019	27.7188	92.8302	15	5.5	4, 2
2019	28.4073	94.5605	14	5.9	4, 2
2019	25.4467	94.4235	61.8	5.1	4, 2
2020	22.1912	94.38	91	5.1	4, 2
2020	23.6114	94.5944	110.5	5	4, 2
2020	24.6513	93.5136	58	5.4	4, 2
2020	27.8464	85.8765	10	5.3	4, 2
2020	23.4098	92.0133	37.8	5.1	4, 2
2020	23.1658	93.3193	10	5.3	4, 2
2020	23.1162	93.3092	10	5.1	4, 2
2020	23.1449	93.2856	10.8	5.6	4, 2
2020	23.8756	93.071	40.4	5.2	4, 2
2020	24.3856	93.9197	57.9	5.1	4, 2
2020	22.8004	94.0292	10	5.9	4, 2
2020	28.5896	87.3081	10	5.7	4, 2
2020	26.3386	90.7847	10	5	4, 2
2021	22.8217	93.52	42.7	6.2	4, 2
2021	22.3074	94.7616	110	5.5	4, 2
2021	25.2256	94.8803	80.1	5	4, 2
2021	25.9603	90.3499	10	5.3	4, 2
2021	26.7489	92.5136	35	5	4, 2

Year	Latitude	Longitude	Depth (km)	Moment Magnitude	Reference*
2021	26.7746	92.4364	34	6	4, 2
2021	22.5129	94.1955	24.7	5.1	4, 2
2021	27.1863	88.9412	10	5.2	4, 2
2021	27.6146	92.6806	24.8	5	4, 2
2021	22.1989	88.9914	10	5.7	4, 2
2023	24.8172	92.0359	31.8	5	4, 2
2023	24.951	92.24	33.7	5.5	4, 2

*List of Reference of the Earthquake Event Catalogue:

1 – NDMA: National Disaster Management Authority, India

2 – ISC: International Seismological Centre

3 – NEIC: National Earthquake Information Center, USA

4 – GlobalCMT: Global Centroid-Moment-Tensor Project

5 – BNBC: Bangladesh National Building Code

6 – ISET: Indian Society of Earthquake Technology

7 – ISS: International Seismological Summary

8 – IMD: India Meteorological Department

APPENDIX – B: GEOTECHNICAL INVESTIGATION DATA

Table B – 1: Geotechnical investigation information

Borehole	Easting (m)	Northing (m)	Project	Type
CDMP BH-01	237550.536	2642506.685	CDMP	SPT
CDMP BH-02	237204.4938	2623759.17	CDMP	SPT
CDMP BH-03	244561.0195	2625582.591	CDMP	SPT
CDMP BH-04	237700.2848	2640001.173	CDMP	SPT
CDMP BH-06	231276.0138	2643973.865	CDMP	SPT
CDMP BH-07	229892.3278	2634810.026	CDMP	SPT
CDMP BH-08	229452.9476	2630854.212	CDMP	SPT
CDMP BH-09	240459.1638	2628321.828	CDMP	SPT
CDMP BH-10	240602.2726	2634472.267	CDMP	SPT
CDMP BH-11	231738.9741	2625275.1	CDMP	SPT
CDMP BH-12	232321.0077	2626126.586	CDMP	SPT
CDMP BH-13	233098.4594	2626789.411	CDMP	SPT
CDMP BH-14	237757.772	2630552.18	CDMP	SPT
CDMP BH-15	240307.6861	2633676.811	CDMP	SPT
CDMP BH-16	242551.0699	2634190.796	CDMP	SPT
CDMP BH-17	240415.3238	2638077.809	CDMP	SPT
CDMP BH-18	243798.297	2637247.177	CDMP	SPT
CDMP BH-19	245202.5408	2623709.363	CDMP	SPT
CDMP BH-20	241006.1631	2625229.784	CDMP	SPT
CDMP BH-21	237964.2826	2627870.972	CDMP	SPT
CDMP BH-22	235867.0331	2634034.3	CDMP	SPT
CDMP BH-23	236854.0632	2636940.956	CDMP	SPT
CDMP BH-24	233556.0444	2640819.439	CDMP	SPT
CDMP BH-25	234389.6308	2643020.606	CDMP	SPT
CDMP BH-26	231912.2091	2637709.014	CDMP	SPT
CDMP BH-27	231127.5453	2632028.096	CDMP	SPT
CDMP BH-28	238797.4082	2631641.61	CDMP	SPT
CDMP BH-29	233853.5225	2624566.786	CDMP	SPT
CDMP BH-30	231139.4339	2626951.936	CDMP	SPT
CDMP BH-31	232391.5492	2632485.66	CDMP	SPT
CDMP BH-32	232717.9081	2637998.853	CDMP	SPT
CDMP BH-33	230373.0105	2637070.481	CDMP	SPT
CDMP BH-34	239824.1823	2621445.366	CDMP	SPT
CDMP BH-35	239419.3001	2624022.54	CDMP	SPT
CDMP BH-36	239126.3516	2628670.092	CDMP	SPT
CDMP BH-37	235462.3942	2626282.859	CDMP	SPT
CDMP BH-38	232458.4266	2628431.467	CDMP	SPT
CDMP BH-39	233970.289	2644260.628	CDMP	SPT
CDMP BH-40	240852.0521	2622616.217	CDMP	SPT
CDMP BH-41	229148.1403	2639609.398	CDMP	SPT
CDMP BH-42	234266.9129	2637607.359	CDMP	SPT

Borehole	Easting (m)	Northing (m)	Project	Type
CDMP BH-44	232775.9425	2633706.647	CDMP	SPT
CDMP BH-45	230231.305	2629105.212	CDMP	SPT
CDMP BH-48	241021.493	2643622.896	CDMP	SPT
CDMP BH-49	244337.5796	2626894.778	CDMP	SPT
CDMP BH-50	236133.2844	2640864.028	CDMP	SPT
CDMP BH-51	242083.1833	2637936.598	CDMP	SPT
CDMP BH-52	234567.5438	2636090.279	CDMP	SPT
CDMP BH-53	242636.2734	2622810.449	CDMP	SPT
DK_BM1872	239998.8346	2630413.816	GSB	SPT
DK_BM2849	232275.5304	2643560.262	GSB	SPT
DK_BM2890	230845.0771	2643106.044	GSB	SPT
DK_BM2891	237487.6495	2643374.419	GSB	SPT
DK_BM2897	230052.9568	2640869.148	GSB	SPT
DK_BM2898	233597.006	2640897.124	GSB	SPT
DK_BM2899	236715.4585	2641053.178	GSB	SPT
DK_BM2900	240546.4684	2638571.193	GSB	SPT
DK_BM2902	230736.1667	2633379.669	GSB	SPT
DK_BM2903	239562.3455	2627566.786	GSB	SPT
DK_BM2904	238611.6252	2634457.637	GSB	SPT
DK_BM2905	240118.2171	2636472.977	GSB	SPT
DK_BM2910	242424.7405	2628554.577	GSB	SPT
DK_BM2914	239592.5433	2630319.222	GSB	SPT
DK_BM2917	232549.9774	2626099.767	GSB	SPT
DK_BM2918	238152.9192	2623757.123	GSB	SPT
DK_BM2919	238926.9383	2625248.505	GSB	SPT
DK_BM2921	240090.0048	2621820.23	GSB	SPT
DK_BM2931	236205.8501	2631780.286	GSB	SPT
DK_BM2942	229449.6168	2634887.575	GSB	SPT
DK_BM2958	233908.4467	2635273.973	GSB	SPT
DK_BM2959	238299.2047	2638100.444	GSB	SPT
DK_BM2961	232830.1758	2636640.117	GSB	SPT
DK_BM2962	232183.1758	2641500.553	GSB	SPT
DK_BM2963	236944.6697	2638142.921	GSB	SPT
DK_BM2969	229104.1875	2632188.543	GSB	SPT
DK_BM2971	232660.2189	2624775.822	GSB	SPT
DK_BM2973	232242.3763	2626909.244	GSB	SPT
DK_BM2978	233972.6537	2637990.821	GSB	SPT
DK_BM2993	245284.0422	2624939.464	GSB	SPT
DK_BM2994	237165.0488	2629902.851	GSB	SPT
DK_BM2995	240188.2587	2631733.185	GSB	SPT
DK_BM3266	230027.8497	2638271.559	GSB	SPT
DK_BM3267	233802.2478	2641784.573	GSB	SPT
DK_BM3277	239718.561	2630630.95	GSB	SPT
DK_BM3284	240007.2883	2630521.714	GSB	SPT
DK_BM3296	240707.6464	2626624.608	GSB	SPT

Borehole	Easting (m)	Northing (m)	Project	Type
MRT5S1	229124.422	2632606.649	MRT	SPT
MRT5S16	234171.63	2628984.29	MRT	SPT
MRT5S19	235858.7	2630241.6	MRT	SPT
MRT5S20	236007.812	2630418.282	MRT	SPT
MRT5S24	237485.709	2630990.506	MRT	SPT
MRT5S25	237623.93	2630907.83	MRT	SPT
MRTS5_26	238066.18	2630658.43	MRT	SPT
MRTS5_27	238555.14	2630462.174	MRT	SPT
MRTS5_28	238796.686	2630605.563	MRT	SPT
MRTS5_29	239018.86	2620616.46	MRT	SPT
MRTS5_30	239825.94	2630535.95	MRT	SPT
MRTS5_31	240697.34	2630469.4	MRT	SPT
SW BH 01	229362.6	2632641	SW	SPT
SW BH 02	235070.1	2631467	SW	SPT
SW BH 03	233400	2640510	SW	SPT
SW BH 04	235971.4879	2624792.634	SW	SPT
SW BH 05	235971.4879	2623990.669	SW	SPT
SW BH 07	233664.195	2636787.19	SW	SPT
SW BH 08	237554.486	2627164	SW	SPT
SW BH 09	234433.491	2643502.9	SW	SPT
SW BH 10	239870.88	2636901.09	SW	SPT
SW BH 11	236782.969	2632265.27	SW	SPT
SW BH 12	234472.8125	2627007.679	SW	SPT
SW BH 13	238639.705	2627045.55	SW	SPT
SW BH 14	229680.205	2630655.615	SW	SPT
SW BH 15	236703.807	2629408.595	SW	SPT
SW BH 16	237288.144	2635846.355	SW	SPT
SW BH 17	236113.1863	2636139.104	SW	SPT
SW BH 18	230401.378	2631452.847	SW	SPT
SW BH 19	233019.7747	2637163.765	SW	SPT
SW BH 20	231669.71	2636851.964	SW	SPT
SW BH 21	230303.0657	2636246.384	SW	SPT
SW BH 22	229629.353	2635026.293	SW	SPT
SW BH 23	229406.3956	2633767.049	SW	SPT
SW BH 24	229211.352	2632693.601	SW	SPT
SW BH 25	230044.4108	2631918.916	SW	SPT
SW BH 26	233713.8574	2641438.065	SW	SPT
SW BH 27	230575.0084	2629690.264	SW	SPT
SW BH 28	230785.829	2628694.448	SW	SPT
SW BH 29	231061.5619	2627452.143	SW	SPT
SW BH 30	231656.159	2626474.506	SW	SPT
SW BH 31	232509.2344	2625834.313	SW	SPT
SW BH 32	233633.533	2625320.644	SW	SPT
SW BH 33	234778.1143	2624692.308	SW	SPT
SW BH 36	234713.503	2644480.53	SW	SPT
SW BH 37	234285.1522	2642360.76	SW	SPT

Borehole	Easting (m)	Northing (m)	Project	Type
SW BH 38	230776.292	2630800.702	SW	SPT
SW BH 39	237061.1597	2628754.054	SW	SPT
SW BH 40	236137.839	2627518.482	SW	SPT
SW BH 41	236969.7828	2624304.583	SW	SPT
SW BH 42	235706.298	2627604.939	SW	SPT
SW BH 43	237036.2118	2627742.978	SW	SPT
SW BH 44	238127.358	2627827.81	SW	SPT
SW BH 45	239110.927	2628206.096	SW	SPT
SW BH 47	241407.1933	2628330.813	SW	SPT
SW BH 48	242447.933	2628417.609	SW	SPT
SW BH 49	243504.713	2628543.805	SW	SPT
SW BH 50	233107.1477	2639361.801	SW	SPT
SW BH 51	232794.2567	2638374.367	SW	SPT
SW BH 52	233230.502	2636365.733	SW	SPT
SW BH 53	233513.2265	2635445.635	SW	SPT
SW BH 54	233868.8252	2633223.708	SW	SPT
SW BH 55	234650.965	2632015.583	SW	SPT
SW BH 56	235957.697	2630632.131	SW	SPT
SW BH 57	233796.139	2634310.969	SW	SPT
SW BH 58	229846.209	2628592.203	SW	SPT
SW BH 59	229344.9468	2629609.17	SW	SPT
SW BH 60	231978.5132	2631061.281	SW	SPT
SW BH 61	233283.6329	2631046.141	SW	SPT
SW BH 62	234342.1036	2631252.438	SW	SPT
SW BH 63	236476.334	2631637.216	SW	SPT
SW BH 64	237675.7648	2631092.14	SW	SPT
SW BH 65	238640.717	2631447.995	SW	SPT
SW BH 66	239918.7798	2631537.011	SW	SPT
SW BH 67	240466.695	2631497.092	SW	SPT
SW BH 68	241022.3004	2631511.861	SW	SPT
SW BH 69	232223.6293	2627732.859	SW	SPT
SW BH 70	233286.442	2627804.227	SW	SPT
SW BH 71	234675	2627640	SW	SPT
SW BH 73	232633.979	2625294.439	SW	SPT
SW BH 74	234625.435	2625332.596	SW	SPT
SW BH 75	235642.9166	2625027.516	SW	SPT
SW BH 76	237049.4	2625038.665	SW	SPT
SW BH 77	238577.5765	2624447.23	SW	SPT
SW BH 78	239535.8331	2623925.247	SW	SPT
SW BH 79	240581.6584	2623321.989	SW	SPT
SW BH 80	241678.5297	2622763.82	SW	SPT
SW BH 81	242878.1588	2622551.211	SW	SPT
SW BH 82	244034.2504	2622718.637	SW	SPT
SW BH 83	244907	2622772	SW	SPT
SW BH 84	246180.704	2623082.258	SW	SPT
SW BH 90	240523.512	2629365.848	SW	SPT
SW BH 94	231546.81	2633747.104	SW	SPT

Borehole	Easting (m)	Northing (m)	Project	Type
SW BH 95	232521	2633749	SW	SPT
SW BH 96	235409.6295	2632842.539	SW	SPT
SW BH 97	237582.6581	2632316.114	SW	SPT
SW BH 98	238496	2632402	SW	SPT
SW BH 99	239499	2632679	SW	SPT
SW BH 100	240841.24	2633024.46	SW	SPT
SW BH 101	241931.9152	2632936.101	SW	SPT
SW BH 112	240157.802	2635862.095	SW	SPT
SW BH 113	247276.4764	2623797.853	SW	SPT
SW BH 115	232689.003	2639357.523	SW	SPT
SW BH 117	230390.3136	2633609.471	SW	SPT
SW BH 118	241887.444	2636958.82	SW	SPT
SW BH 119	241793.2749	2638161.654	SW	SPT
SW BH 120	241636.9006	2639537.443	SW	SPT
SW BH 128	236925.9366	2623137.833	SW	SPT
SW BH 129	237516.183	2622393.234	SW	SPT
SW BH 133	236028.24	2626217.999	SW	SPT
SW BH 134	235475.278	2628357.843	SW	SPT
SW BH 135	235354.814	2635122.145	SW	SPT
SW BH 144	242043.231	2620326.886	SW	SPT
SW BH 145	241417.482	2621108.128	SW	SPT
SW BH 146	240944.2496	2621965.456	SW	SPT
SW BH 147	240843.884	2622997.156	SW	SPT
SW BH 148	240876.878	2624032.285	SW	SPT
SW BH 151	240330.546	2626843.506	SW	SPT
SW BH 152	240369.926	2630565.27	SW	SPT
SW BH 153	240158.3231	2633792.049	SW	SPT
SW BH 154	240044.704	2634465.318	SW	SPT
SW BH 155	233102.135	2628533.757	SW	SPT
SW BH 156	239719.512	2638894.085	SW	SPT
SW BH 157	238839.0109	2639777.524	SW	SPT
SW BH 158	238316.964	2640457.713	SW	SPT
SW BH 159	238189.4754	2641664.005	SW	SPT
SW BH 160	235961.8297	2642016.468	SW	SPT
SW BH 161	235061.1761	2642015.352	SW	SPT
SW BH 162	232876.8071	2642200.731	SW	SPT
SW BH 163	231742.2979	2642130.755	SW	SPT
SW BH 164	230729.004	2642272.937	SW	SPT
SW BH 174	236613.7696	2633723.168	SW	SPT
SW BH 175	236158.855	2634709.376	SW	SPT
SW BH 176	234384.3759	2635785.73	SW	SPT
SW BH 177	234146.723	2636827.19	SW	SPT
SW BH 178	233701.6847	2638284.544	SW	SPT
SW BH 179	237120.8656	2642074.054	SW	SPT
SW BH 180	240006.7745	2637800.735	SW	SPT
SW-PZ-005	230702.62	2629203.97	SW	SCPT
SW-PZ-006	235933.95	2645158.81	SW	SCPT

Borehole	Easting (m)	Northing (m)	Project	Type
SW-PZ-007	235138.82	2644628.92	SW	SCPT
SW-PZ-008	234378.53	2644094.9	SW	SCPT
SW-PZ-009	234193.65	2641886.64	SW	SCPT
SW-PZ-014	233093.07	2636689.27	SW	SCPT
SW-PZ-015	233319.96	2635809.14	SW	SCPT
SW-PZ-020	235716.87	2631090.15	SW	SCPT
SW-PZ-021	236128.22	2629874.89	SW	SCPT
SW-PZ-023	237260.47	2628109.66	SW	SCPT
SW-PZ-025	237489.13	2624544.24	SW	SCPT
SW-PZ-026	236145.47	2623888.16	SW	SCPT
SW-PZ-027	229178.38	2630262.43	SW	SCPT
SW-PZ-028	230209.88	2630809.59	SW	SCPT
SW-PZ-030	232560.88	2631023.71	SW	SCPT
SW-PZ-031	234667.38	2631305.12	SW	SCPT
SW-PZ-032	235587.96	2631816.84	SW	SCPT
SW-PZ-033	237816.55	2629375.87	SW	SCPT
SW-PZ-035	241007.15	2631501.32	SW	SCPT
SW-PZ-036	231803.05	2627118.79	SW	SCPT
SW-PZ-039	235042.88	2627886.32	SW	SCPT
SW-PZ-041	239615.41	2628445.54	SW	SCPT
SW-PZ-042	231545.49	2624502.21	SW	SCPT
SW-PZ-043	232526.86	2625457.96	SW	SCPT
SW-PZ-044	232849.03	2625694.8	SW	SCPT
SW-PZ-045	235166.46	2625121.11	SW	SCPT
SW-PZ-046	236230.25	2625291.1	SW	SCPT
SW-PZ-047	238046.39	2625160.28	SW	SCPT
SW-PZ-052	245638.71	2622858.73	SW	SCPT
SW-PZ-054	240097.97	2631479.28	SW	SCPT
SW-PZ-056	234097.78	2625085.57	SW	SCPT
SW-PZ-057	232147.32	2626107.18	SW	SCPT
SW-PZ-058	231300.53	2626882.57	SW	SCPT
SW-PZ-059	230940.37	2628056.35	SW	SCPT
SW-PZ-061	229532.52	2629741.1	SW	SCPT
SW-PZ-062	229652.28	2632410.43	SW	SCPT
SW-PZ-064	229481.94	2634404.7	SW	SCPT
SW-PZ-065	229831.66	2635709.96	SW	SCPT
SW-PZ-068	234345.44	2636300.81	SW	SCPT
SW-PZ-070	236717.31	2635750.92	SW	SCPT